SPATIAL DISTRIBUTION AND GEOMORPHIC FACTORS OF LEAD CONTAMINATION ON FLOODPLAINS AFFECTED BY HISTORICAL MINING, BIG RIVER, S.E. MISSOURI

A Masters Thesis

Presented to

The Graduate College of

Missouri State University

In Partial Fulfillment

Of the Requirements for the Degree

Master of Science, Geospatial Science and Environmental Geology

By

David B. Huggins

May 2016

SPATIAL DISTRIBUTION AND GEOMORPHIC FACTORS OF LEAD CONTAMINATION ON FLOODPLAINS AFFECTED BY HISTORICAL MINING, BIG RIVER, S.E. MISSOURI

Geography, Geology, and Planning

Missouri State University, May 2016

Master of Science

David B. Huggins

ABSTRACT

Historical mining in the Old Lead Belt resulted in lead (Pb) contamination of floodplain soils for over 170 km along the Big River in southeastern Missouri. The overall patterns of contamination are understood. However, Pb distribution across floodplain surfaces has not been investigated at the scale needed for site-level remediation planning. The goal of this project is to examine spatial distribution of Pb with more detail and identify the role of geomorphic processes. Predictive models are needed to evaluate factors affecting Pb distribution such as elevation, distance from the channel, and geochemistry. This study evaluates Pb distribution at three ~1km sites on the Big River with varying floodplain conditions: (1) human-altered topography, (2) narrow valley and, (3) wide valley. Surface soil samples were collected to quantify Pb, geomorphic maps were created using LiDAR, and spatial patterns were analyzed using regression models. Results show that Pb levels at the three sites pose an ecological problem. The most effective predictive model was created at the narrow floodplain site using distance from the channel, elevation, and Fe as independent variables. Less sensitive models were created at the two other sites which had more complicated geomorphological characteristics and less variability in Pb. Using landform/soil series associations and examining the influence of watershed-scale factors such as valley width and proximity to source are likely more effective approaches for understanding Pb distribution on Big River floodplains.

KEYWORDS: geomorphology, mining contaminates, floodplains, Missouri, GIS

This abstract is approved as to form and content

_____

Dr. Robert Pavlowsky
Chairperson, Advisory Committee
Missouri State University

SPATIAL DISTRIBUTION AND GEOMORPHIC FACTORS OF LEAD CONTAMINATION ON FLOODPLAINS AFFECTED BY HISTORICAL MINING, BIG RIVER, S.E. MISSOURI

By

David Huggins

A Masters Thesis
Submitted to the Graduate College
Of Missouri State University
In Partial Fulfillment of the Requirements
For the Degree of Master of Science, Geospatial Science and Environmental Geology

May 2016

Approved:

_____
Robert Pavlowsky, PhD

_____
Jun Luo, PhD

_____
Xin Miao, PhD

_____
Julie Masterson, PhD: Dean, Graduate College

ACKNOWLEDGEMENTS

A great number of people were involved in this research project, and I would like to thank them for all their help. First, I would like to thank my committee members Drs. Robert Pavlowsky, Jun Luo, and Xin Miao for support and guidance in developing and executing this project. I would like to especially thank Dr. Robert Pavlowsky for mentoring and guiding me from start to finish, including suggesting the Big River for this study. I would also like to thank Marc Owen for the extensive help in field, laboratory and GIS method support. A special thanks to Ralph Hill, Karen Zelzer, Felix Corrodi, Kathryn Martin, Lisa Andes, Adam Mulling, Ali Keppel, Megan Hente, and Rachael Bradley who helped make sampling possible.

I would like to thank the United States Environmental Protection Agency as well as the Fish and Wildlife Service for partial funding of this research. Funding for supplies, field work, and travel to conferences was from Graduate College at Missouri State University, Ozark Environmental and Water Resource Institute, the Department of Geography, Geology, and Planning, and the College of Natural and Applied Sciences.

Finally, a huge thank you to all of my family and friends that supported me through this process. I could not have completed this project without the encouragement of the people closest to me.

TABLE OF CONTENTS

LIST OF TABLES

LIST OF FIGURES

CHAPTER 1 - INTRODUCTION

Floodplains control the spatial distribution of flood energy, sediment storage, and riparian habitat in river systems. They act as an intermediate step for sediment within a watershed, representing both a significant sediment sink by deposition, as well as a source by bank erosion (Jain et al., 2008; Lecce and Pavlowsky, 1997). Sediment from within the watershed is stored in floodplains as it gets deposited through accretionary processes (Nanson and Croke, 1992). Once sediment is deposited, it can remain in floodplain deposits for a period of decades to centuries (Macklin et al., 2006) and can later be remobilized through bank erosion and mast wasting (Leece and Pavlowsky, 2001; Phillips et al., 2007; Hürkamp et al., 2009). Phillips et al., 2007 found that in the Waipaoa River in New Zealand, 30 to 40% of alluvium becomes remobilized from the floodplain within a century of deposition. Once remobilized, sediment is transported downstream to potentially become stored in new floodplain deposits. This process continues as the fine-grained sediment that dominates floodplain deposition moves through a watershed (Nanson and Croke, 1992).

When anthropogenic activity within a watershed introduces contaminated sediment into a river, it is transported, deposited, and reworked in the same manner as natural sediment (Miller, 1996; Macklin et al., 2006). Historically, mining activity has contributed significant quantities of sediment containing high concentrations of heavy metals into fluvial systems (Gazdag and Sipter, 2008; Gäbler and Schneider, 1999; Zornoza et al., 2011). Through overbank deposition and point bar accretion, contaminants can accumulate on floodplain surfaces and within bank deposits where they can pose

serious problems to stream ecosystems and human health (Dennis et al. 2009; Macklin et al., 2006; Ciszewski and Turner, 2009). Bioaccumulation of metals stored in floodplains can then be passed through food chains in the tissue of organisms and can cause significant damage to riparian ecosystems (Schipper et al., 2008; Gazdag and Sipter, 2008; Appleton et al., 2001; Thonon, 2006; Kooistra et al., 2001). Heavy metal pollutants do not break down in the environment and remain geochemically and biologically active. Consequently, even during post-mining periods the remobilization of contaminated floodplain sediment can represent a long-term non-point source for channel contamination which can damage fisheries and macroinvertebrate populations (Dennis et al., 2009; Lecce and Pavlowsky, 2014; Hürkamp et al., 2009; Clements et al., 2000; Leece and Pavlowsky, 2001). Therefore, understanding the spatial distribution of metal contaminants in floodplains along rivers affected by historical mining is important for understanding and monitoring long-term toxic risks in affected watersheds.

A period of lead mining from 1869 through 1972 in the Old Lead Belt in the Ozarks has created a serious contamination problem within the Big River watershed in southeast Missouri (Meneau, 1997; MDNR, 2007). Through the ore milling process, coarse and fine-grained mine wastes were produced and dumped into large piles or stored in retention ponds on or near floodplains near Leadwood, Desloge, and Bonne Terre, Missouri. These mining wastes contained high concentrations of heavy metals including Pb and Zn (Smith and Schumacher, 1993). Through erosion, runoff, and retention pond dam failure, large quantities of heavy metal-rich sediment were able to enter the local streams. Fluvial processes have since reworked contaminated sediment and distributed it downstream (Meneau, 1997; Mosby et al., 2009). Transportation and deposition of

contaminated mining sediment in the Big River has resulted in the accumulation of toxic levels of both lead (Pb) and zinc (Zn) along 171 river kilometers of floodplain deposits from the Leadwood tailings pile and Eaton Creek confluence to where the Big River connects with the Meramec River (Pavlowsky et al., 2010a).

Major tailings piles contributing to Big River contamination include the Bonne Terre, Desloge, National, Elvins, Federal and Leadwood piles (Figure 1). The Leadwood and Desloge piles contaminate the Big River above the Flat River confluence. The Elvins, Federal, and National piles contaminate the Flat River, which then flows into the Big River in Desloge, MO. The Bonne Terre Pile contaminates the Big River downstream of the Flat River confluence near Bonne Terre, MO.

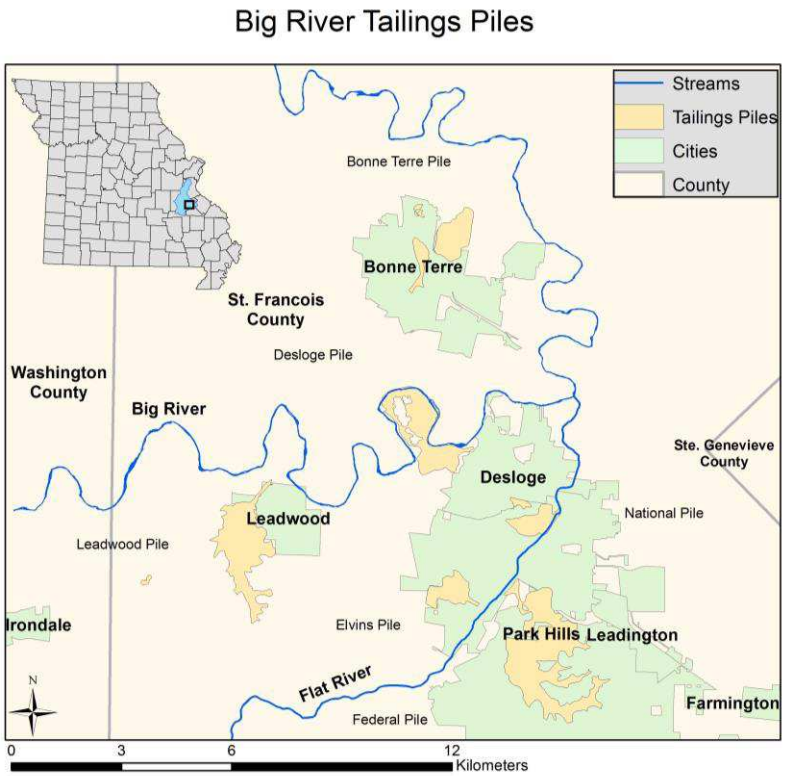

Figure 1 – Big River tailings piles. Tailings have been show to contaminate the Big River and the Flat River with heavy metals.

In compliance with the Comprehensive Environmental Response Compensation Liability Act, all six major tailings piles have since been stabilized to limit contamination potential, however the contaminated sediment within floodplain deposits acts as a significant non-point source for heavy metal contamination for the watershed (Mosby et al., 2009; Pavlowsky et al., 2010a).

Extensive studies and reports have been conducted on the contamination of the Big River in order to assess soil, ecosystem, and water quality (Pavlowsky et al., 2010a; Meneau, 1997; Smith and Schumacher 1993; Mosby et al., 2009; Young, 2011). While these reports offered detailed information about the mining contamination across the watershed, there is limited knowledge about the variables driving patterns of surface soil contamination across Ozark floodplains on a scale needed for soil remediation planning. This type of planning requires the examination of spatial trends in contamination through detailed landform mapping, as well as the quantifying and modeling of contamination concentrations across a study site. Specifically, this allows for the prediction of areas of high and low risk ecologically across floodplains (Macklin et al., 2006; Brewer and Taylor, 1997). Previous studies suggest factors such as floodplain elevation in relation to flood stage, number and pattern of secondary channels along a reach, and sediment composition and transport rate controls play a key role in explaining the spatial variation of heavy metal contamination across floodplains (Brewer and Taylor, 1997; Middelkoop, 2000; Ciszewski and Malik, 2004; Lecce and Pavlowsky, 1997). However, in order to effectively develop remediation plans for Big River floodplains, more knowledge about how to predict the locations of contaminated floodplain soils is needed.

Mining-Contaminated Sediment Characteristics

In order to understand the effects of mining activity on a fluvial system, it is important to characterize the associated contaminated sediment. Mining and milling operations in a watershed create an artificial source of sediment in fluvial systems. These activities typically create an influx of sediment with physical, geochemical, and mineralogical characteristics different than that of natural sediment (Lecce and Pavlowsky, 1997; Leopold, 1980). Altering the geochemistry of stream sediment can cause toxicological effects to the stream ecosystem and can pose a serious pollution problem (Schipper et al., 2008; Dennis et al. 2009; Macklin et al., 2006). Mining contaminated sediment, like the sediment that pollutes the Big River, is formed though the separation processes that mining operations use to extract heavy metals from mined rock. The milling process begins with crushing and grinding the rock to allow for the separation of the economically viable fractions of rock from the waste rock, called tailings (Bussiere, 2007).

In the Old Lead Belt, three defined types of tailings were produced and are identified by differences in particle size. The first and coarsest is described locally as "chat," which ranges from 4-16 mm in diameter and is formed through dry gravity milling. The next is fine-tailings which have been further crushed for separation using flotation processes and range anywhere from 0.06-0.20 mm in diameter. Finally, fine rock powders sometimes referred to as "slimes" are created during the physical crushing of the rock and are less than 32 μm in diameter (Pavlowsky et al., 2010a). All size fractions of tailings tend to contain residual heavy metal concentrations, thus becoming a pollutant if they are not properly managed. Weathering of tailings can release dissolved

metals into the environment which can then bond with very fine clay minerals and organic rich sediment. Consequently, the finest fraction of tailings particles tends to have the highest concentrations of heavy metals (Smith and Schumacher, 1993; Smith et al., 1998). Contaminated sediment in the Big River in areas below mining sources tend to contain high concentrations of lead and other metals across a range of particle sizes related to the three types of tailings inputs (Pavlowsky et al., 2010a).

Geographic Factors in Contaminant Distribution

Once contaminated sediment enters a stream, contamination concentrations in a watershed are generally related to distance from the point source and physiographic controls (Lecce and Pavlowsky, 2001; Leece and Pavlowsky, 2014; Axtmann and Luoma, 1991). With mining contamination, it is important to examine the downstream distribution of contaminants to better understand spatial trends seen on specific floodplains study sites.

Longitudinal Trends in Concentration and Sorting. Longitudinal trends in contamination concentrations depend on sediment inputs as well as downstream sorting. Natural sediment inputs from eroding hillslopes, runoff, and uncontaminated tributaries, causes a dilution effect in contamination concentrations within streams. This paired with will channel and floodplain contaminated sediment storage, will effectively reduce concentrations of contaminants downstream from the point source (Lecce and Pavlowsky, 2001; Axtmann and Luoma, 1991). Grain size also plays significant role in the longitudinal extent of contaminants within a river. Rivers naturally fine with increased distance downstream due to its ability to transport different sized sediment.

Fine-grained sediment will be able to remain entrained in rivers for greater distances than coarse-grained sediment. This means that finer fractions of contaminated sediment will have more downstream mobility than coarser fractions, so fine-grained floodplain contaminant storage would likely be more dominant downstream (Figure 2) (Axtmann and Luoma, 1991; Lecce and Pavlowsky, 2001; Leopold and Maddock, 1953).

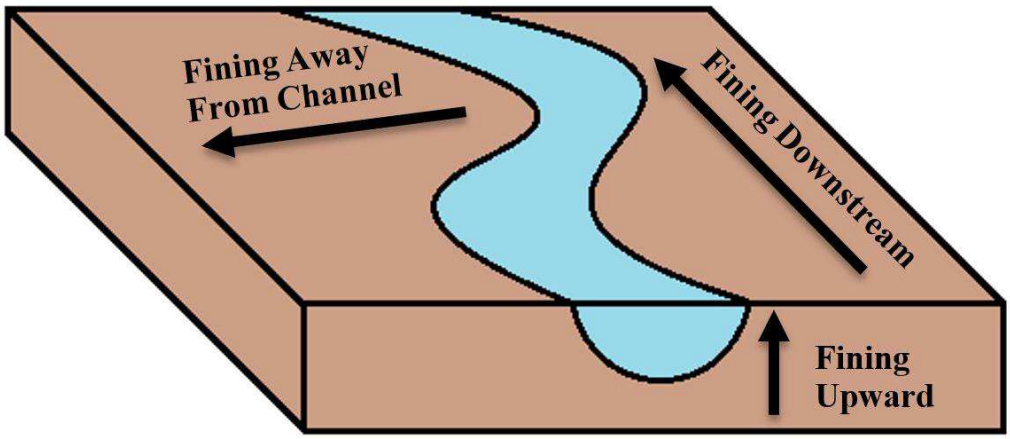

Figure 2 – General longitudinal, stratigraphic, and across-floodplain sorting trends in floodplain sediment.

Valley Width. Physiographic characteristics such as valley width will also play a significant role in floodplain sedimentation rates. Valley width and the associated hydrologic characteristics can affect erosional and depositional trends longitudinally downstream. Typically, narrow valley segments of a stream favor transportation and erosion of sediment, whereas wide valley segments favor more deposition (Leece and Pavlowsky, 2014; Howard, 1996). For example, Magilligan, 1985 created a theoretical model examining a narrowing/widening sequence of valley width along a river and the resulting sedimentation trends (Figure 3). The study labeled wide valley areas above the constriction "Zone 1," narrow valley areas in the constriction "Zone 2," and wide valley

areas below the constriction “Zone 3.” Magilligan, 1985 found that in Zone 1, flood waters dam up behind the narrowing valley and increase overbank flow and deposition. In Zone 2, a narrow confining valley increases flow depth and velocity causing erosion and transportation of sediment. In Zone 3, as the valley widens, flow velocity decreases and sediment deposits as flood waters are able to spread out across the valley. Generally, wide floodplains like Zones 1 and 3 favor deposition, whereas narrow floodplains like Zone 2 favor transport and erosion. Due to the large surface area in wide valley floodplains, overbank accumulations may be thinner as they are spread across the floodplain, but will have a greater volume of sediment (Faulkner, 1998).

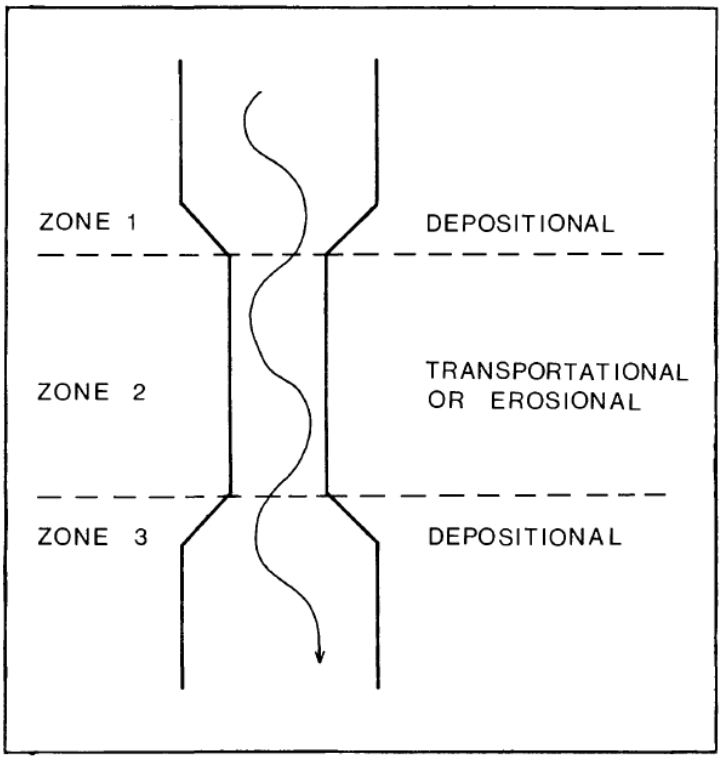

Figure 3 – Valley width effects on sediment deposition and transport (from Magilligan, 1985).

In the context of contaminated sediment, this means that narrow valley segments of the stream will promote downstream transport of contaminants, whereas wide valley segments will act as significant sinks (Leece and Pavlowsky, 2001). Wider valleys also tend to have increased development of floodplain chutes and drainage features which can result in a wider spatial variation in deposition rates and resulting contamination (Howard, 1996; Leece and Pavlowsky, 2014).

Floodplain Sedimentology and Landforms in Contaminated Environments

Floodplains are defined differently in terms of hydrology and geomorphology. The hydrologic floodplain is defined as: "the surface next to a channel that is inundated once during a given return period regardless of whether this surface is alluvial or not". In geomorphology, a floodplain is defined in a sediment transport and deposition context as: "the largely horizontally-bedded alluvial landform adjacent to a channel, separated from the channel by banks, and built of sediment transported by the present flow-regime" (Nanson and Croke, 1992). This study is focused on sedimentation, thus the geomorphic definition is used. Knowledge of floodplain development and sediment deposition is critical in understanding the variables that control mining-contaminated sediment deposition and distribution across floodplains. Sedimentation rates and associated contaminant concentrations can be related to geomorphic processes that develop floodplain morphology and control sediment distribution (Miller, 1996; Macklin et al., 2006; Graf, 1996). Having a detailed understanding of natural floodplain development can aid in understanding and predicting contamination deposition in mining districts.

Floodplain Deposition. The function of a floodplain is to store sediment and dissipate flood water energy by allowing banks to overflow and flood waters to spread out across it (Leopold, 1994; Wolman and Leopold, 1957). The formation of floodplains is driven by two main accretionary processes. First is the lateral accretion of point bars and channel deposits across the valley as the channel migrates (Figure 4). This occurs as the progressive bank cutting along the outside of meander bends is in equilibrium with the deposition of sediment in the lower-velocity flows found on the opposite bank. This simultaneous erosional and depositional progression causes the channel to move laterally across the valley and accrete channel sediment to build the floodplain (Wolman and Leopold, 1957; Leopold, 1994). There is also deposition of sediment that occurs during flooding events. When overbank floods occur, sediment is carried by the flow across the floodplain and caps channel deposits as flood waters dissipate and sediment settles (Figure 4) (Hupp et al., 2015; Wolman and Leopold, 1957).

Laterally accreted channel deposits are made up of coarse-grained sands and gravels including lag, bed, and bar deposits. Lag deposits are the coarsest fraction, and are a result of the reworking of channel sediment to separate out fine material. Channel bed gravels are then deposited atop the basal lag, followed by the finer-gravel and sands of point bars. This forms a fining-upward sorting pattern within these deposits (Figure 2 and Figure 4) (Nanson and Croke, 1992; Huggett, 2007).

Overbank deposits can range from sand-sized sediment to clay. Sand fractions have a more limited mobility than finer clay and silt fractions causing them to accumulate close to channel margin creating a natural levee on the bank. Levees can be breached during large flows which can result in the deposition of a thin layer of sand called a splay

to be deposited greater distances from the channel. Silt and clay fractions have a greater ability to remain entrained in overbank flows and consequently can be deposited farther from the channel. This causes a fining of sediment with increasing distance from the channel (Figure 2 and Figure 4) (Martin, 2009; Leopold, 1994; Nanson and Croke, 1992; Huggett, 2007; Hupp et al., 2015).

Due to the limits of sediment mobility within overbank flows, sediment deposition rates across the floodplain tend to be related to proximity to the channel. As flood waters dissipate, flows have a declining capacity to transport sediment which results in a much lower deposition rate with increasing distance from the channel. This means that in general, higher deposition rates are associated with levee deposits, and lower deposition rates are associated with distal floodplain deposits (Piegay et al., 2008).

In the context of mining sediment deposition on floodplains, the fining trend of floodplain sediment in relation to proximity to the channel dictates the spatial distribution of different size fractions of mining waste. For example, chat will be limited to channel and bar deposits where gravel deposition occurs. Therefore, chat will not be a significant contaminant in floodplains. Sand-sized tailings associated with floatation, will be an important contaminant in levee and splay deposits where sand deposition dominates naturally. Silt and clay-sized slimes will have the most mobility, and thus can be a significant floodplain contamination source at distance from the channel. It is expected to see increased accretion of contaminated sediment closer to the channel since it is the direct source of contamination on a site scale (Chen et al., 2012; Middelkoop, 2000; Pavlowsky et al., 2010a).

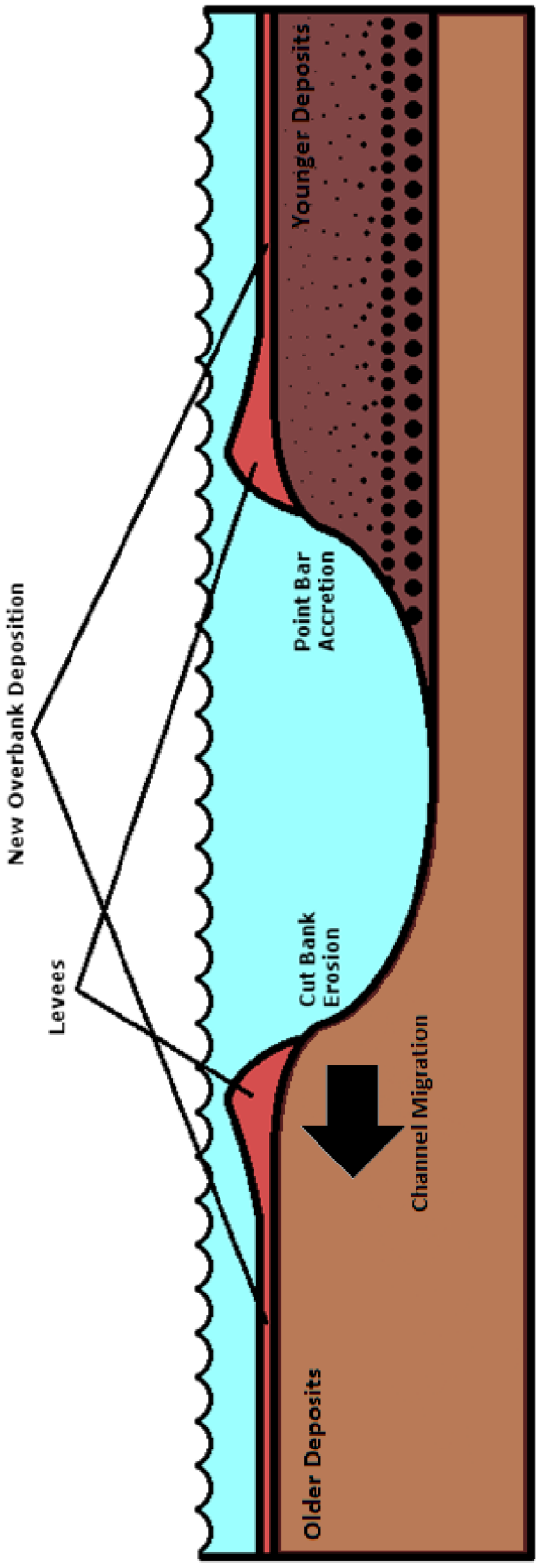

Figure 4 – Floodplain accretion and erosion.

Floodplain Landform Deposition Patterns. Floodplain landforms differ in elevation and will have a different flood frequency, and consequently different levels of contamination. Landforms at a lower elevation will have a higher flood frequency than landforms at a higher elevation (Leece and Pavlowsky, 2001). With an increase in flood frequency, there is an increase in the available sediment entrained in overbank flows, thus lower elevation floodplain landforms will have the ability to accrete more contaminated sediment in mining environments (Chen et al., 2012; Howard, 1996; Ciszewski and Malik, 2004; Owen et al, 2011).

For example, if the stream is incising due to a drop in base level or a change in erosional capability, floodplains can be abandoned, the stream will widen, and a new active floodplain called a bench will begin to form (Huggett, 2007). A bench is typically defined as an alluvial feature with similar characteristics as the adjacent floodplain, but has a lower elevation (Owen et al., 2011). The bench will have a higher flood frequency than the floodplain, and will thus have a greater amount of sediment deposition during flooding events allowing for increased surface soil contamination compared to higher floodplains (Figure 5 and Table 1) (Howard, 1996; Lecce and Pavlowsky, 2001). Upland areas such as valley walls are at a higher elevation and are not flooded. Consequently, these areas are not alluvial landforms, and would not allow the deposition of contaminated sediment. (Figure 5 and Table 1) (Lecce and Pavlowsky, 2001).

Sediment deposition is not solely based on elevation; it is also important to look at hydrologic variables. If a floodplain has poor drainage during flooding events, water can pool in depressions within the floodplain allowing for suspended sediment to settle out. Low elevation wetlands like this are called backswamps and can act as important areas

for fine-grained floodplain deposition. Gravel and sand mining is common in floodplains and will create poorly drained artificial depressions that can also act as sediment sinks for fine-grained sediment (Hupp et al., 2015; Box and Mossa, 1999; Howard, 1996). Conversely, if a floodplain is well-drained, drainage features or chutes can begin to down-cut behind levees and across the floodplain channelizing the drainage of floodwaters and runoff. Channelized flows such as this will have a higher velocity than the poorly drained backswamps, and will likely deposit less fine grained sediment and scour existing deposits. However, chutes can facilitate sediment transport across floodplains which can increase sedimentation at greater distance from the channel (Howard, 1996). As runoff erosion occurs on valley uplands and moves downslope to the floodplain, drainages features receive a mixture of alluvial and colluvial sediment which can dilute alluvial sediment signatures (Lecce and Pavlowsky, 2001). In mining contaminated systems, there would consequently be high concentrations of heavy metals in poorly drained depressions, and lower contamination concentrations in chutes and drainage features. These hydrological and topographical differences can create significant spatial variation in contaminant concentrations across a floodplain (Figure 5 and Table 1) (Schipper et al., 2008).

Table 1 – General floodplain landform characteristics.

Landform	Relative Elevation	Flood Frequency	Depositional Capability	Erosional Capability	Sediment Size	Sediment Source
Bank	Low/Moderate	Moderate/High	Moderate/High	High	Silt to Sand	Alluvial
Bench	Low/Moderate	Moderate	Moderate/High	Moderate	Clay to Sand	Alluvial
Floodplain	Moderate	Low/Moderate	Moderate	Low	Clay to Silt	Allvuvial
Drainage/Chute	Low/Moderate	Moderate	Low	High	Silt to Sand	Alluvial/Colluvial
Backswamp	Low/Moderate	Moderate	Moderate/High	Low	Clay to Silt	Alluvial
Upland	V. High	Never	Low	Low to High	Clay to Boulders	Colluvial

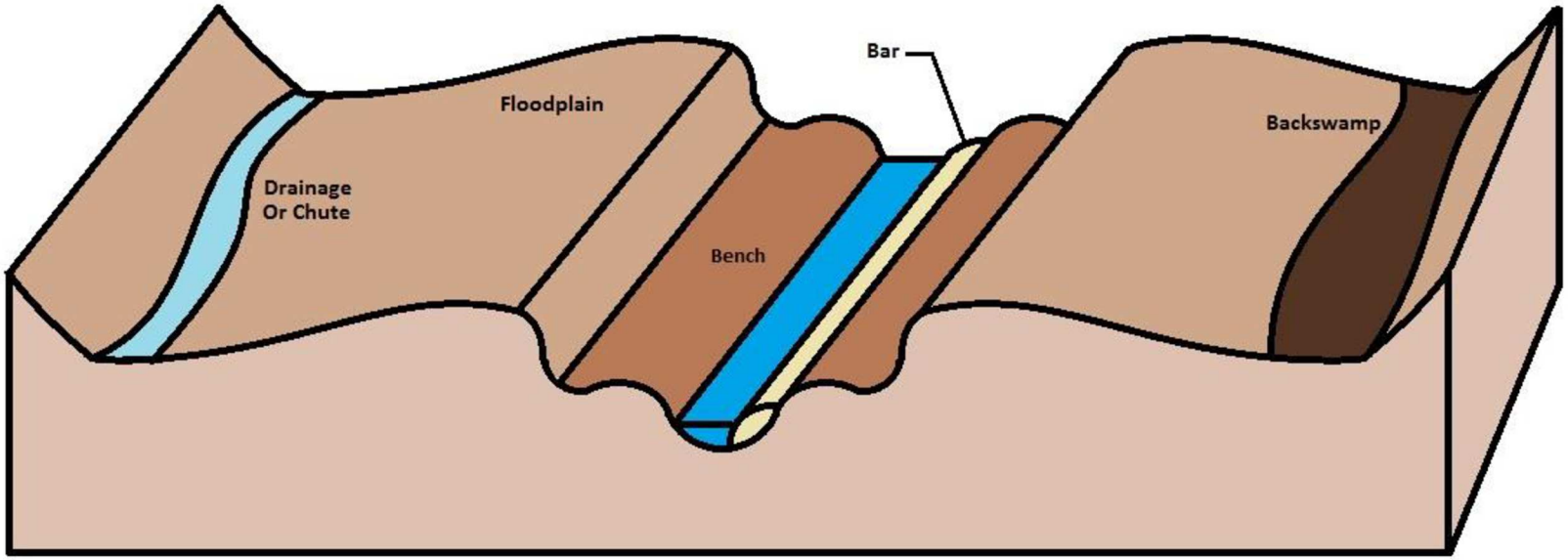

Figure 5 – Common floodplain landforms.

Geochemical Contamination Patterns

Floodplain soil and mine tailing geochemistry can play a significant role in spatial distribution of contaminants in mining-affected areas as well. Depending on the host rock targeted in mining activities, tailings can have a distinct signature that can act as a geochemical proxy for mining sediment deposition (Pavlowsky et. al., 2010a). For example, dolomite mined during the Old Lead Belt mining activity, was introduced into the Big River after being crushed into tailings during the milling process (Smith and Schumacher, 1993). Dolomite ($CaMg(CO_3)_2$) is rich in calcium (Ca), so it was found that there is a significantly higher concentrations of Ca in soils that contain mining sediment than would be expected in natural sediment (Smith and Schumacher, 1993; Pavlowsky et. al., 2010a). Therefore Ca can be used as a proxy for tailing deposition and may be indicative of coarse grained floatation sands especially. Consequently, Ca concentrations could be used as a predictive variable in heavy metal contamination.

Floodplain soil geochemistry can also aid in dictating contamination patterns. For example, high iron (Fe) content in floodplain soils can be related to the weathering of mine tailings which releases Fe/Mn-oxides into the fluvial system. It can then be stored in floodplain soils allowing Fe to be a proxy for tailings deposition in the same way Ca was described (Smith and Schumacher, 1993). There is also natural Fe clays from the weathering of residuum in Ozark uplands (USDA, 1981). Dissolved heavy metals from mining activity can precipitate on natural clay mineral surfaces and can be a source of highly-contaminated fine grained sediment (Schröder et al., 2008; Laing et al., 2009; Smith and Schumacher, 1993). In fact, other studies have shown due to the preferential precipitation of heavy metals, Fe/Mn-oxides can be beneficial in soil remediation

(McCann et al., 2015). This means that floodplain soils rich Fe, may likely be correlated with high concentrations of heavy metals in mining districts.

Mapping of Floodplain Contamination

There is a need to develop a mapping procedure and resulting maps of Pb contamination patterns for Big River floodplains. In order to effectively examine spatial variations in contamination trends and predict areas with high or low risk across floodplains, it is important to develop spatial relationships and models that reflect depositional processes, landform influence, and geochemistry. Contamination patterns are best mapped through a combination of sample collection, remote sensing, and landform mapping. Sample collection of contaminated soils allows for the quantification of contaminant concentrations in floodplain soils (Leece and Pavlowsky, 2014). Technologies such as LiDAR and historical aerial photographs allow for a continuous view of topography and land cover both spatially and temporally (Jones et al., 2007; Gilvear et al., 1995; Hohenthal et al., 2011; Notebaert et al, 2009). These remote sensing data types combined with geomorphic assessment and topographic surveys allows for detailed landform mapping which can be used to interpret sediment depositional trends and the resulting contamination (Jones et al., 2007).

Contamination mapping methodologies can variety depending on the goals of the study. For example, in a floodplain ecology study on the Dutch River by Kooistra et al., 2001, researchers developed a methodology for pollution mapping that focused on landform classification. By developing different homogeneous landform units using the sedimentological history and hydrologic context of the site, this study summarized

contamination by landform and highlighted which contained the greatest ecological risk. On the other hand, if spatial continuity is desired for trends across a land surface, interpolation techniques can be utilized. In a mining contamination study of Geul River floodplains in Belgium, Leenaers et al., 1989 utilized co-kriging and other interpolation methods to develop continuous surface maps of Zn concentrations. They found that interpolation methods such as this are efficient and cost effective methods for viewing trends in top soil contamination. Utilizing a combination of both methods to map Big River floodplain contamination may allow for a more detailed look at spatial trends across a study area to focus remediation efforts.

Modeling Contamination Trends

With a wide range of both geomorphic and geochemical variables controlling contamination concentrations in fluvial studies, regression can be a beneficial tool in developing predictive models for sediment deposition. Developing regression equations can aid in identifying variables that drive deposition and contamination (Lecce and Pavlowsky, 2004; Pavlowsky et al., 2010b; Pavlowsky, 2013; Magilligan, 1985). For example, in Pavlowsky et al., 2010b, Hg and Cu contamination related to mining activities was accurately modeled using geomorphic and sedimentological variables such as distance downstream and grain size. This model then offers a way in which managerial bodies related to the watershed protection could effectively monitor contamination trends within this river. Regression models such as this one could be an integral tool in predicting and monitoring contamination within Big River floodplains.

Purpose and Objectives

The purpose of this study is to analyze the patterns of mining-related Pb contamination on floodplains along the Big River to better assess contamination risk on the scale needed for remediation planning and land management. To accomplish this, examining the spatial variation in Pb concentrations in surface soil on floodplains, and the factors that drive the variation will be necessary. The relationships between Pb concentrations, landforms, valley width, longitudnal trends in contamination, elevation, distance to the channel, and geochemistry, are also necessary in understanding spatial variation. Finally, it will be necessary to take into account the toxic potential of the contamination within Big River floodplains in order to understand the human and ecological risk. This will be accomplished through the following objectives:

1) Quantify Pb, Zn, Fe, and Ca concentrations in surface soils on floodplains along the Big River for three sites, one with a narrow valley, one with a wide valley, and one with human-modified topography. This will allow for the examination of contamination patterns across floodplains with varying physiographic and hydrologic characteristics as well as assess the effects of human-interaction on floodplain surfaces. Geochemical analysis will be accomplished through sediment sampling of floodplain top soils.

2) Utilize existing LiDAR data sets for the Big River to develop geomorphic maps for use in contamination mapping. Understanding contamination in a morphological context will provide insight into the role different landforms have in contamination patterns, and allow for the identification of highly contaminated landform types. A heads-up classification of floodplain landforms based on changes in elevation and geomorphic interpretation will be used in development of these maps.

3) Examine and visualize spatial trends in contaminated sediment distribution through interpolation mapping, which allow for a continuous view of contamination concentrations across a floodplain. This will be accomplished through inverse-distance weighted interpolation techniques.

4) Identify important reach-scale variables that control Pb concentration patterns. By understanding important variables in spatial distribution, multiple regression

models can be developed that can be used to predict Pb contamination trends at other floodplain sites.

Hypotheses

In developing this study and examining the background literature within this field, there are four guiding relationships that are expected to surface:

1) Lead concentrations will be inversely related to both elevation above the active bankfull floodplain and to increasing distance from the channel due to sedimentation controls and flood regime.

2) Calcium and iron concentrations will be positively related to lead concentrations due to geochemical signatures of dolomite ore and the precipitation of Pb on the surface of Fe/Mn-oxide clays.

3) Micro-topographic depressions and local lowlands will contain higher concentrations of Pb due to selective accumulation of finer, more contaminated sediment.

4) Wider valleys with more variable floodplain planform and chute channel topography will yield a more complex pattern of contamination, have a greater variability in Pb concentration, and contain higher concentrations of metals, including Pb due to the higher rates of fine-grained deposition.

Benefits

This thesis will provide valuable insights into the geomorphic processes that dictate the spatial variability of mining-derived contaminated sediment on the Big River. There is a gap in knowledge in examining floodplain contamination at a level necessary for remediation planning. It is also beneficial to assess commonly used techniques in the field, laboratory, and computationally in order to utilize the most effective methodology to yield the most useful results and models in remediation planning. By understanding the controls on contamination variability, this study will aid in planning projects and the models used can act as predictive tools to be used in similar floodplain studies. By aiding

in the remediation and implementation of appropriate best management practices in floodplain environments, ecosystems, wildlife, and people interacting with these areas can be protected from the toxicity of mining contaminants.

CHAPTER 2 - STUDY AREA

Physiography and Geology

The Big River watershed covers roughly 2,500 km^2 on the Ozark Plateau in south eastern Missouri (Figure 6). The headwaters begin in the St. Francois mountains at 530 meters above sea level from where the river flows 225 km north, until it flows into the Meremec River near Eureka, MO (Meneau, 1997; Adamski et al., 1995). The Meremec River then continues approximately 60 km until it meets up with the Mississippi River near St. Louis (Meneau, 1997). The watershed is within the Salem Plateau physiographic region with its headwaters in St. Francois Mountains. The St. Francois Mountains were formed from the upwelling of Precambrian igneous bodies, which created a structural dome. Dominate rock types in the mountains include granite, diabase and rhyolites. Headwater streams in this area have a steep gradient as they flow down from the mountains and create a valley form called a shut-in as they downcut into the ignous bedrock. This creates steep valleys and cascading waterfalls throughout this region. Downstream, the majority of the watershed flows is through Cambrian and Ordovician dolomites with local shale, limestone and sandstone units which dip away from the St. Francois Mountains (Figure 7 and Table 2) (Bretz, 1962; Adamski et al., 1995). Streams within the Salem Plateau downcut through the sedimentary bedrock creating deep valleys with moderately steep gradients. Stream morphology is dominated by riffle-pool sequences with gravely bed material (Heeren et al., 2012; Adamski et al., 1995).

The regional ore deposits throughout southeast Missouri are a type of ore deposit called Mississippi Valley-type, and develop as a result of hydrothermal fluids associated

with orogenic belts (Bradley and Leach, 2003). The Bonne Terre formation is a key formation in mining activity in the area. This formation is 375-400 foot thick Cambrian rock composed predominately of dolomite ($CaMg(CO_3)_2$). Hydrothermal mineralization crystalized significant amounts of galena, or lead sulfide (PbS), as well as zinc, copper and silver (Gregg and Shelton, 1989) . Another important formation in local mining is a dolomite called the Potosi formation, which lies above the Bonne Terre stratigraphically. This formation is also Cambrian, predominately dolomite, and is approximately 200 feet thick (Figure 7 and Table 2) (Smith and Schumacher, 1993).

Climate and Hydrology

The Ozark Plateau lies within a moist continental climate. Average temperatures range from 32°F in the winter to 77°F in the summer. Annual average rainfall for the region is about 100 cm (USDA, 1981). In the spring, the area receives the highest amount of rain as warm, moist airmasses move morth from the Gulf of Mexico. This period of increased storms and rainfall usually occurs from March to June (Adamski et al., 1995).

Southeastern Missouri has a prominent karst topography with abundant sinkholes and caves. This makes for a dynamic hydrology with springs, sinkholes and significant groundwater flow. Streams generally follow a radial pattern, emminating out from the ingneous highlands. In the lowlands, much of the topography is due to the downcutting of streams through the sedimentary substrate (Adamski et al., 1995). Beginning upstream, three USGS discharge gaging stations along the Big River measure median flows of 4.7 m^3/s (Irondale, MO: 07017200), 20 m^3/s (Richwoods, MO: 07018100), and 23.8 m^3/s (Byrnesville, MO: 07018500).

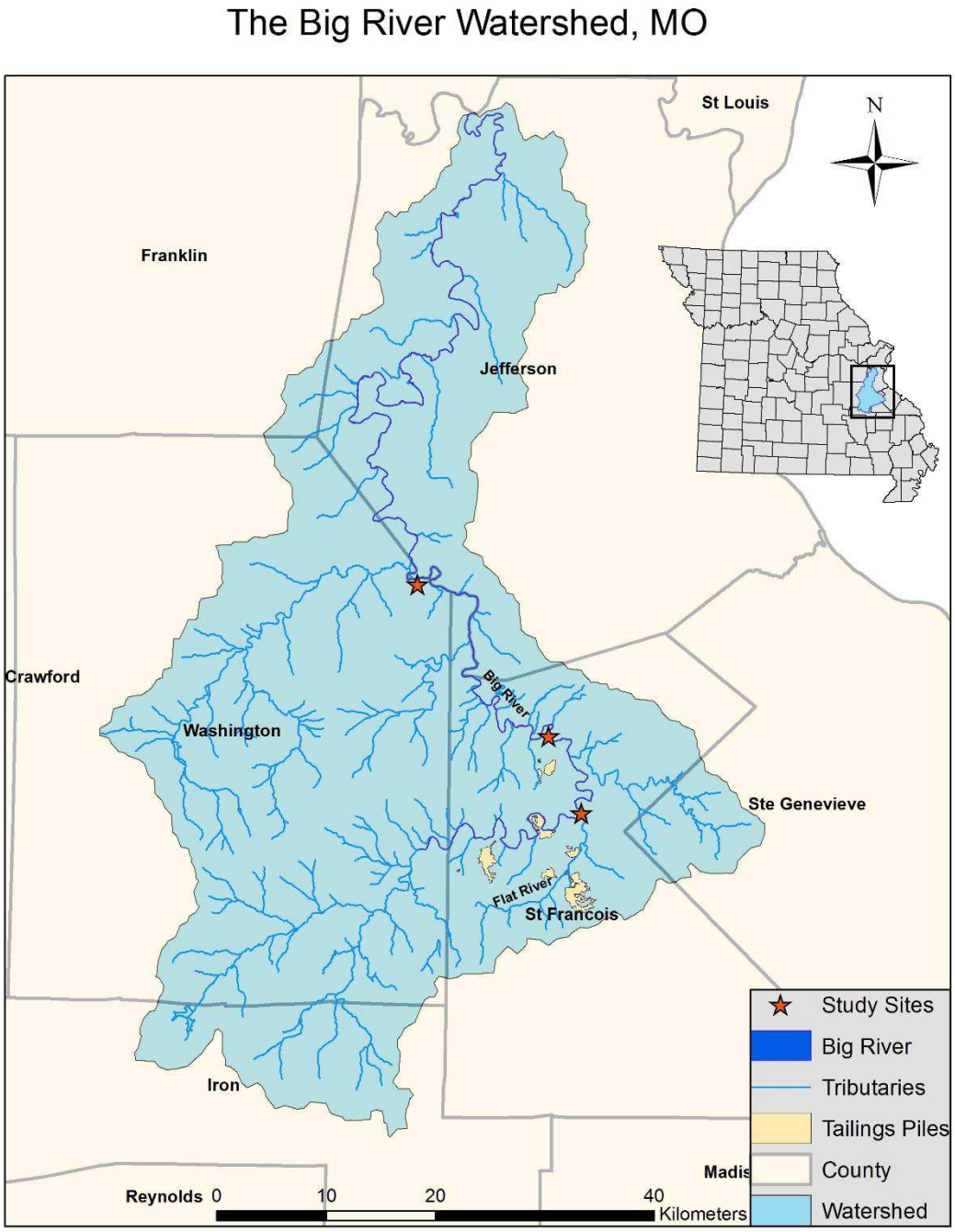

Figure 6 – Big River Watershed and tailings piles.

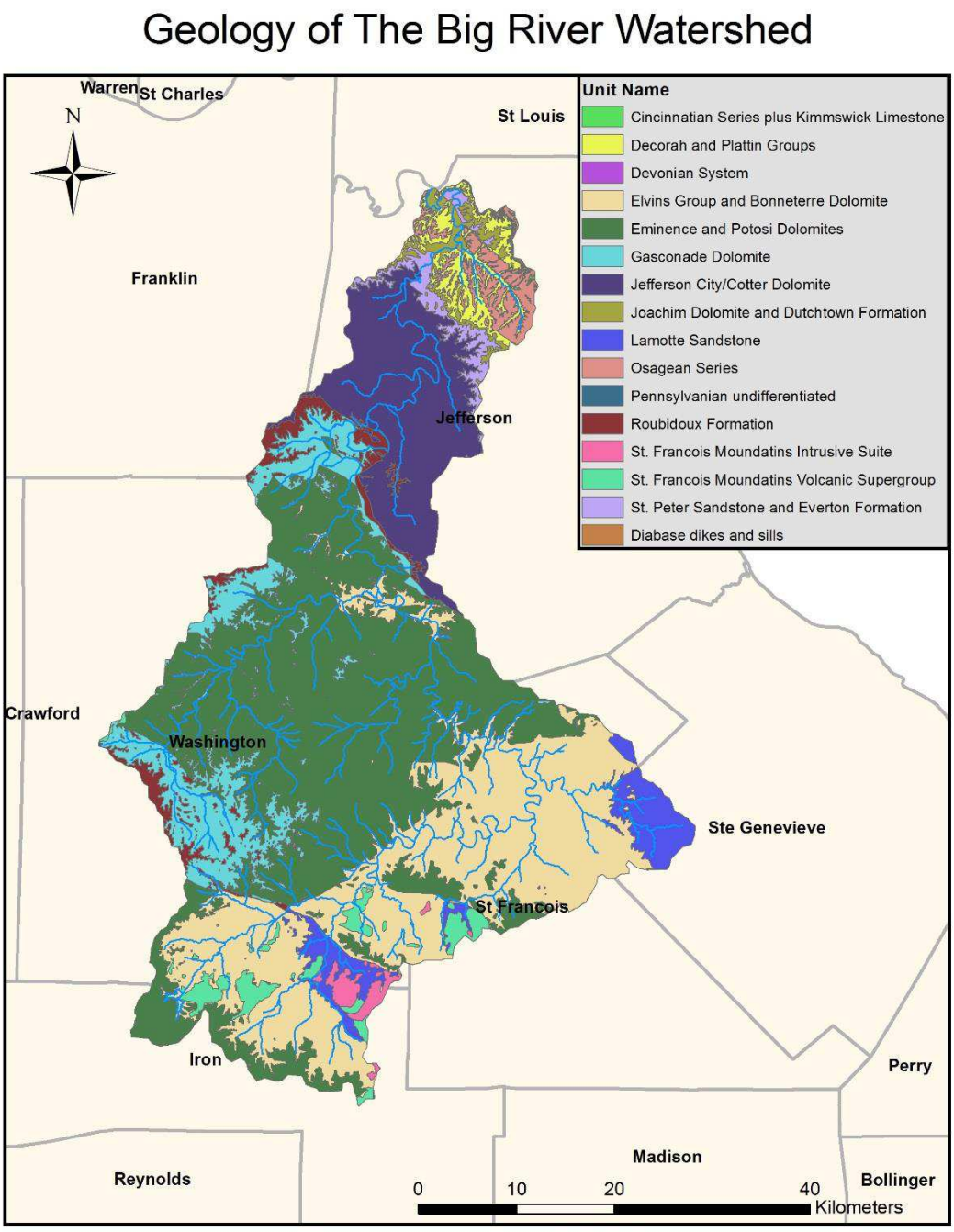

Figure 7 – Geology of the Big River Watershed.

Table 2 - Geological units in the Big River Watershed.

Unit Name	Geologic Age	Primary Rock Type	Secondary Rock Type
Pennsylvanian Undifferentiated	Pennsylvanian	Shale	Limestone, Sandstone, Coal
Osagean Series	Mississippian	Limestone	Chert, Dolomite, Shale
Devonian System	Devonian	Limestone	Sandstone, Shale, Chert
Cincinnatian Series/Kimmswick Limestone	Ordovician	Limestone	Shale, Sandstone
Decorah and Plattin Groups	Ordovician	Limestone	Shale
Gasconade Dolomite	Ordovician	Dolomite	Sandstone
Jefferson City/Cotter Dolomite	Ordovician	Dolomite	Sandstone, Shale, Chert, Conglomerate
Joachim Dolomite and Dutchtown Formation	Ordovician	Dolomite	Limestone, Shale, Sandstone, Siltstone
Roubidoux Formation	Ordovician	Sandstone	Chert, Dolomite
St. Peter Sandstone and Everton Formation	Ordovician	Dolomite	Sandstone, Limestone
Elvins Group and Bonneterre Dolomite *	Cambrian	Dolomite	Shale, Siltstone, Sandstone, Limestone, Conglomerate
Eminence and Potosi Dolomites *	Cambrian	Dolomite	Chert
Lamotte Sandstone	Cambrian	Sandstone	
Diabase Dikes and Sills	PreCambrian	Diorite	Gabbro
St. Francois Mountains Intrusive Suite	PreCambrian	Granite	
St. Francois Mountains Volcanic Supergroup	PreCambrian	Rhyolite	Trachyte

* Indicates mineralized units important to Old Lead Belt mining

Regional Soils

The Ozark Plateau predominately is comprised of alfisols and utisols (Adamski et al., 1995). In the Salem Plateau physiographic region, these soils are overtop the dolomite bedrock which weathers to produce significant residuum (Jacobson and Primm, 1994). In St. Francois county, the Big River down cuts into two main soil groups called the Caneyville-Crider-Gasconade Association, and the Crider-Fourche-Nicholson Association. The first group of soils is characterized by well drained loess and clayey soils that vary significantly in slope and depth. Slope tends to range between 2 to 35 percent and represents terraces and upland areas within the Big River watershed. The second group is composed of deep, moderate to well-drained loess and clayey soils. The slopes range from 2 to 14 percent and also represent high terraces and uplands. As the Big River incises, alluvial soils are then deposited as floodplains build. Common floodplain soils include the Haymond, and Horsecreek series (USDA, 1981). In Jefferson County, the Big River incises into the Sonsac-Useful-Moko Association. This represents a rocky, loess and residuum group that makes up the ridgetops and backslopes of the valleys. Slopes can range between 3 and 55 percent. In the valley, common floodplain units include the Haymond, Horsecreek and Kaintuck series (USDA, 2000).

Land Use

Before the settlement of the Ozark Plateau, praries and oak savannahs dominated. Deciduous and pine forests occupied valleys before settlers clear-cut for pasture and agriculture use. Deforestation and woodland grazing practices caused a large increase in valley slope erosion (Jacobson and Primm 1994; MDNR, 2007). Present day land use

classifcation is as follows: 68% forested, 23% grasslands, 4% urban, 3% barren and open water, 2% row crops (MDNR, 2007).

Mining History

Lead deposits were first discovered in this area around 1700 to the west of St. Francois County. Small mining operations began to operate in about 1720 to the south of St. Francois County. Significant early mining in The Old Lead Belt began with shallow open-pit mines that opened in 1742 as mining activity moved north more into St. Francois County and Washington County (Smith and Schumacher, 1993). These small scale operations mined large galena crystals from shallow pits until more organized mining began in the mid 1800's. The first large-scale mines to open were in the area surrounding Bonne Terre, MO around 1904. It is estimated that as many as 15 mines were operational during the late 1800s to the early 1900s. Mining in the Old Lead Belt peaked in 1942 and continued until 1972, when the majority of mining operations moved to the Vibernum Trend for more economic deposits (Pavlowsky et al., 2010a; Smith and Schumacher, 1993).

Early operations accumulated large chat piles as waste gathered from gravity milling through the 1930s. Beginning in 1917, froth and floatation milling techniques were implemented which resulted in the increased production of fine-grained tailings. These tailings were stored in impoundments as a slurry. Fine-grained impounded slurries and course chat piles together make up about 227 million Mg of tailings produced from mining within the Old Lead Belt (USFWS, 2008). The Missouri Department of Natural Resources estimates that tailings piles cover as much as 12 km^2 in the Old Lead Belt.

Remediation efforts have stabilized these tailings piles to limit the leaching and erosion of contaminated sediment, however, a large amount of contamination from before remediation efforts remains in the river systems, stored in both channel and floodplain deposits (Pavlowsky et al., 2010a; Smith and Schumacher, 1993).

Study Site Characteristics

Three study sites along the Big River were chosen to examine contamination trends. Sites were chosen based on variations in valley width, degree of human interaction, distance from tailings piles, and floodplain area to assess contamination patterns in relation to these factors. Summarized characteristics of each site can be found in Table 3. Characteristics of USDA mapped soil series at each site can be found in Table 4.

Big River/Flat River Confluence. The first field site chosen for this study is at the confluence of the Big River and the Flat River (BR/FR) (Figure 8 and Table 3). This site is the furthest upstream site along the Big River, about 155 river kilometers above the Meramec River confluence and about 16 river kilometers downstream from the tailings piles in Bonne Terre. This site represents a relatively wider valley with a width of about 370 meters on the meander bend. The river is confined by bedrock bluffs on the east side of the stream with a large floodplain to the west. Significant human influence has altered the natural planform of the floodplain at this site. There is evidence of soil mining excavation as well as the dumping of a fill dirt to build a road across the property. The road runs parallel to the Big River channel and sits at a higher elevation than the floodplain on either side of it.

The primary floodplain soil series at this site is the Haymond silt loam (Figure 9 and Table 4). It is a frequently flooded soil and is anywhere from 30 to 60 inches deep with a slope ranging from 0-2%. The Haymond is predomiately formed from alluvium washed downhill from nearby loess deposits and till plains (USDA, 2011). Higher terraces at this site are made up of a silt loam called the Horsecreek silt loam. This series is only occasionally flooded during larger floods. The Horsecreek is a deep soil reaching more than 80 inches thick and has a slope anywhere from 0-5%. It is a mixture of primarily loess alluvium with some residuum from local sedimentary units (USDA, 2002). Upland soils include the Crider silt loam, the Caneyville silt loam, and the Gasconade-Rock outcrop complex (USDA, 2002). Pavlowsky et al. 2010a found that floodplain soils contained Pb levels as high as 4,000 ppm within core samples.

The Environmental Protection Agency, in conjunction with the U.S. Army Corp of Engineers is working on a remediation project at this site funded through the Comprehensive Environmental Response Compensation Liability Act (CERCLA). Construction on a riffle and basin sediment catchment project was completed in late 2015.

Table 3 - Study site characteristics. Measurements and landcover were estimated from aerial photographs and LiDAR data.

	BR/FR	SFSP	WSP
River-km	155	140.5	102
Drainage Area (km^2) [1]	821	1,008	1,363
Valley Width (m)	370	80	430
Valley Slope	0.00088	0.00050	0.00050
Active Channel Width (m)	40	35	45
Sampling area (m^2)	160,238	30,901	121,319
% Grass	48%	35%	67%
% Road	3%	19%	5%
% Forest	49%	46%	28%

[1] Pavlowsky et al., 2010a

Table 4 - Soil series present at BR/FR, SFSP, and WSP (USDA, 1981 and USDA, 2000).

Series Name	Study Site Where Present	Landform	Slope	Flood Frequency	Drainage
Caneyville Silt Loam	SFSP, BR/FR	Upland	3-20%	Never	Well
Crider Silt Loam	SFSP, BR/FR	Upland	1-8%	Never	Well
Gasconade Rock Outcrop Complex	BR/FR	Upland	3-35%	Never	V. Well
Haymond Silt Loam	WSP, SFSP, BR/FR	Floodplain	0-3%	Frequently	Well
Horsecreek Silt Loam	SFSP, BR/FR	Terrace	0-2%	Occasionally	Well
Ogborn Silt Loam	SFSP	Upland	1-5%	Never	Somewhat Poor
Goss Very Cobbly Silt Loam	SFSP	Upland	15-50%	Never	Well
Fourche Silt Loam	SFSP	Upland	2-15%	Never	Moderately Well
Kaintuck Fine Sandy Loam	WSP	Floodplain	0-3%	Frequently	Well
Moko Rock Outcrop Complex	WSP	Upland	3-50%	Never	Well
Sonsac Gravelly Silt Loam	WSP	Upland	3-40%	Never	Well

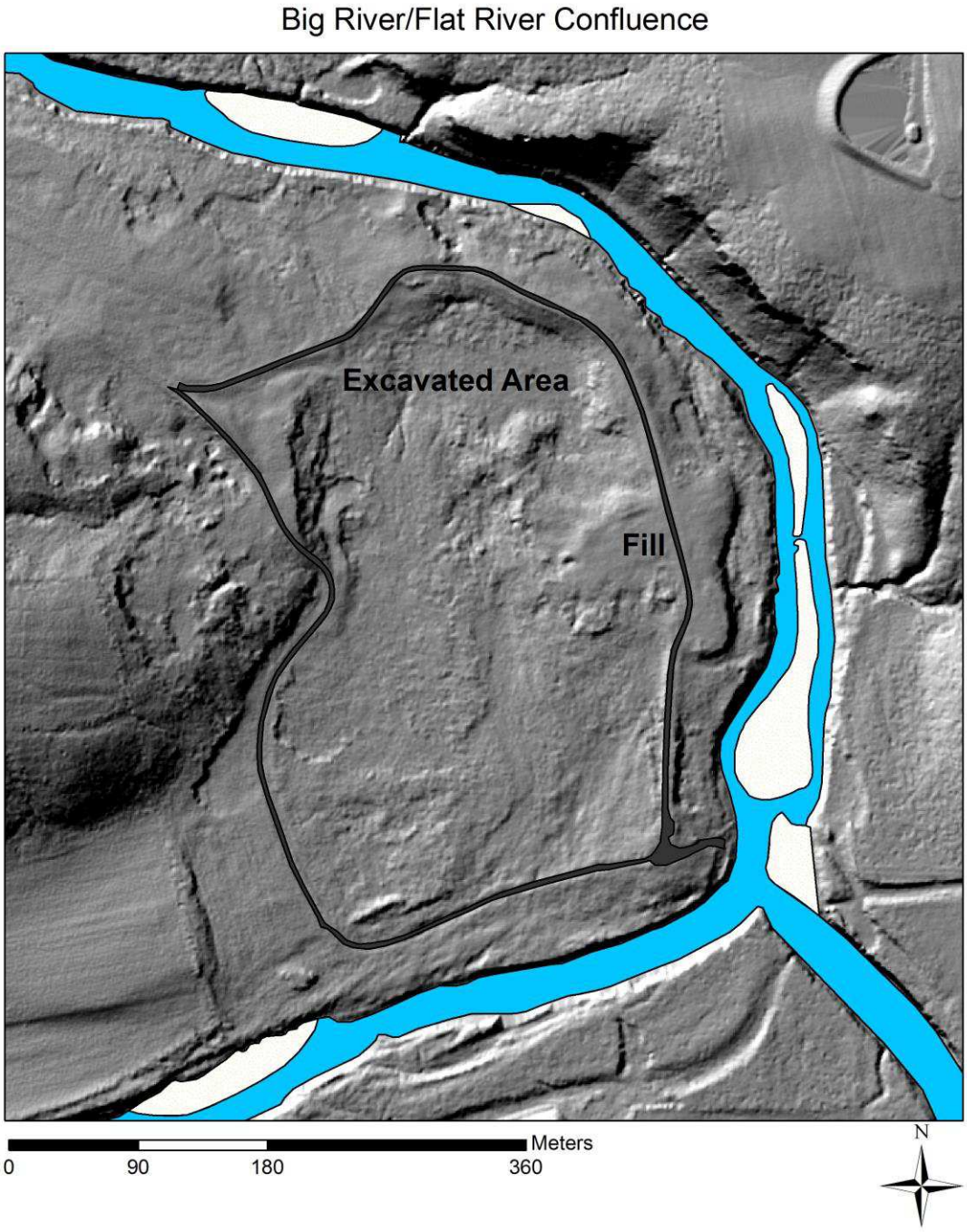

Figure 8 – The Big River/Flat River Confluence, Missouri.

Figure 9 – Soil series at the Big River/Flat River Confluence.

St. Francois State Park. St. Francois State Park (SFSP) is about 140.5 river kilometers above the Meramec River confluence with the Big River, and about 30.5 river kilometers below the Leadwood tailings pile (Figure 10 and Table 3). The valley is about 80 meters wide at the study site and the channel is confined by a narrow valley with bluffs to the west and a rapid rise in landscape to the east. This results in a relatively smaller floodplain with less variability in planform. St. Francois State Park represents more natural floodplain with minor human influence on topography. A road, parking lots, and park buildings with small footprints are built on the upper floodplain.

The floodplain soil series at this site are the same as at the Big River/Flat River Confluence (Figure 11 and Table 4). Lower bench units are the Haymond silt loam, and upper floodplains and terraces are the Horsecreek silt loam. Upland soils include the Ogborn silt loam, the Goss very cobbly silt loam, the Fourche silt loam, the Crider silt loam, and the Caneyville silt loam. None of the upland units are flooded (USDA, 2002; USDA, 2011;USDA, 2012). Pavlowsky et al., 2010a reported that floodplain soils contained Pb levels as high as 5,500 ppm within core samples.

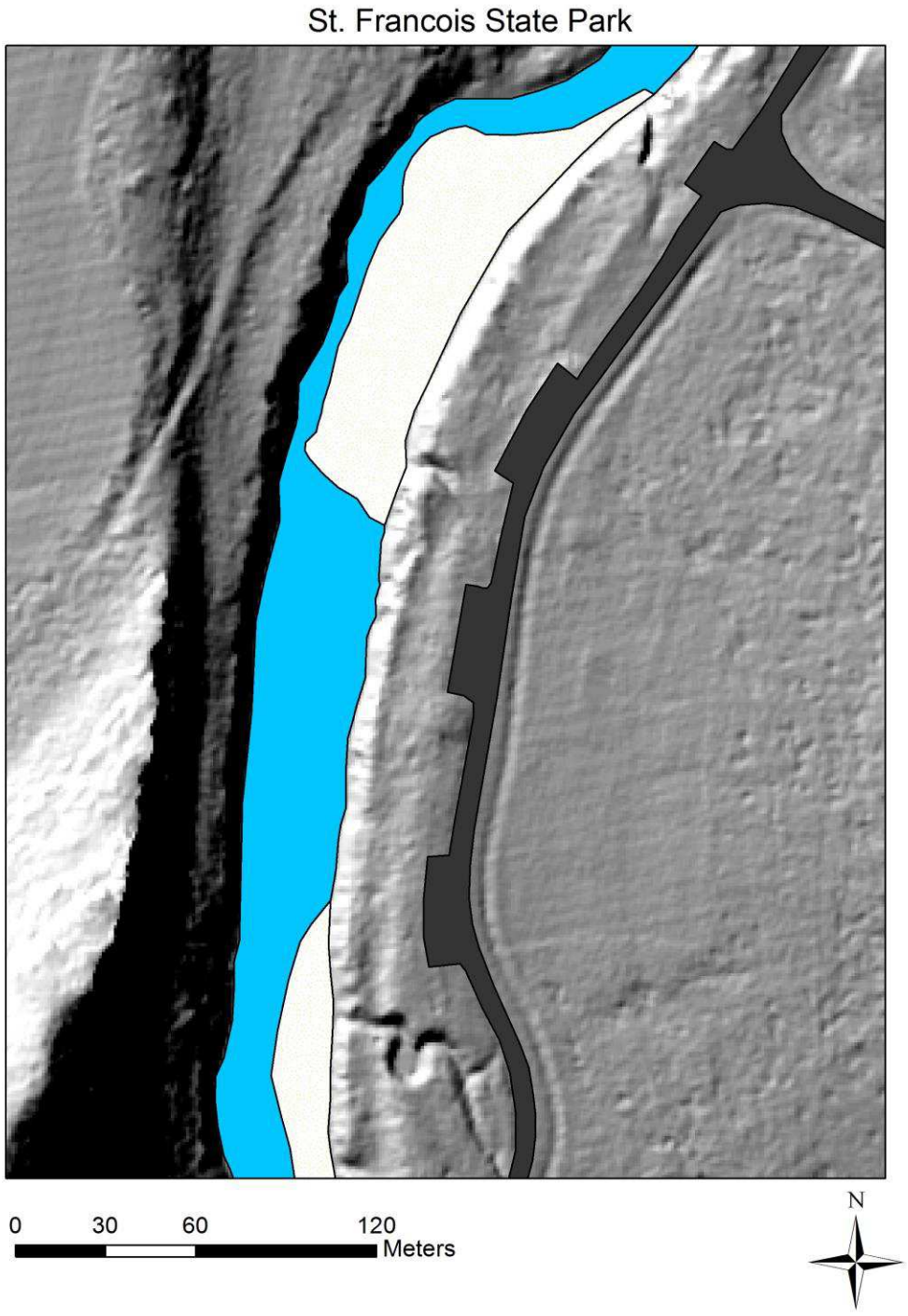

Figure 10 – St. Francois State Park, Missouri.

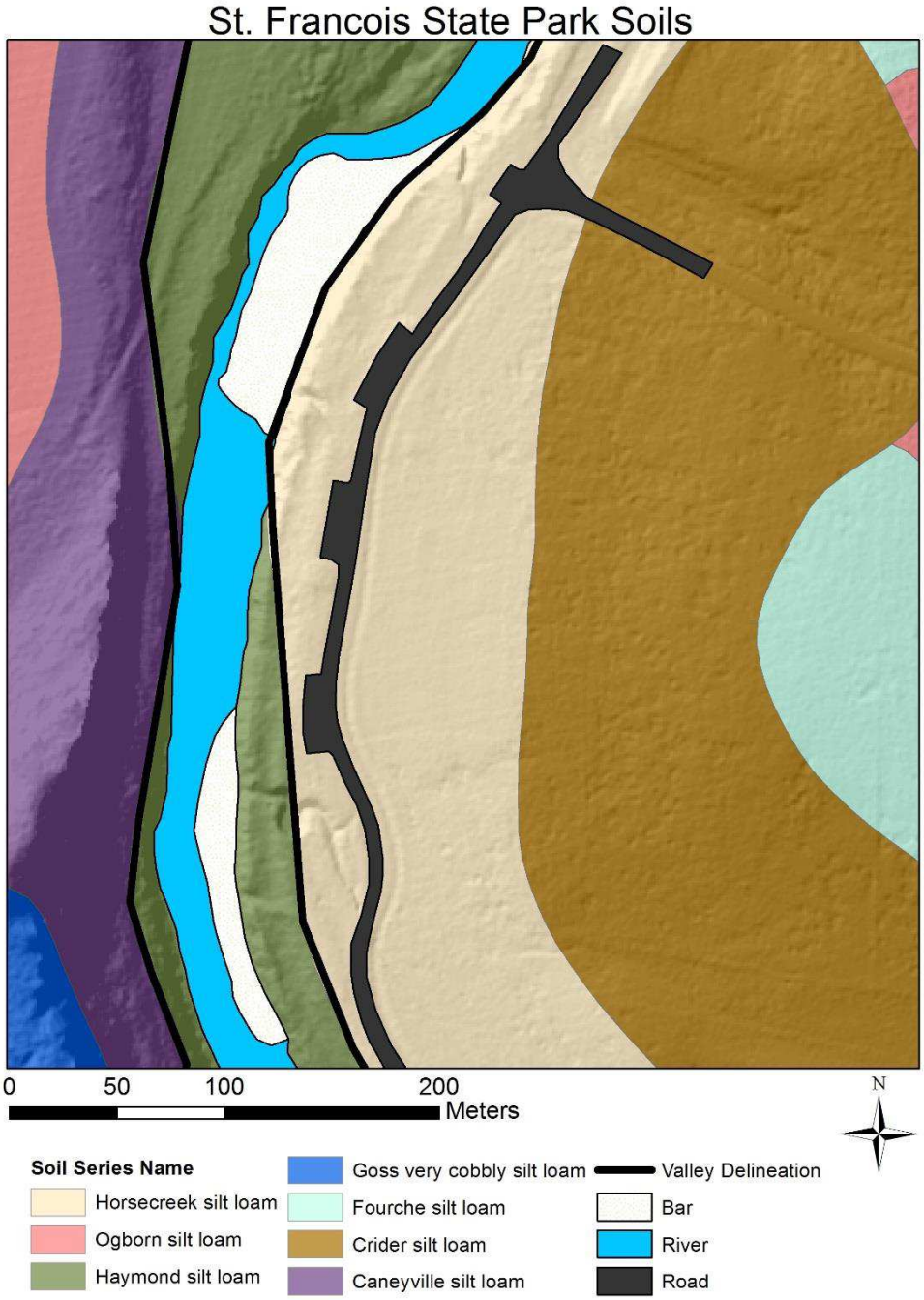

Figure 11 –Soil series at St. Francois State Park.

Washington State Park. Washington State Park (WSP) is the furthest site downstream at about 102 river kilometers above the Meramec River confluence with the Big River (Figure 12 and Table 3). This site has a wide valley of about 430 meters. A large floodplain extends south away from the channel until it meets the toe of a steep valley bluff. Washington State Park represents a more natural floodplain as well with minor human influence on topography. A road, parking lot, and small outhouse are the only structures built on the floodplain.

The floodplain contains two main soil series at this site (Figure 13 and Table 4). The first is the Kaintuck fine sandy loam. It is a frequently flooded soil and is reaches more than 60 inches thick with a slope ranging from 0-3%. It is a coarse-loamy alluvium that is well drained. The second frequently flooded soil series is the Haymond silt loam. Upland soils that make up the valley bluff include the Moko-Rock outcrop complex and the Sonsac gravelly silt loam (USDA, 2006; USDA, 2001; USDA, 2000).

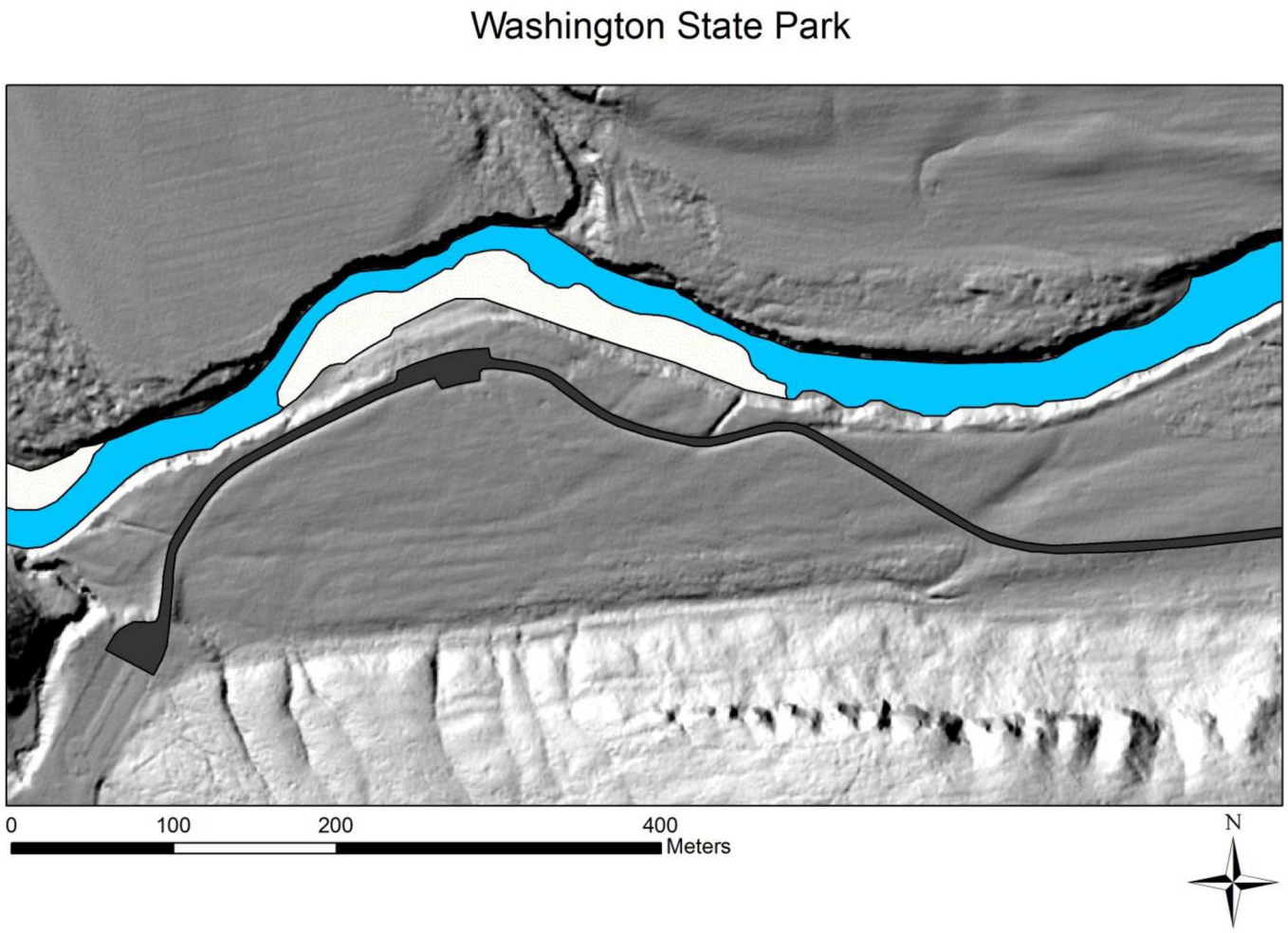

Figure 12 – Washington State Park, Missouri.

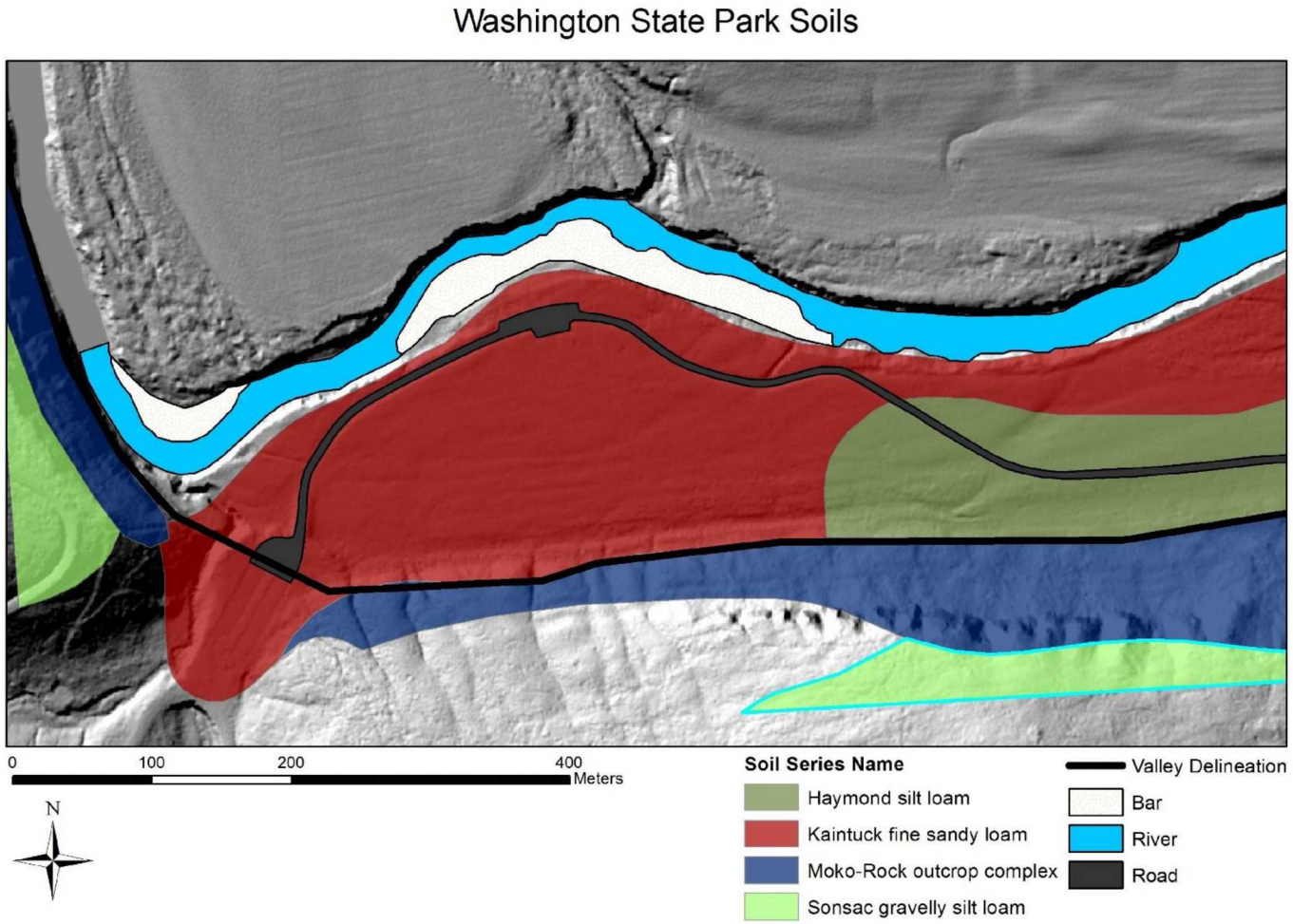

Figure 13 –Soil series at Washington State Park.

CHAPTER 3 - METHODS

Contamination mapping and the analysis of spatial variability in geochemical studies are most effectively done with a combination of field, laboratory, and Geographic Information Systems (GIS) methods. Sample collection and laboratory methods allow for geochemical analysis (Leece and Pavlowsky, 2001), while GIS analysis allows for spatial relationships to be examined and mapped efficiently (Kooistra et al., 2001). This study utilizes existing LiDAR-derived digital elevation models (DEM) and aerial photographs to classify planform, field sediment sampling and GPS data collection, GIS to compile data and develop maps, and statistical analysis to examine trends and develop predictive models.

Field Sampling

Soil sampling for spatial variability studies needs to be a balance between cost-effectiveness and coverage (Andronikov et al., 1999). Many contamination spatial analysis studies develop a regular grid to sample locations at equal intervals across the study area (Liu and Yang, 2007; Andronikov et al., 1999; Fleming et al., 2000). While this is effective in achieving uniform coverage of the study site, it does not account for landform variations. This study examines contamination with respect to landform, so it is important to ensure sufficient sample numbers are collected within each distinct topographic difference. With this in mind, sample collection was conducted along adjacent transects to develop a rough grid across each study site for sufficient coverage. Spacing between samples was estimated using pacing to try and keep the distance

between samples relatively consistent. While walking a transect, whenever a change in elevation that could represent a rise to a different landform surface was noted (i.e. the rise from a bench to a floodplain surface), careful consideration was taken to collect multiple samples within each landform. This ensured that there was sufficient spatial coverage with the rough grid, while gathering enough samples within each landform to effectively characterize the geochemistry. Grid spacing varied based on the size of the study site.

Collecting top soil was done using a hand trowel to carefully dig under vegetation or litter cover, and collect roughly a fist-sized amount of soil from the top 10 centimeters (Andronikov et al. 1999; Xiao et al., 2011). Samples were then bagged and labeled with a name, date, and transect number. Careful consideration to clean excess soil off of the trowel was ensured to avoid inter-sample contamination. At each sample site, a GPS point was collected using a handheld Trimble unit and labeled with the sample name. The Big River/Flat River Confluence had a total of 174 top soil samples, St. Francois State Park had a total of 140 samples, and Washington State Park had a total of 154 samples. Samples at the Big River/Flat River confluence were collected on November 20, 2014, and samples at St. Francois State Park and Washington State Park were collected on July 7, 2015. The Missouri Department of Natural Resources permit for sampling can be found in Appendix A.

Laboratory

Samples were processed at Missouri State University in the geomorphology laboratory. They were first placed in an oven to dry at 60 degrees Celsius. Next, they were sieved using a 2 mm sediment sieve and placed into a small lead-free plastic bag for

use on the X-ray fluorescence (XRF) instrument according to Environmental Protection Agency XRF analysis protocol (EPA, 2007). A handheld XRF was used in a benchtop stand to collect elemental concentrations for Pb, Zn, Ca, and Fe. The XRF was set to collect data for 90 seconds per sample and create an output with elemental content in parts per million (ppm). Twenty samples were run at a time, including one duplicate sample. Geochemistry for all samples can be found in Appendix B.

Accuracy is a measurement of the "closeness of agreement between a test result and the true value" (ISO, 2011). Assessment of accuracy is important to ensure laboratory instruments are yielding reliable results that reflect true values. Calculations for accuracy in XRF analysis are done by analyzing a known standard, and assessing the difference between the true value and the instrument reading. For this study, a USGS standard (Jasperoid, GXR-1) was analyzed with a known Pb concentration of 856 ppm. Then, by comparing the value read by the XRF to the known standard, accuracy could be quantified (EPA, 2007). For the samples from the confluence site (n = 174), the accuracy for Pb was -3.45%, for Zn was -7.63%, for Fe was -1.34%, and for Ca was -1.80%. For the samples from Washington State Park and St. Francois State Park (n = 294), the accuracy for Pb was -1.34%, for Zn was -8.37%, for Fe was -3.19%, and for Ca was -4.02%.

Precision is also an important measurement for laboratory instruments because it assesses the consistency of the results allowing for the identification of systematic error. Precision is defined as "the closeness of agreement between independent test/measurement results obtained under stipulated conditions" (ISO, 2011). Precision was calculated for this XRF analysis by running duplicate samples to compare the results

of the same sample (EPA, 2007). At the Big River/Flat River confluence site (n = 174), the precision values were -0.88% for Pb, -2.78% for Zn, -0.46% for Ca, and 0.93% for Fe. At St. Francois State Park and Washington State Park (n = 294), the precision values were 0.89% for Pb, -1.70% for Zn, 0.50% for Ca, and 0.85% for Fe.

Fifteen subsamples selected from the three sites were then sent to ALS Chemex Laboratories, Sparks, Nevada for aqua-regia digestion and ICP analysis (Appendix C). Aqua-regia extracts metals from sediment samples using a mixture of hot nitric and hydrochloric acids. It is not a total digestion of the sample, but the metals that are extracted represent the environmentally mobile fraction (EPA, 2007) Regression equations that compare XRF to ICP results indicate a strong linear relationship between the two analytical methods. In order to maintain absolute variability of the XRF analysis among all samples in the data set, ICP: XRF ratios were used to correct the XRF results to equivalent aqua-regia concentrations (EPA, 2007). The ratios were as follows: Pb = 0.82, Zn = 0.88, Ca = 1.00, Fe = 0.77 (Appendix C).

Geospatial and Computational

Base Maps and Cross Sections. In order to create maps needed for the study site, aerial photographs and LiDAR data were needed. Georeferenced aerial photographs from 2010, collected as part of the National Agriculture Imagery Program (NAIP), were obtained from the Ozarks Environmental and Water Institute (OEWRI) database at Missouri State University. LiDAR data with 1 meter resolution, collected between December 10, 2010 and April 6, 2011, was downloaded from the Missouri Spatial Data Information Service (MSDIS) at the University of Missouri. LAS point data was

classified by MSDIS and a digital elevation model (DEM) was available for download. In Arcmap 10.2.2, hillshade basemap layers were created using the tools within the Spatial Analyst toolbox, and were used for topographic visualization. Geochemical data was then matched with the corresponding GPS points and mapped on the hillshade basemap in ArcMap. By extracting DEM data, elevation values were attributed to each GPS point as well. The distance from each point to the channel was also calculated using a distance algorithm tool in ArcMap called Near. This measured the shortest distance to the channel for each point and added the value to the attribute table.

Cross sections were also created by extracting elevation data from the DEM using the Extract Values to Points tool within the Spatial Analyst toolbox. Cross-sectional data was then be plotted in Excel to view elevation changes across the study site. Each cross section was drawn in close proximity to a sample transect so geochemical concentration data could be plotted across a representative cross section at each site to examine topographical/geochemical relationships.

Landform Classification and Mapping. Landform mapping was then conducted using a methodology similar to Jones et al. (2007) in which landforms were defined by breaks in slope visualized using LiDAR data, in a similar manner as field geomorphic mapping. Utilizing geomorphic background knowledge about floodplain morphology as outlined in Chapter 1, along with field observations and LiDAR elevation maps, heads-up digitization of distinct landforms was performed. A total of eight landform classes were developed over the three sites based on characteristic fluvial landforms outlined in Chapter 1. Sand bars within the channel were identified by elevated surfaces within the bankfull channel. The bank was classified as the rise from the channel including the

natural levees. Floodplains were broken up into two classes when distinct surfaces could be identified. Lower surfaces were classified as benches, and higher surfaces were classified as a floodplain. Low areas within the floodplain were classified as either disturbed area/backswamps or drainages features/chutes. The drainage feature/chute classification was used when clear channelization could be seen in the topography. These areas either show evidence of runoff drainage or connectivity to the main channel. The disturbed low areas at the Big River/Flat River confluence site were classified as a backswamp due to fine grained sediment deposition and lack of channel form which would promote the pooling of flood waters unlike chutes and drainages. An additional, unnatural classification was created for the excavation fill dirt present at the Big River/Flat River confluence. Finally, the rise in the river valley was classified as the upland.

Landform Flood Frequency. Once landforms were classified, recurrence intervals of the floods that inundate bench and floodplain landform surfaces were calculated in order to better understand the frequency of the overbank events that promote deposition. This was accomplished through the measurement of cross sectional geometry of the channel and floodplain landforms and the quantification of flows with USGS gage data.

Peak surface flows from the last 30 years were collected from the three USGS gaging stations on the Big River. The data was then analyzed in PEAKFQ, a program created by the USGS. This program used gaging records to calculate the probability and discharge of different magnitude floods. Probability from PEAKFQ was then converted to recurrence intervals (RI) of 1.05, 1.25, 1.5, 2, and 5 years for each gage station (RI =

1/probability of flood). Regression equations were then developed for each of the five recurrence intervals to relate the drainage area of each station to the discharge associated with each RI. Then, using the drainage area of each of the three study sites, the expected discharge of the 1.05, 1.25, 1.5, 2, and 5 year floods could be calculated.

Next, cross sections from all three study sites from surveys conducted by OEWRI were used to measure channel geometry for different flow heights that correspond to the inundation of benches and floodplains. With the channel geometry, flow velocity was calculated using the Manning equation. This equation is:

$$V = (1.5/n)\, R^{2/3}\, S^{1/2}$$

Where V is velocity, n is a roughness coefficient, R is the hydraulic radius defined by cross sectional area divided by the wetted perimeter, and S is the slope of the stream. Discharge can then be calculated by multiplying the velocity by the cross sectional area (Ward and Elliot, 1995). Using a program called Hydraflow Express, cross sectional area, wetted perimeter, and width were measured for different flow heights that correspond to the inundation of floodplains and benches. The measured area and perimeter were then used to calculate R. Then, using LiDAR data, stream slope was calculated by dividing rise over run for the change in elevation across a 1 km section of the stream at each study site. Finally, n was estimated based on the surface roughness of different river stages. Ward and Elliot, 1995 lists recommended n values for different surface and channel types. Calculated velocity for each flow of interest was then multiplied by the area to yield a discharge (Ward and Elliot, 1995).

Discharges calculated using the Manning equation for benches and the floodplains were then correlated with the discharges for the five different recurrence intervals

calculated from USGS gage data. This allowed for the flooding events that represent the inundation of the benches and floodplains to be attributed with a recurrence interval. An additional flood recurrence interval was calculated at the Big River/Flat River confluence site to estimate how often floods overtop the road.

Interpolations. Using inverse distance weighted interpolations (IDW), rasters showing continuous surfaces for Pb, Zn, Fe, and Ca were created. Inverse distance weighted interpolations are a simple technique that can be calculated without knowledge about the spatial structure of the data, and with any sample size (Kravchenko, 2003). The IDW calculation interpolates unknown areas using sample values weighted by distance from the unknown point in question (Gotway et al., 1995). Interpolation techniques work under the assumption that points in closer proximity to one another are more related than points farther from each other. Inverse distance weighting estimates an unknown point in space by using this assumption to assign a weight to neighboring known points. Known points closer to the unknown point will have a higher weight, and consequently have a greater effect on the interpolated unknown value. The number of closest known points used in the prediction will affect the smoothness of the resulting interpolation. A larger neighborhood will yield a smoother result than a smaller neighborhood. An exponent value determined based on the variation within a data set is used to adjust the effect of each known point. The resulting equation for IDW calculations is:

$$z_j = \frac{\sum_i \frac{z_i}{d_{ij}^n}}{\sum_i \frac{1}{d_{ij}^n}}$$

Where z_j is an unknown point to be estimated, z_i is a known control point, d_{ij} is the distance to the known point, and n is an exponent affecting the weighting. Using the

number of control points defined, unknown points across a surface are calculated and a continuous raster is created (Franke, 1982; O'Sullivan and Unwin, 2010).

The goal of creating interpolated contamination maps is to visualize the spatial trends and draw qualitative conclusions based on patterns. In an accuracy study by Kravchenko, 2003, it was found that despite the simplicity, the difference in accuracy between IDW and other methods such as Kriging is minimal. Gotway et al., 1995 found that when conducting IDW interpolations, if the data set has a coefficient of variation less than 25%, a higher order power produces better accuracy. If the coefficient of variation is greater than 25%, accuracy is increased with a lower power. For each element at each site, the coefficient of variation value was calculated and the appropriate power was used in the IDW tool within the Spatial Analyst toolbox in ArcMap 10.2.2. The search radius was set to use the twelve closest points to interpolate unknown areas across the study sites with a smooth surface. Since this study is focused on floodplain contamination, bar samples were not used in interpolation calculations

The study site at the Big River/Flat River confluence is split by a road that runs parallel to the river. Based on the elevation of the road above the surrounding areas, continuity of sediment deposition between the bench to the east and the floodplain to the west could not be assumed. To address this, interpolations will be conducted on both sides of the road independently.

Statistical

Descriptive statistics for geochemical data at each site were calculated for each site as well as by landform. This includes measures of central tendency (mean and

median), measures of variability (standard deviation, inter-quartile range and coefficient of variation), and range. This study focuses on floodplain variability, so besides general descriptive statistics, bar samples were excluded from other statistical analyses.

Pearson correlation matrices were then created to look at relationships between geochemical variables and physical variables for each sample point. Correlation was assessed for all samples at a site, as well as for a subsample including only samples in the floodplain landform classes. This was done to see if correlations varied if landform was kept constant. Next, simple linear regression models between Pb and geochemical and physical variables were developed and residual plots were created. Residuals are defined as the difference between the expected value from the model, and the observed value from sampling. Residual plots were then used to identify any samples with anomalously high residuals and consider the possibility of outliers. Finally, a multiple linear regression analysis was conducted. Regression analysis allows for the quantification of relationships between Pb and geochemical and physical variables, and the development of a predictive model in spatial trends (Rogerson, 2010; Pavlowsky et al., 2010b).

A stepwise selection of the independent variables was utilized to develop regression equations. This method adds independent variables that are most highly correlated with the dependent variable to the equation in an attempt to explain the variability, so long as they have a significant positive effect on the R^2 value. As new variables are added to the equation, previous variables are reassessed for significance and removed if they are not beneficial in the equation. With each variable added and removed, the analysis conducts an F-test. If the p-value of a variable is less than 0.05, it is added to the equation. If the p-value of any variable in the equation is more than 0.10, it

is removed. This analysis goes through iterations of this process until it identifies the most important variables in determining the variability (Rogerson, 2010). Then, to avoid multicollinearity between similar variables, an assessment of the variance inflation factor (VIF) was needed. If the VIF value is above five for any independent variable, there is significant overlap with another independent variable, and the variable cannot be used in the equation (Rogerson, 2010). Through step-wise analysis and assessment of multicollinearity, regression models with the highest R^2 values were determined to describe spatial variability in Pb. Independent variables used were elevation, distance from the channel, Ca concentration, and Fe concentration. Variables were converted to a logarithmic scale to be used in regression analysis as well. A combination of logarithmic and arithmetic variables were combined to form the best models. Hypothesis testing for each variable in the model was conducted to ensure statistical significance using a t-test. Possible outliers identified in the residual plots were removed to see if any improvement of model fit could be seen (Rogerson, 2010). All analysis was conducted in IBM SPSS Statistics 23.

CHAPTER 4 – RESULTS AND DISCUSSION

The purpose of this chapter is to present and discuss the results of landform classification, flood frequency calculations, geochemical analysis, and interpolation mapping. Results are discussed for each study site individually. Tables for landform classification area (Table 5), flood frequency (Table 6), and geochemistry (Appendix D) include information about all sites for comparison. This chapter will also evaluate large-scale geographic controls such as valley width and distance from the source, and determine the effects of these controls on contamination patterns. It will then examine relationships between the spatial distribution on a site-scale of Pb, and geochemical and spatial variables such as elevation, distance from the channel, and Ca and Fe concentrations. Next, simple linear regression models comparing Pb to these variables to will be developed to further investigate relationships, and identify outliers to be removed for multiple linear regression models. Using both geochemical and spatial variables, multiple linear regression models for Pb distribution are developed and assessed. Finally, management implications in regards to findings are discussed.

Big River/ Flat River Confluence

Landform Classification. The relatively wide valley and the human-altered landscape create unique geomorphic and hydrologic characteristics at this site. There are five distinct floodplain landform classes created at this site (Figure 14 and Table 5). The study site is divided into two areas: the disturbed area where excavation and soil mining history have created a topographic low, and the undisturbed are near channel that has

been less affected by human-influence. The road is the boundary between the disturbed and undisturbed areas separating them due to its high relative elevation to the surrounding area. In the undisturbed area, the rise from the channel including the levee represents the bank class. Adjacent to this is a lower depositional floodplain surface that was called a bench. There is an upper floodplain unit higher than the bench located in both the disturbed and undisturbed areas. The excavated disturbed area is a local lowland cut into the upper floodplain unit that is connected by a small channelized area to the Big River at the southern end of the study area. Within this channelized area, there is abundant sand splay deposition across the road. This channelized area feeds into a basin with significant mud deposition towards the north end of the disturbed area. Due to the ability for the sediment to pool in the basin, the whole disturbed area was classified as a backswamp. Near the road, there is an area of fill dirt and gravel that was dumped during excavation activity.

Flood Inundation Frequency. At the Big River/Flat River confluence site, the bench was found to have a recurrence interval of less than a year indicating frequent inundation (Table 6). The floodplain inundation was calculated for the disturbed area near the chute connecting to the disturbed area at the southern end. The disturbed area recurrence interval was between 1.05 and 1.25 years. This suggests that the disturbed area does inundate frequently, but not as regularly as the bench. Both of these landforms would be expected to have significant alluvial deposition potential with the high frequency of overbank events. For the road dividing the undisturbed and disturbed areas, the recurrence interval was 1.5-2 years indicating that larger floods are needed for the mixing of flood waters and sediment between the two areas.

Table 5 – Area of mapped landforms at BR/FR, SFSP, and WSP.

Landforms	BR/FR		SFSP		WSP	
Bank	7,406	4%	3,963	5%	11,614	9%
Bench	9,844	5%	8,578	12%	NA	NA
Floodplain	96,084	53%	50,919	69%	78,781	63%
Backswamp	53,035	29%	NA	NA	NA	NA
Drainage/Chute	NA	NA	4,588	6%	29,487	23%
Road	4,879	3%	5,948	8%	6,231	5%
Fill	11,248	6%	NA	NA	NA	NA
Total	182,496	100%	73,996	100%	126,113	100%

Table 6 – Flood frequency for benches and floodplains at BR/FR, SFSP, and WSP.

Landform	Site	Recurrence Interval (yr)	Approx. Landform Elevation (m)	Stage from Bed (m)	Discharge (m^2/s)
Bench	BR/FR	< 1 year	201	2.21	86
	SFSP	1.25 - 1.5	194	5.64	309
	WSP	NA	NA	NA	NA
Floodplain	BR/FR	1.05 - 1.25	202	2.87	134
	SFSP	1.5 - 2	196	7.16	365
	WSP	1.05 - 1.25	172	5.79	212
Road	BR/FR	1.5 - 2	205	6.13	445
	SFSP	NA	NA	NA	NA
	WSP	NA	NA	NA	NA

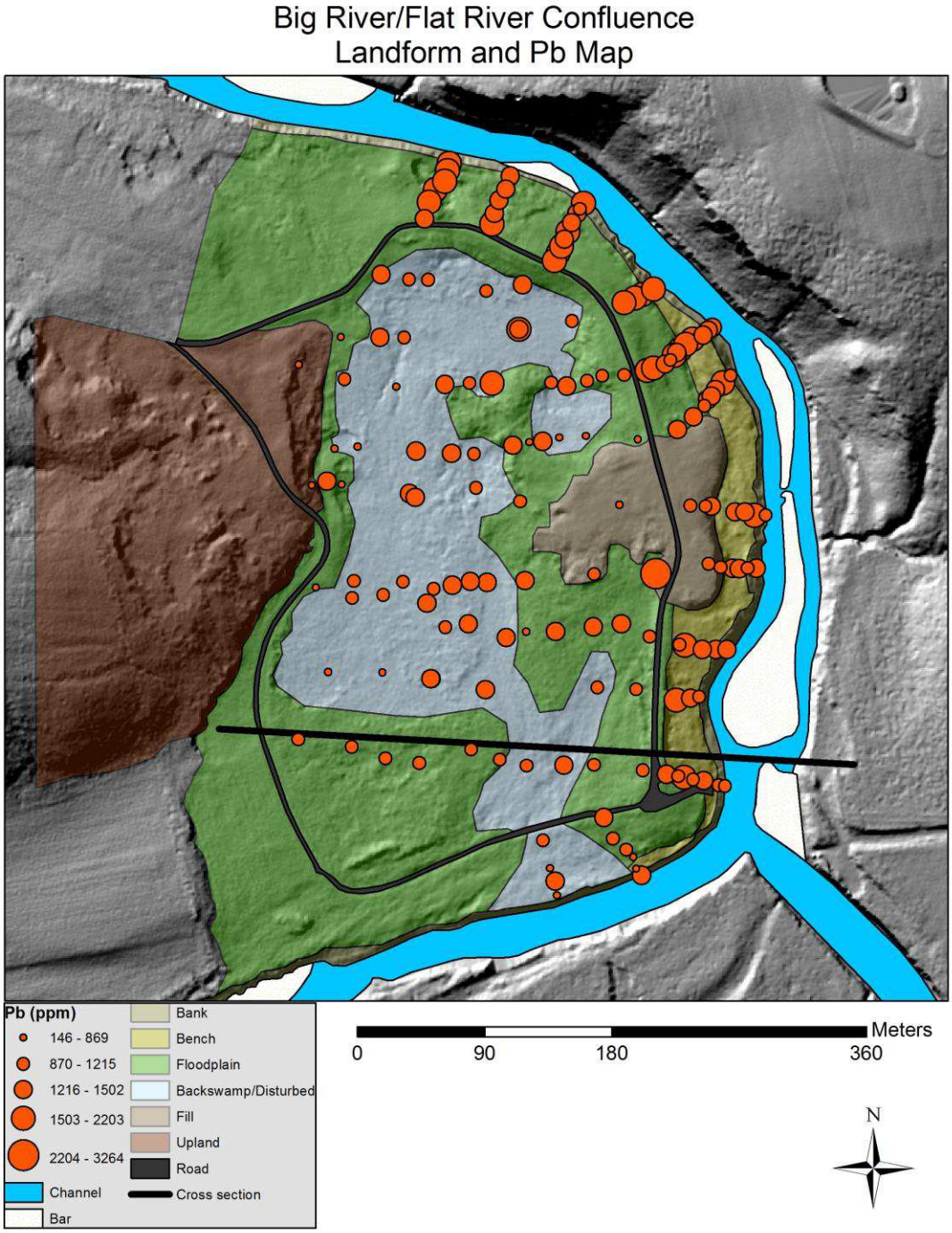

Figure 14 – BR/FR landform and Pb map.

Geochemistry. At the Big River/Flat River confluence, 174 samples were collected and each sample was attributed a landform classification based on location, and descriptive statistics for Pb, Zn, Ca, and Fe data was summarized for the whole site (Table 7). Bar samples were not included. Mean value of Pb concentration for all of the samples is 1,257 ppm, with the maximum mean concentration found in the bench, and the minimum in the backswamp. The mean for Zn is 1,118 ppm, with the maximum mean concentration in the bench, and the minimum in the floodplain. Mean calcium was 47,744 ppm, with maximum mean concentrations found in the bank, and the minimum in the backswamp. Mean Fe was 17,534 ppm, with highest concentrations found in the bank, and the lowest in the backswamp. The coefficient of variation was 29%, indicating a low variability in Pb between all samples. Landform concentrations and variability are summarized in Appendix D and Figures 15 and 16. Analysis of variance test showed a significant difference ($\alpha = 0.05$) in mean Pb concentrations between the backswamp and the bench.

Samples were split between the disturbed area and the undisturbed area and compared. Samples in the undisturbed area have a higher mean lead (1,371 ppm), zinc (1,200 ppm), and calcium (60,942 ppm) concentrations than the disturbed area (1,124, 1,022, and 32,237 ppm respectively). Iron is relatively uniform in both the disturbed (17,224 ppm) and undisturbed (17,799 ppm) areas. The differences between these sample groups are within one standard deviation, indicating there is not significant variability between the two sample groups.

Table 7 – Big River/Flat River Confluence geochemistry.

Element	Arithmetic			Logarithmic		
	Mean (ppm)	St. Dev. (ppm)	CV (%)	Mean (ppm)	St. Dev. (ppm)	CV (%)
Pb	1,257	365	29	3.08	0.15	4.9
Zn	1,118	362	32	3.02	0.16	5.1
Ca	47,744	30,904	65	4.60	0.27	5.9
Fe	17,534	1,966	11	4.24	0.05	1.1

n = 174

The geochemical cross section at this site displays 20 samples from the bank through the undisturbed and disturbed areas (Figure 14 and Figure 17). Moving from the channel inward beginning at the bank, lead is slightly lower near the channel, but rapidly rises on the bench. Moving across the road away from the bench into the disturbed area, lead drops off significantly between samples 11 and 12. Concentrations continue to fall in the chute that leads into the disturbed area. Throughout the remainder of the lower disturbed area, concentrations remain relatively high. Finally they tail off at samples 2 and 1 as elevation increases moving toward the upland. Zinc follows a similar trend with lower concentrations near the channel, high concentrations in the bench that tail off into the chute, and finally higher concentrations towards the uplands. The lead/zinc ratio shows increases in zinc in relation to lead on the margins of the chute as noted by the decrease in the ratio. Within the chute, however, Pb concentrations are higher. On the bench in the undisturbed area below the confluence, lead concentrations are also higher.

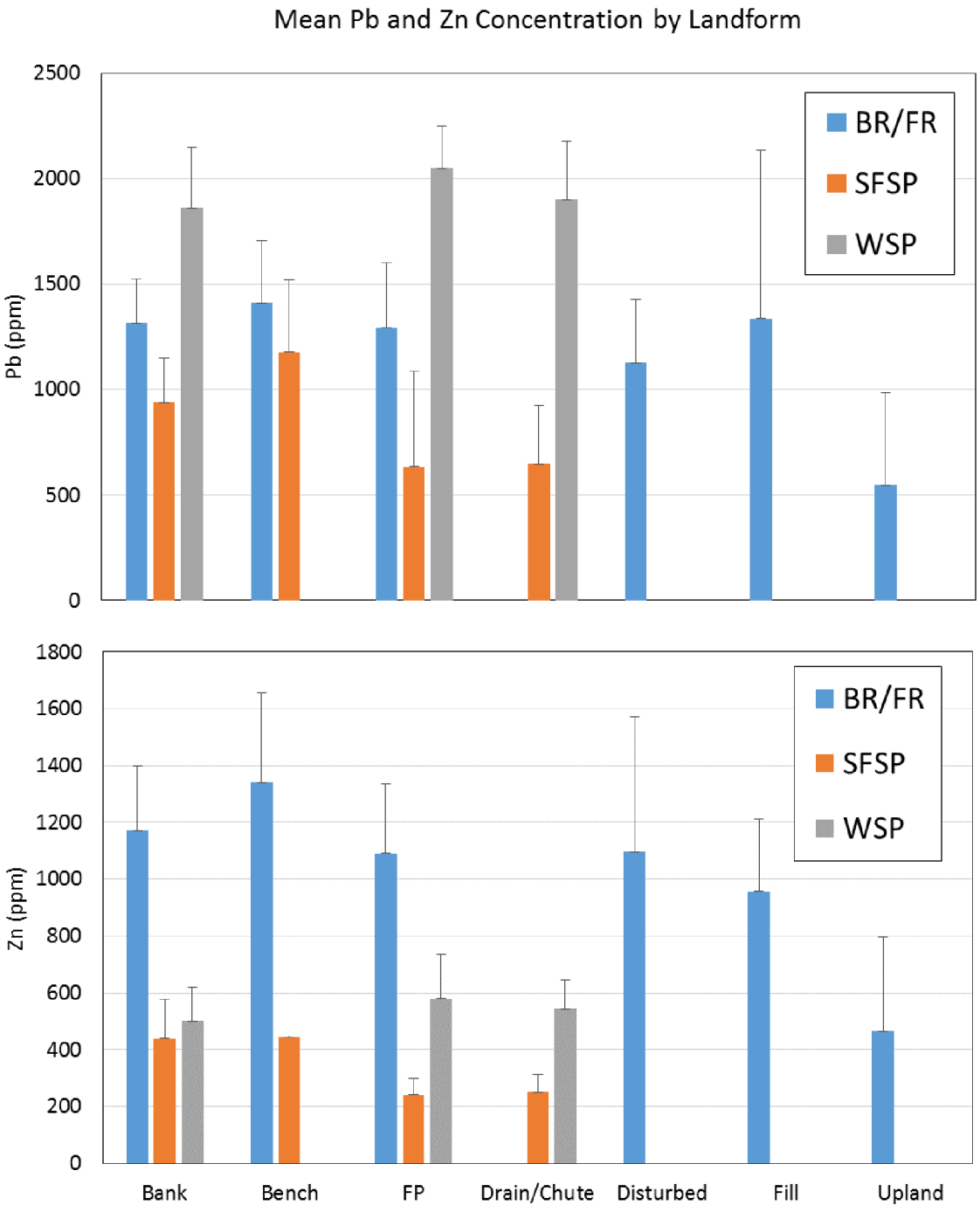

Figure 15 – Mean ± sd concentration of Pb (top) and Zn (bottom) by landform.

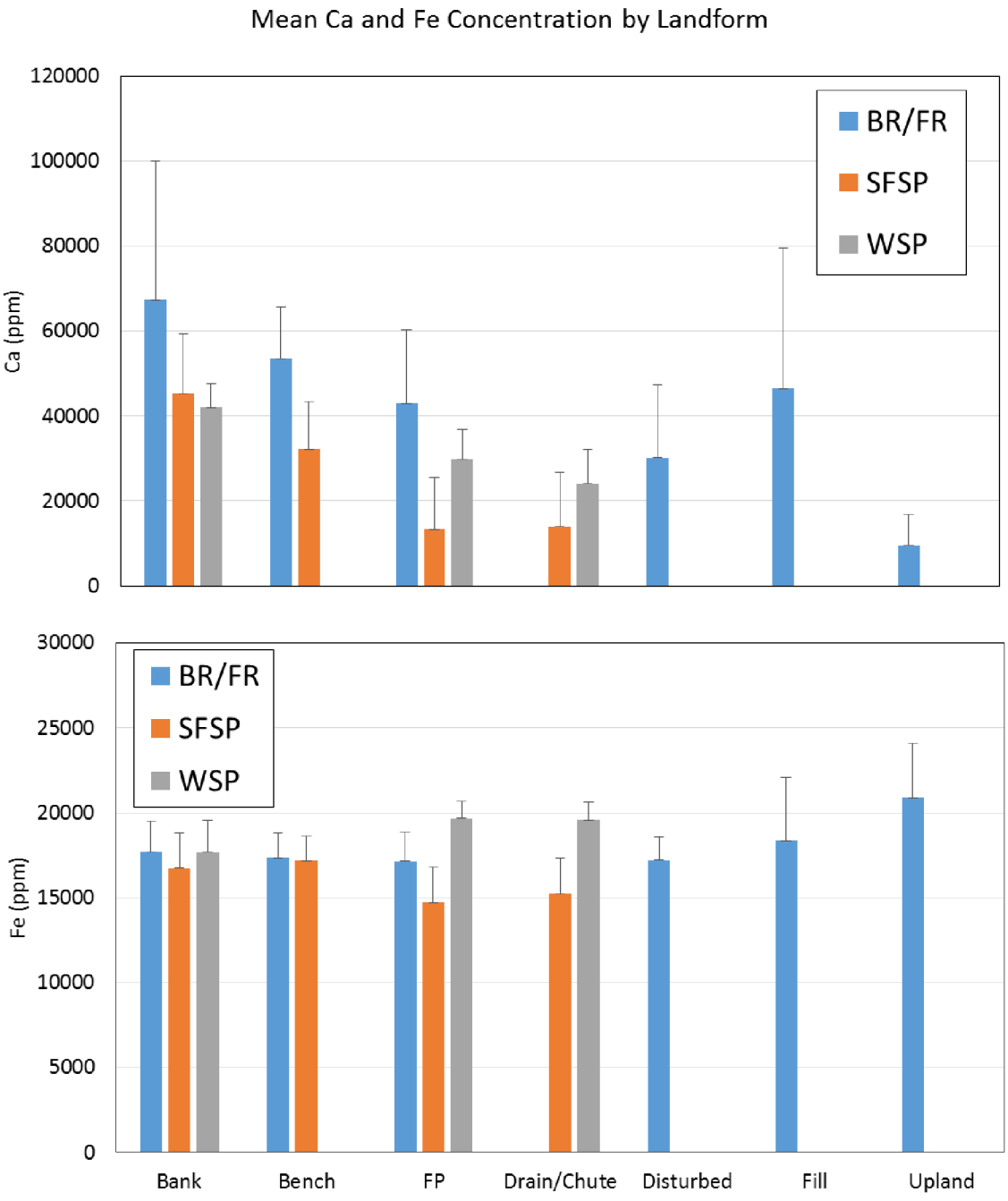

Figure 16 – Mean ± sd concentration of Ca (top) and Fe (bottom) by landform.

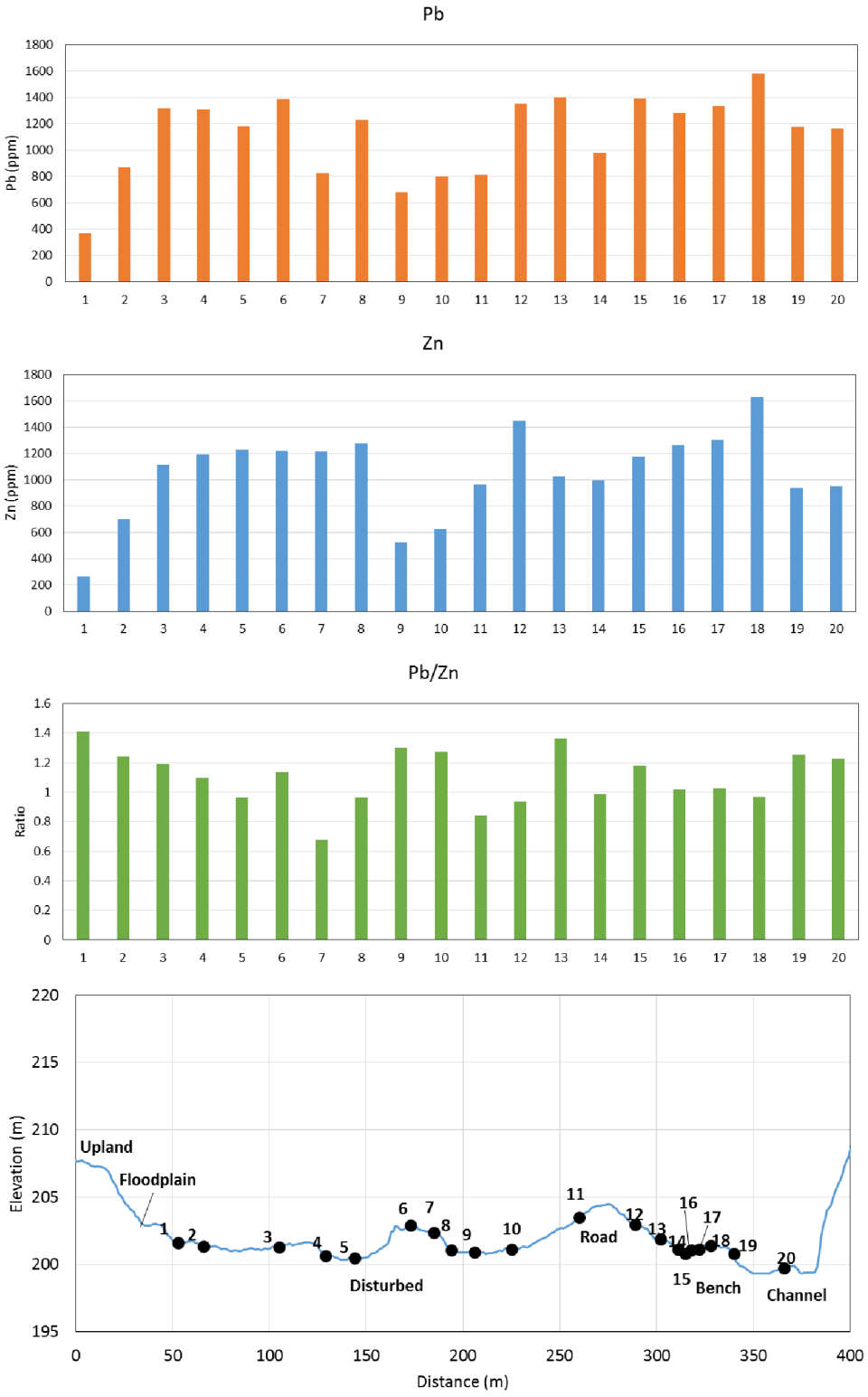

Figure 17 – Geochemical cross section at BR/FR. Cross section location can be found on Figure 14. Numbers are reference points for use in text.

Interpolations. Interpolated Pb maps indicate higher values of Pb are on the undisturbed floodplain and bench landforms closest to the channel (Figure 18). In the disturbed floodplain, there are lower concentrations of Pb, but they show clear topographical trends. Higher interpolated concentrations are found in the disturbed area in the backswamp. Near the road and the floodplain unit, concentrations are still high, but tend to be significantly less than these lowlands.

Sediment sources can be differentiated between Flat River and the Big River when looking at Zn patterns (Figure 19). The highest concentrations of Zn are found around the south end in the small chute leading to the disturbed area. Zinc-rich sediment is able to be transported through the chute during flooding events. The undisturbed floodplain areas below the Flat River confluence show less Zn than the areas above the confluence.

Above the confluence and in the disturbed area, the Pb/Zn interpolation shows much lower ratios indicating more zinc relative to lead (Figure 20). The ratio gets bigger after the confluence along the undisturbed bench, after the confluence with the Flat River. The variation is due a difference in the geochemical signature of the sediment supplied from the Big River above the confluence, and the sediment that is added as Flat River joins the Big River. Mining contaminated sediment from the Flat River has a different geochemical signature than contaminated sediment from the Big River. Leadwood tailings are found to have Zn concentrations more than twelve times higher than tailings from National or Federal, and lead concentrations are similar between these piles. The lead/zinc ratio for the National, Federal, and Leadwood tailings are 6.9, 6.8 and 0.4, respectively (Smith and Schumacher, 1993; Pavlowsky et al, 2010a). Therefore, areas

above the Flat River confluence will have high zinc concentrations from Leadwood tailings. Below the confluence, the influx of sediment from the Flat River with high lead and low zinc concentrations dilutes the high zinc concentration from the Leadwood. Because of this, areas below the confluence tend to have lower concentrations of zinc, than areas above. Therefore, areas such as the disturbed backswamp will have more Zn, whereas such as the undisturbed area below the confluence will likely be diluted in Zn.

High calcium concentrations are typically found close to the channel in the undisturbed area, and near the chute in the disturbed area (Figure 21). The increased Ca near the channel is likely related to the coarse grained floatation sands that would accumulate in the proximal channel areas. Iron concentrations are lowest in the low disturbed backswamp and highest in areas close to the upland (Figure 22). Natural sediment input from upland erosion may be driving this pattern.

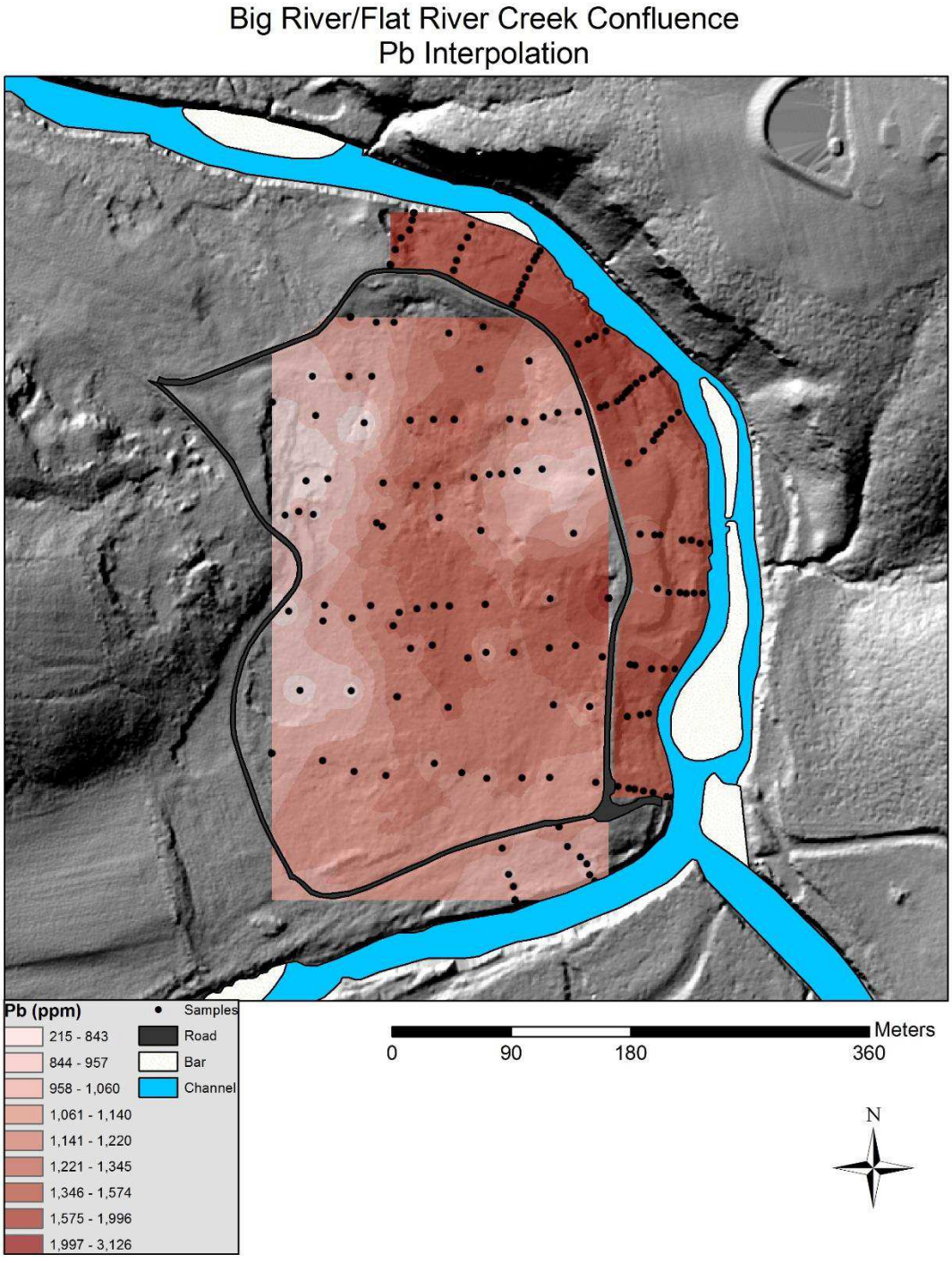

Figure 18 –Pb interpolation at the BR/FR site.

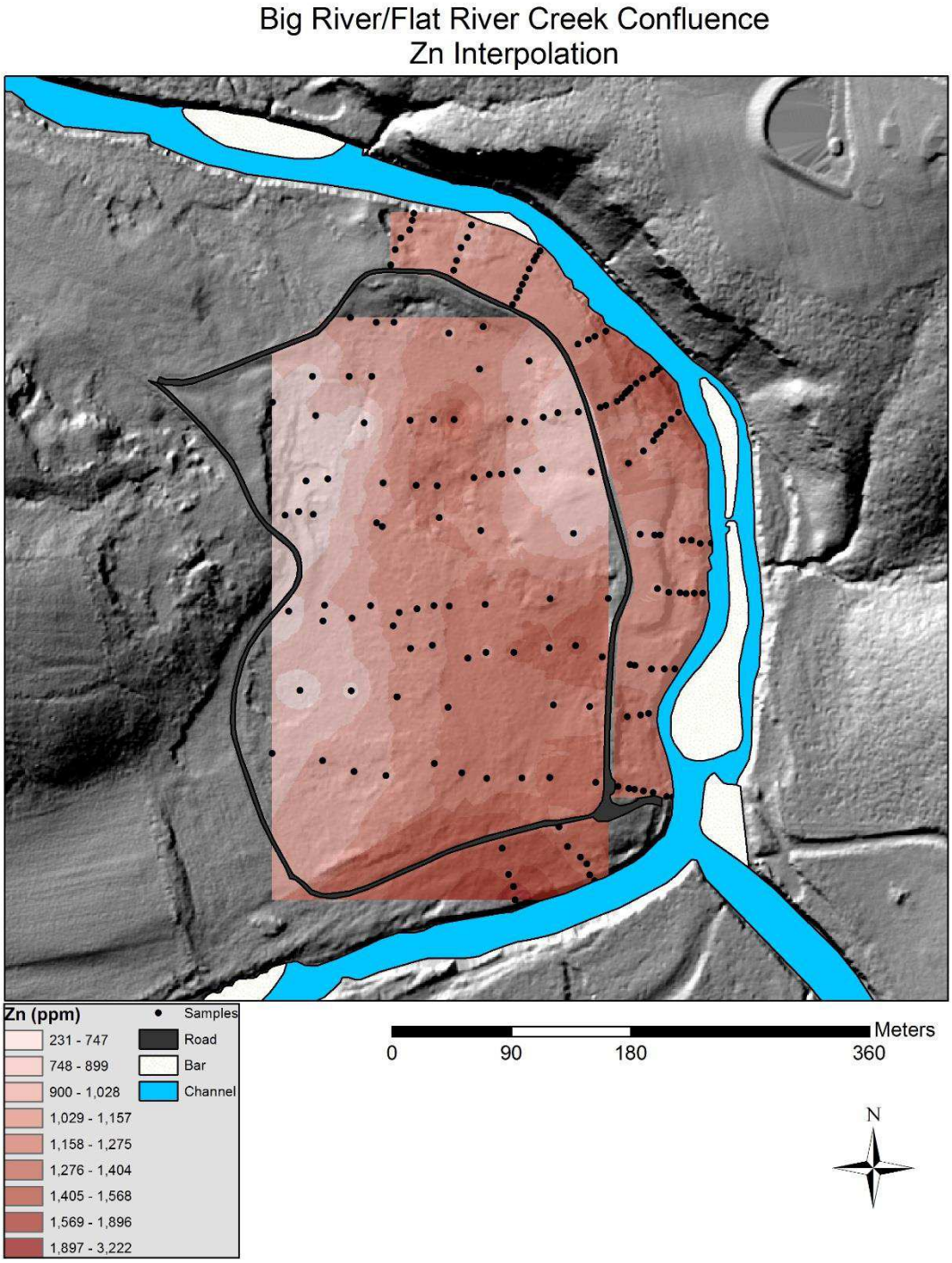

Figure 19 – Zn interpolation at the BR/FR site.

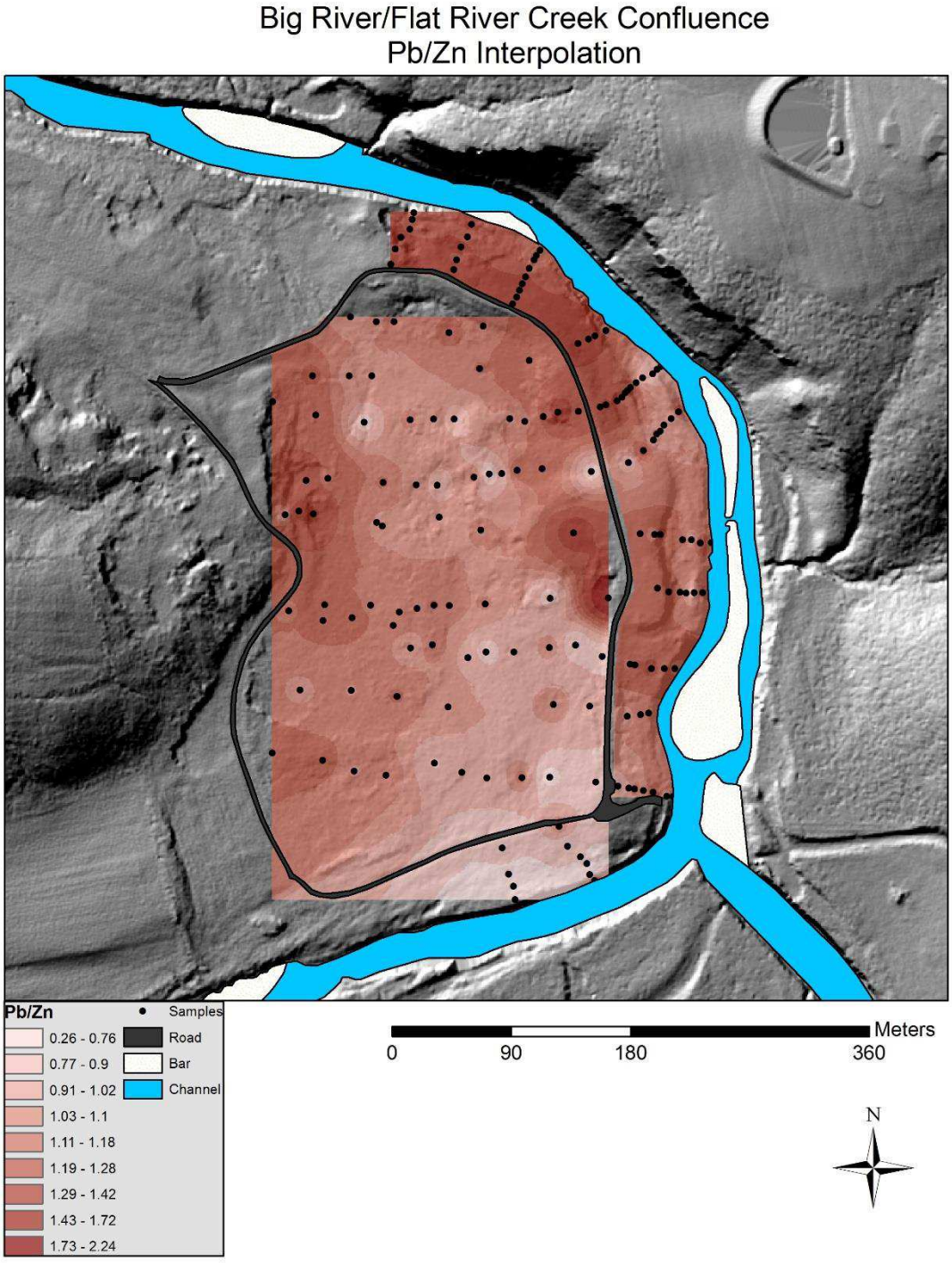

Figure 20 – Pb/Zn interpolation at the BR/FR site.

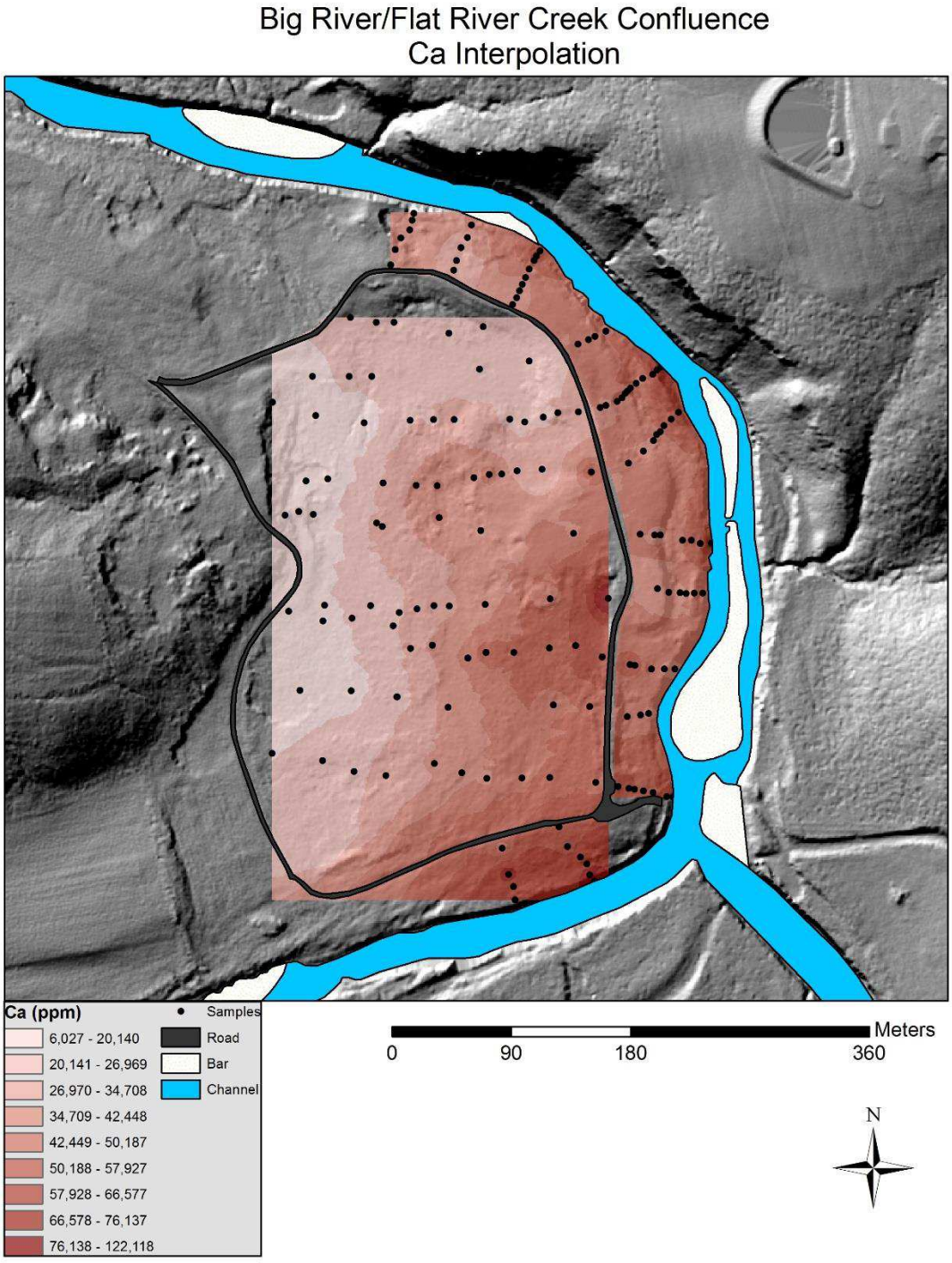

Figure 21 – Ca interpolation at the BR/FR site.

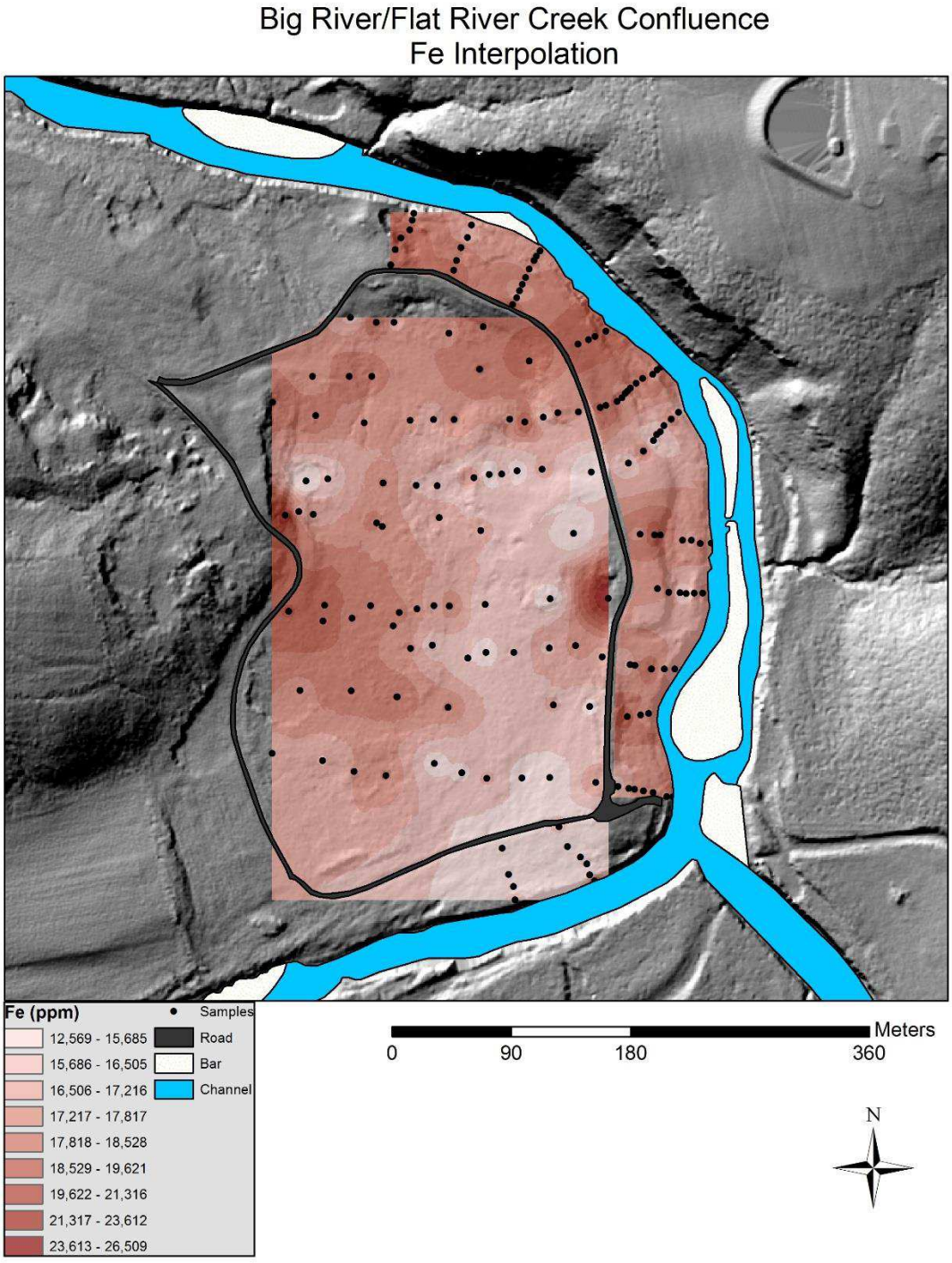

Figure 22 – Fe interpolation at the BR/FR site.

St. Francois State Park

Landform Classification. The confining valley at St. Francois State Park creates a narrow floodplain that rises rapidly with distance from the channel. There are four distinct landform classes created at this site (Figure 23 and Table 5). The channel and floodplain are separated by steep banks that rise to a sand-rich levee. Across the levee is the bench that extends until it meets the road that runs atop the initial rise of the floodplain unit. A drainage channel has been cut by park management along the road in the floodplain for runoff and is connected to the river by deep cuts through the bank. The floodplain has a relatively steep rise as it moves out toward the narrow valley margin.

Flood Inundation Frequency. At St. Francois State Park, the bench was found to flood every 1.25-1.5 years (Table 6). A stage of 5.64 m above the thalweg is needed in order for the river to overtop the levees due to the tall, steep banks. For the flood waters to reach the road where the higher floodplain unit begins, a larger flood with a recurrence interval of 1.5-2 years is needed. Therefore, alluvial sedimentation would be expected to be much less on the higher floodplain surface.

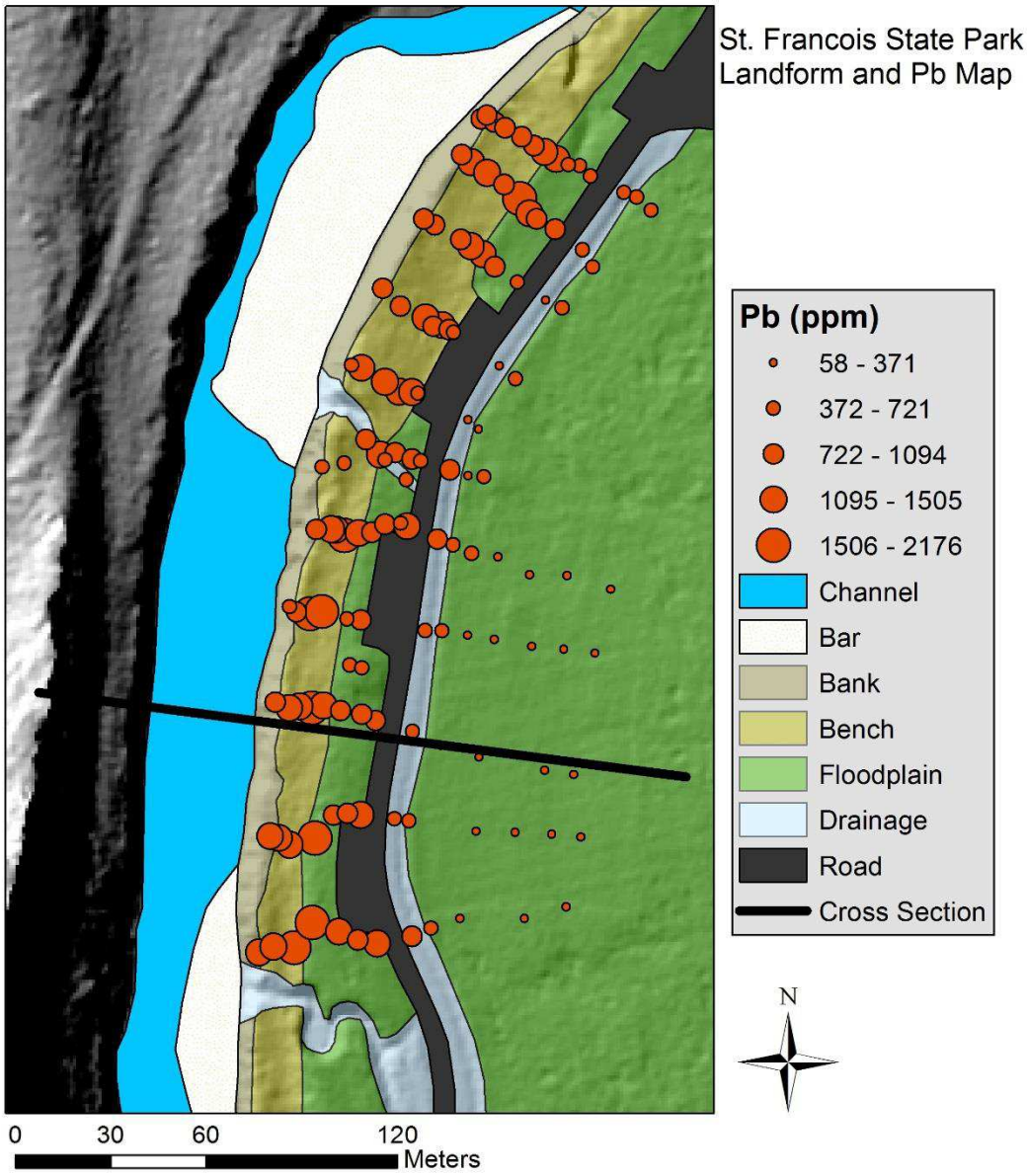

Figure 23 – SFSP landform and Pb map.

Geochemistry. Descriptive statistics were calculated for Pb, Zn, Ca, and Fe concentrations for the 140 samples collected (Table 8). Bar samples were omitted from the data set. Mean Pb concentration for all of the samples is 820 ppm, with the maximum mean concentration found in the bench, and the minimum in the floodplain. The mean for Zn is 326 ppm, with the maximum mean concentration in the bench, and the minimum in the higher floodplain as well. Mean calcium was 26,118 ppm, with maximum mean concentrations found in the bank, and the minimum in the floodplain. Mean Fe was 16,030 ppm, with highest concentrations found in the bench, and the lowest in the floodplain. The coefficient of variation was 55%, indicating significant variability in Pb between all the samples. Landform concentrations and variability are summarized in Appendix D and Figures 15 and 16. Analysis of variance test showed a significant difference ($\alpha = 0.05$) in mean Pb concentrations between the drainage feature and the bench, and between the floodplain and the bench.

The geochemical cross section displays total of 12 samples from the bank into the upper floodplain (Figure 24). Concentrations of these metals started relatively low near the channel in the lower bank deposits. On the other side of the levee on the bench, concentrations rise quickly to the highest levels in the study area. As elevation increases toward the road and the higher floodplain unit, concentrations begin to tail off. Increasing elevation with distance from the channel shows a clear decrease in Pb and Zn into the floodplain landform. Overall, the zinc concentration are much lower than the lead concentrations, but they follow the same trend in contamination across the landforms. Lead/zinc ratios do not show a clear trend because the contamination patterns are very similar.

Table 8 –St. Francois State Park geochemistry.

Element	Arithmetic			Logarithmic		
	Mean (ppm)	St. Dev. (ppm)	CV (%)	Mean (ppm)	St. Dev. (ppm)	CV (%)
Pb	820	451	55	2.83	0.31	11.1
Zn	326	169	52	2.44	0.28	11.7
Ca	26,118	23,741	91	4.22	0.47	11.0
Fe	16,030	3,050	19	4.20	0.07	1.8

n = 140

Interpolations. Lead and zinc interpolation maps indicate that distance from the channel and elevation appear to be strongly related to heavy metal concentrations. (Figure 25 and Figure 26). With increased distance from the channel, Pb and Zn concentrations fall quickly across the study area. In the coarse, sandy levee deposits that are part of the bank deposition, concentrations are lower than the adjacent finer-grained bench. Any increase in elevation above the bench towards the road is related to a drastic decrease in heavy metal contamination. Across the road, very limited contamination exists, likely related to infrequent flooding and limited deposition.

As for calcium, the highest concentrations are limited to areas close to the channel, such as the levee, where sand deposition is more common (Figure 27). Iron trends are similar to the other elements with high concentration across the bench, and much lower concentrations in the floodplain (Figure 28). This could be related to fine-grained tailing input in the bench.

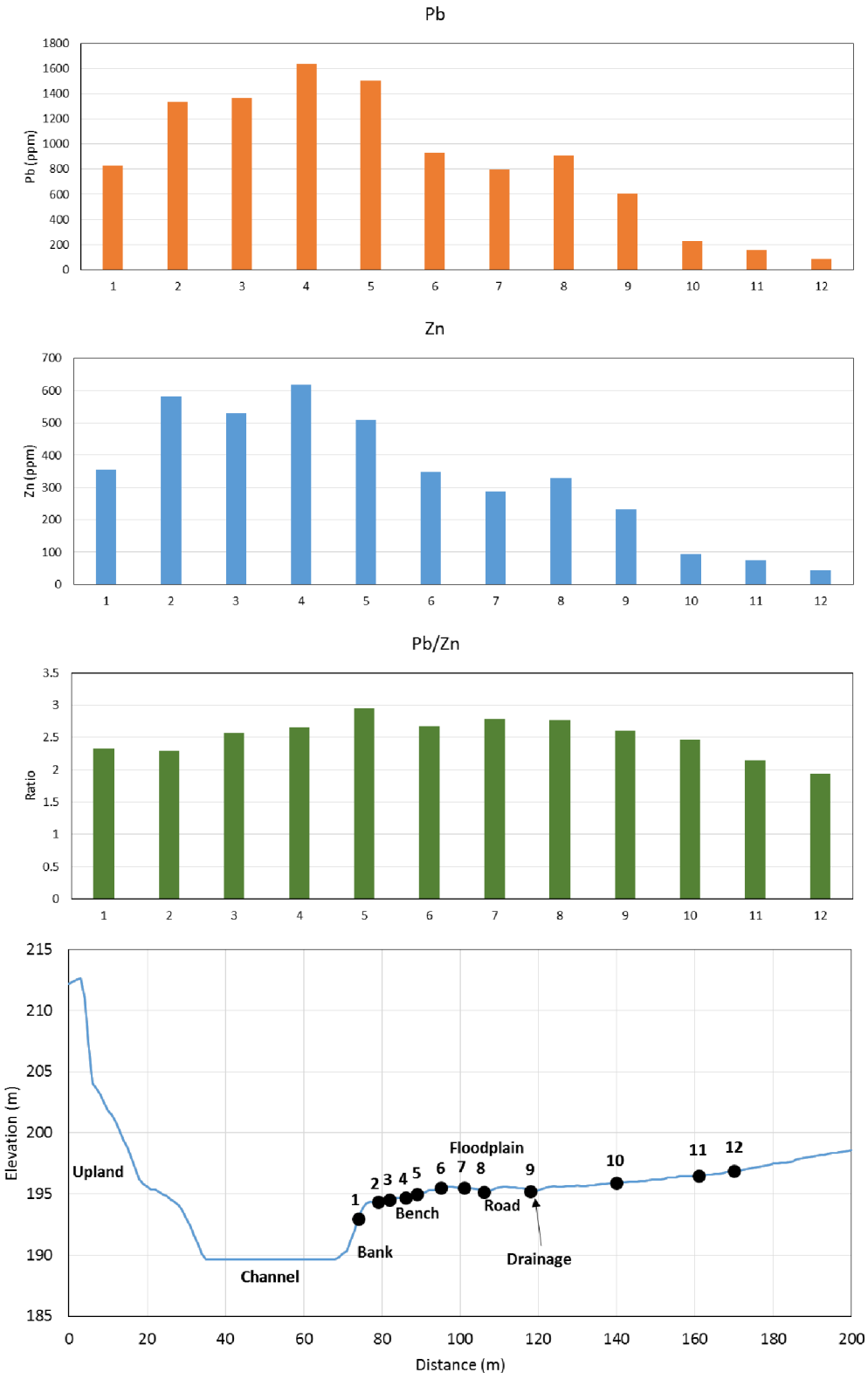

Figure 24 – Geochemical cross section at SFSP. Cross section location can be found on Figure 23. Numbers are reference points for use in text.

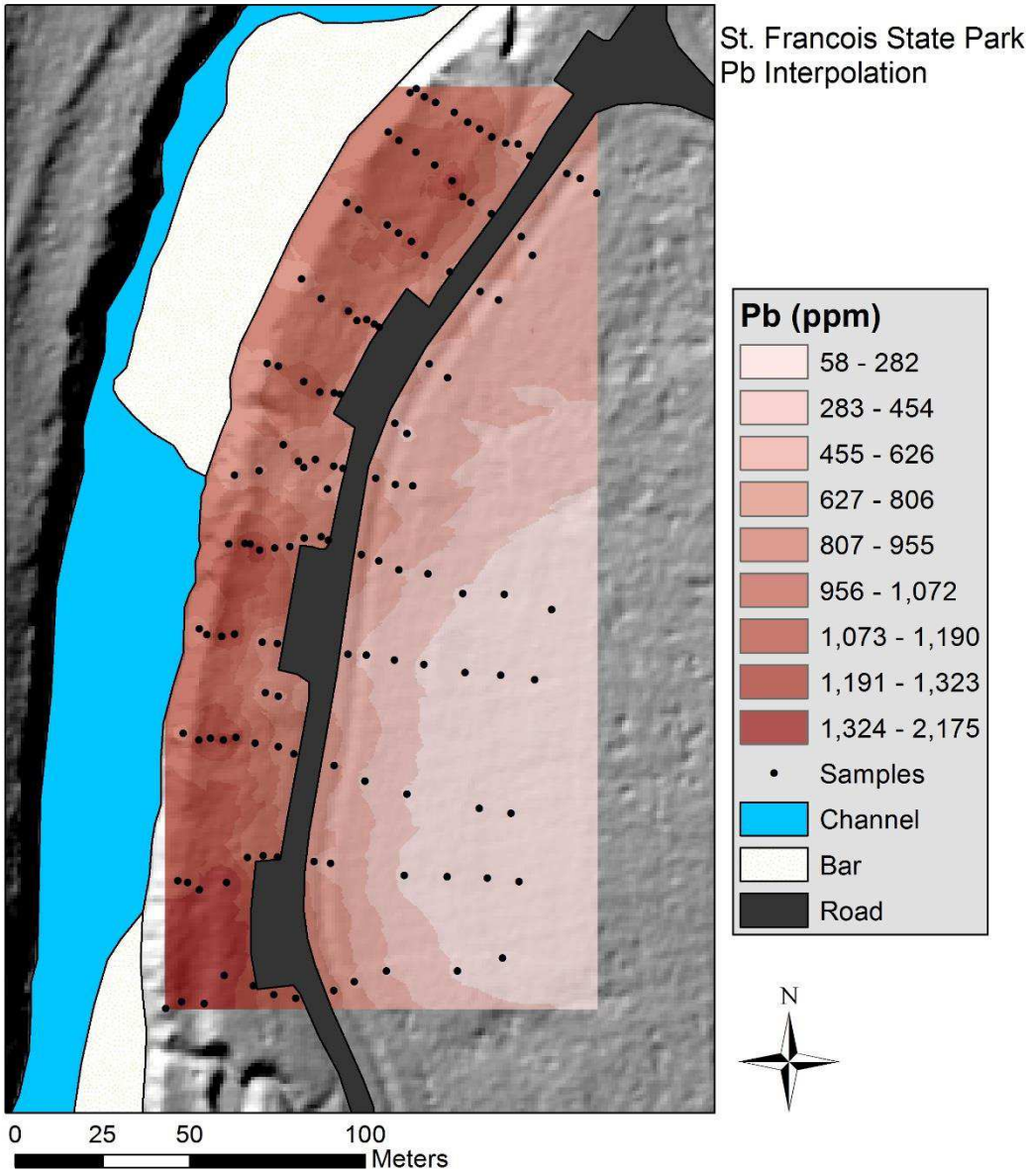

Figure 25 – Pb interpolation at the SFSP site.

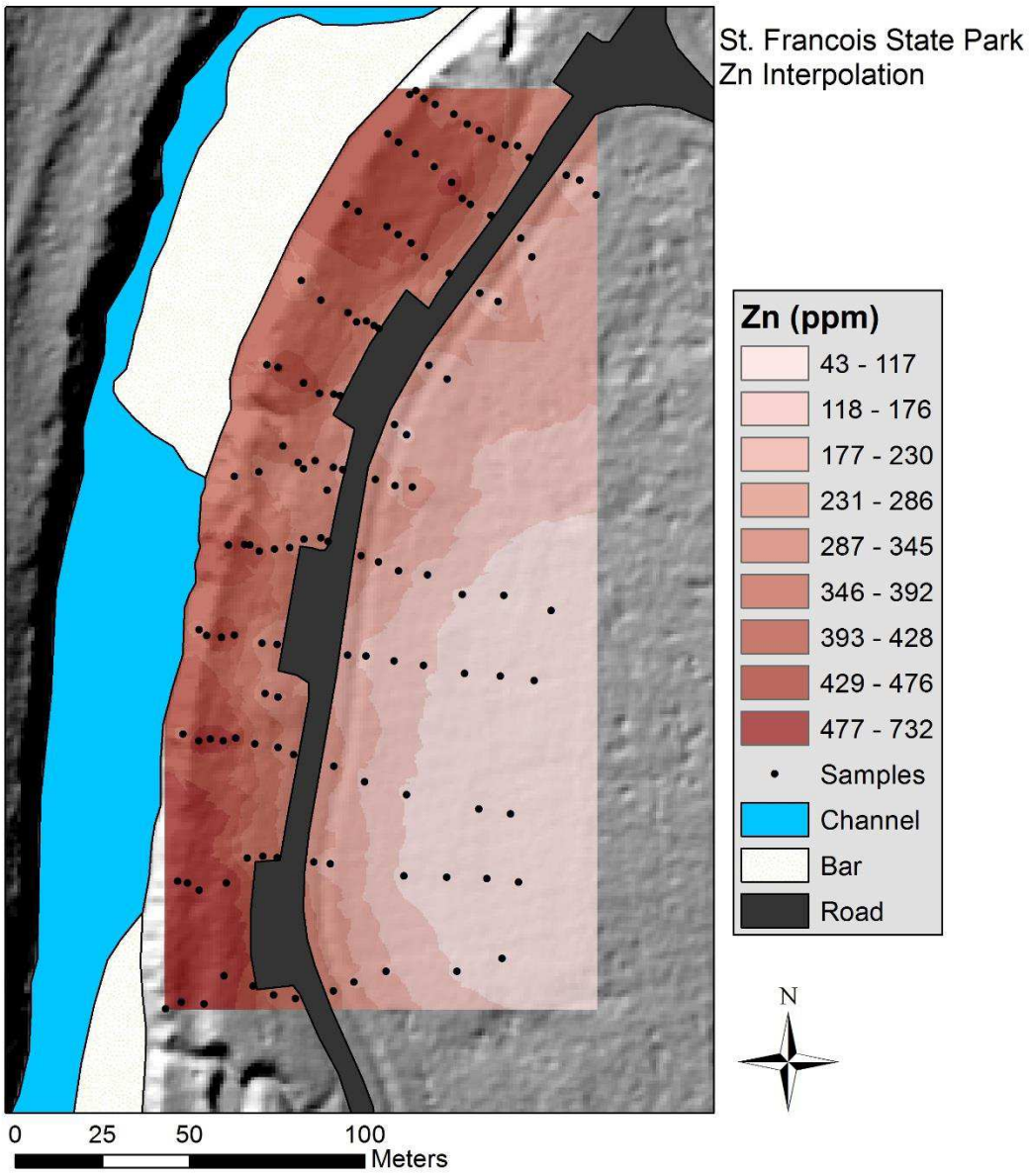

Figure 26 – Zn interpolation at the SFSP site.

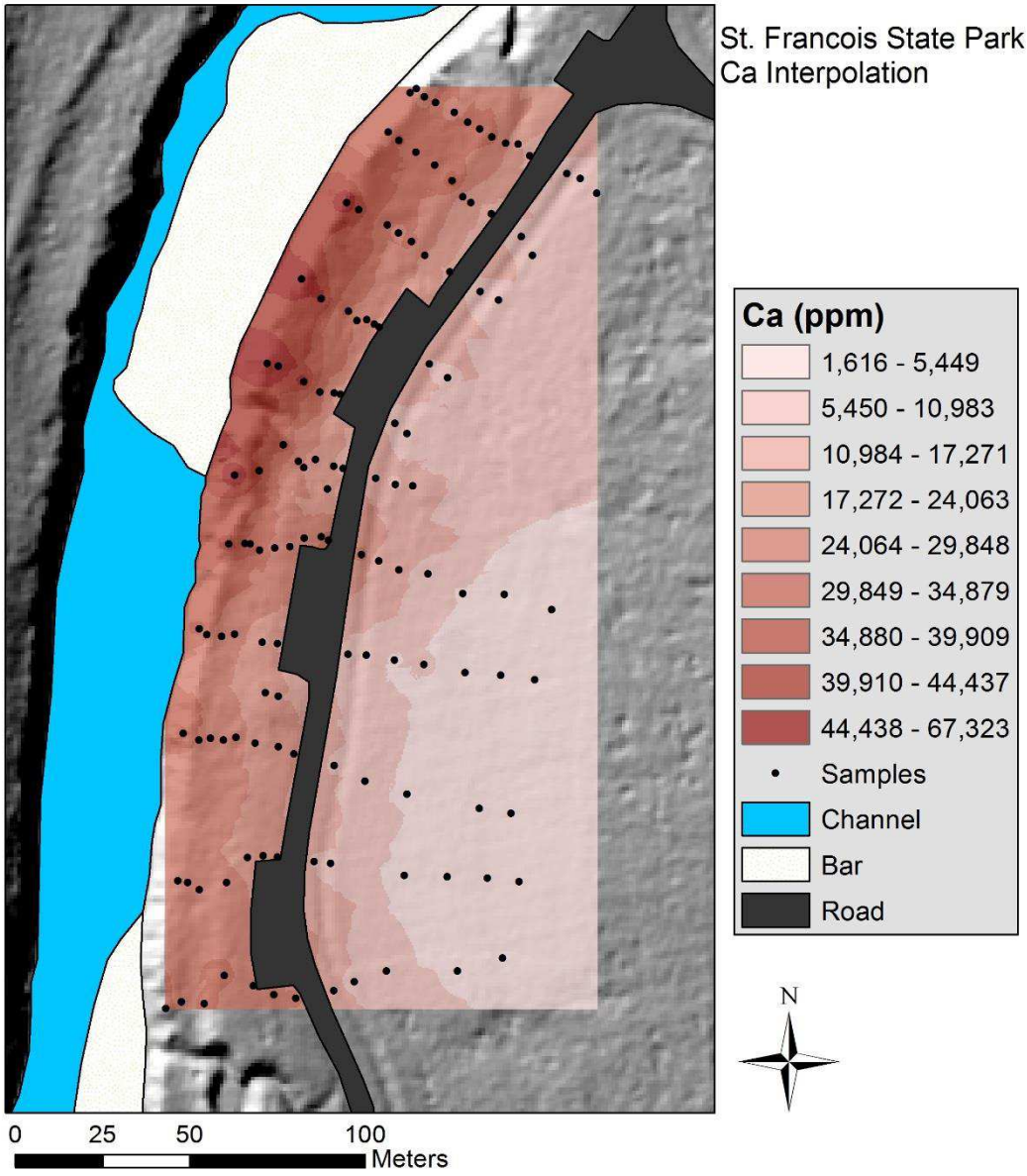

Figure 27 – Ca interpolation at the SFSP site.

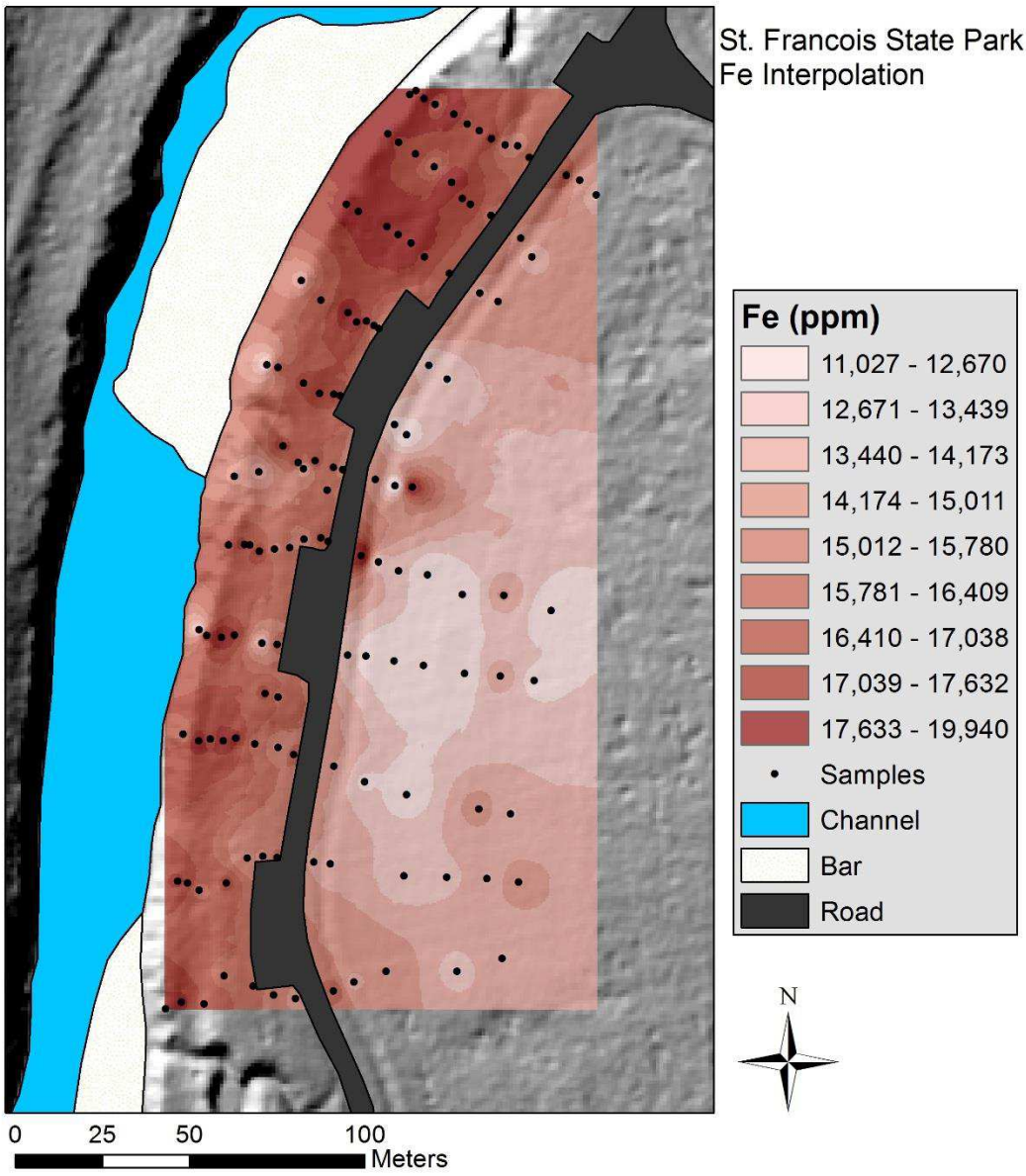

Figure 28 – Fe interpolation at the SFSP site.

Washington State Park

Landform Classification. Washington State Park is characterized by a wide valley and relatively uniform floodplain, and a prominent chute and drainage feature. There are three distinct landform classes at this site (Figure 29 and Table 5). The floodplain elevation is between 171 and 172 m above sea level, and is limited in topographic variation. The elevation across the floodplain does not vary more than about a meter. Since there is only one distinct topographical surface, there is no differentiation between a higher floodplain and a lower bench unit. The bank shows limited levee development based on LiDAR data, likely due to the increased distance from the mining sources. Therefore, there is likely a more limited availability of sand-sized sediment for levee formation. On the eastern end of the study site, the bank is steep as it rises from the channel. To the west, there is a public access area where the bank in has a much shallower slope that leads into a large bar. There is a chute that cuts across the floodplain from the channel and connects with a prominent drainage feature at the toe of the confining bluff on the southern end of the study area. The drainage feature at the base of the bluff drains the upland runoff as clearly seen by erosional cuts on the slope. The chute allows for floodwaters to be channelized across the floodplain and flow along the base of the bluff in the drainage feature until they connect back into the Big River on the west end of the study site. The road is at a lower elevation than the floodplain it is built on, causing it to look inset into the floodplain. This suggests possible high deposition rates on this floodplain building up around the road. Since the road is at a lower elevation, park management has cut a drainage channel that connects the road to the main channel, preventing water from pooling in the road.

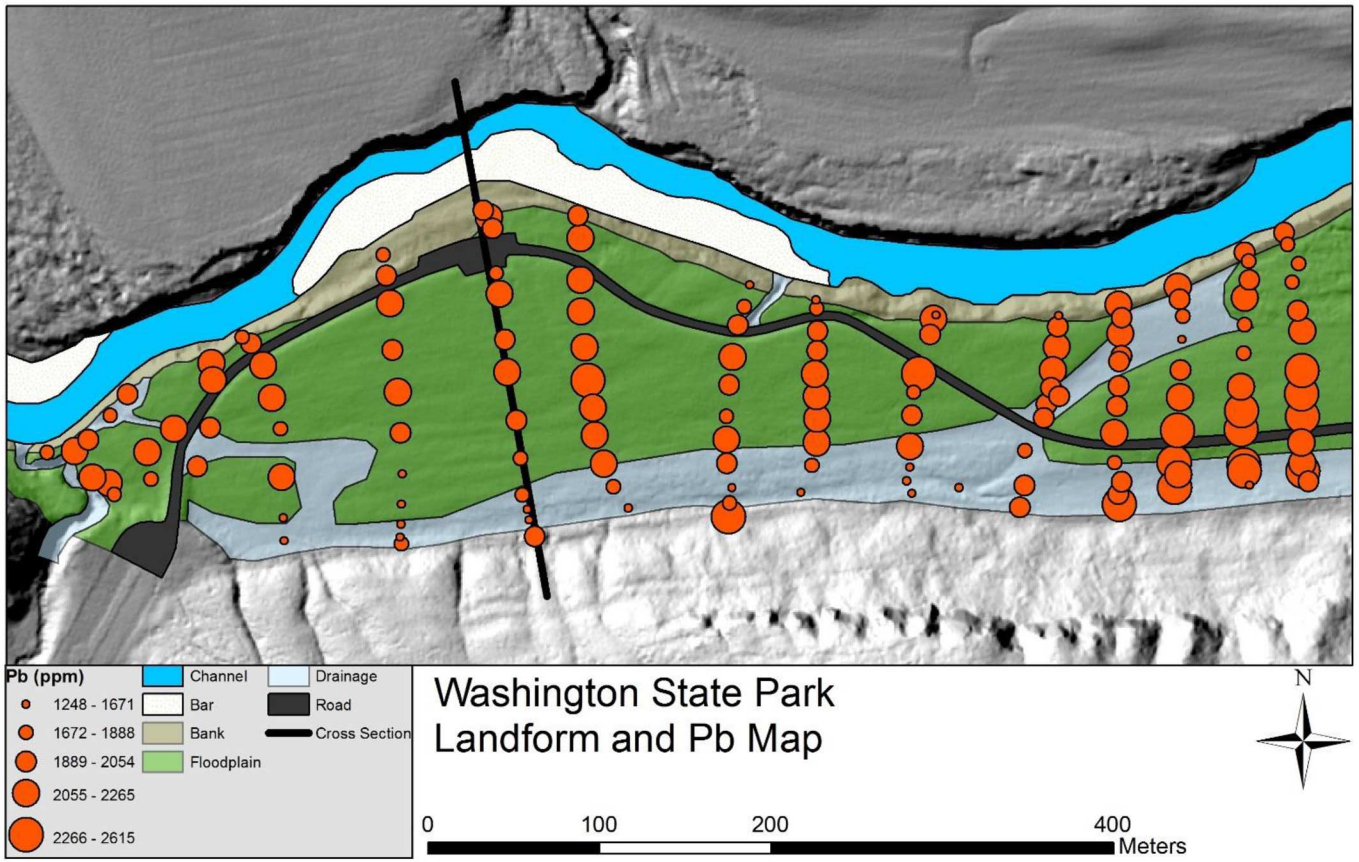

Figure 29 - WSP landform and Pb map.

Flood Inundation Frequency. At Washington State Park, only one recurrence interval was calculated for overbank floods (Table 6). The single floodplain landform was found to flood every 1.05-1.25 years. When this overbank flood occurs, the more uniform and flat topography at Washington allows flood waters to spread across floodplain to the valley wall. Flood water transport into the farther reaches of the floodplain may be facilitated by the chute channel. Wide valley width paired with low recurrence intervals indicates this site may have the ability to accumulate a significant amount of sediment.

Geochemistry. Descriptive statistics were calculated for Pb, Zn, Ca, and Fe concentrations for the 154 samples collected (Table 9). Bar samples were again omitted. Mean Pb concentration for all of the samples is 1,915 ppm, with the maximum mean concentration found in the floodplain, and the minimum in the bank. The mean for Zn is 543 ppm, with the maximum mean concentration in the floodplain, and the minimum in the bank as well. Mean calcium was 28,802 ppm, with maximum mean concentrations found in the bank, and the minimum in the chute/drainage feature. Mean Fe was 19,012 ppm, with highest concentrations found in the floodplain, and the lowest in the bank. The coefficient for Pb is 21% indicating an overall lack in variability in concentrations. Landform concentrations and variability are summarized in Appendix D and Figures 15 and 16. Analysis of variance test showed a significant difference ($\alpha = 0.05$) in mean Pb concentrations between the chute/drainage and floodplain, and between the bank and floodplain.

Table 9 –Washington State Park geochemistry.

Element	Arithmetic			Logarithmic		
	Mean (ppm)	St. Dev. (ppm)	CV (%)	Mean (ppm)	St. Dev. (ppm)	CV (%)
Pb	1,915	407	21	3.26	0.17	5.2
Zn	543	111	20	2.72	0.14	5.1
Ca	28,802	8,978	31	4.44	0.15	3.4
Fe	19,012	2,464	13	4.27	0.08	1.8

n = 154

The geochemical cross section at this site displays a total of 15 samples from the lower bank to the hillslope (Figure 30). Lead and zinc followed the same trend across the cross section with zinc levels much lower than lead. The lowest concentrations for both lead and zinc were found near the channel. Concentrations rise significantly atop the levee and floodplain. Across the floodplain, the concentrations of lead stay consistently high between 1,500 and 2,250 ppm, and zinc stays between 450 and 610 ppm. Point 2 is within the channelized drainage feature near the hillslope and there is a significant decrease in both lead and zinc. Point 1 is no longer in the channel and concentrations are more consistent with the rest of the floodplain. Overall there are high concentrations of heavy metals across the whole floodplain unit, even at distance from the channel.

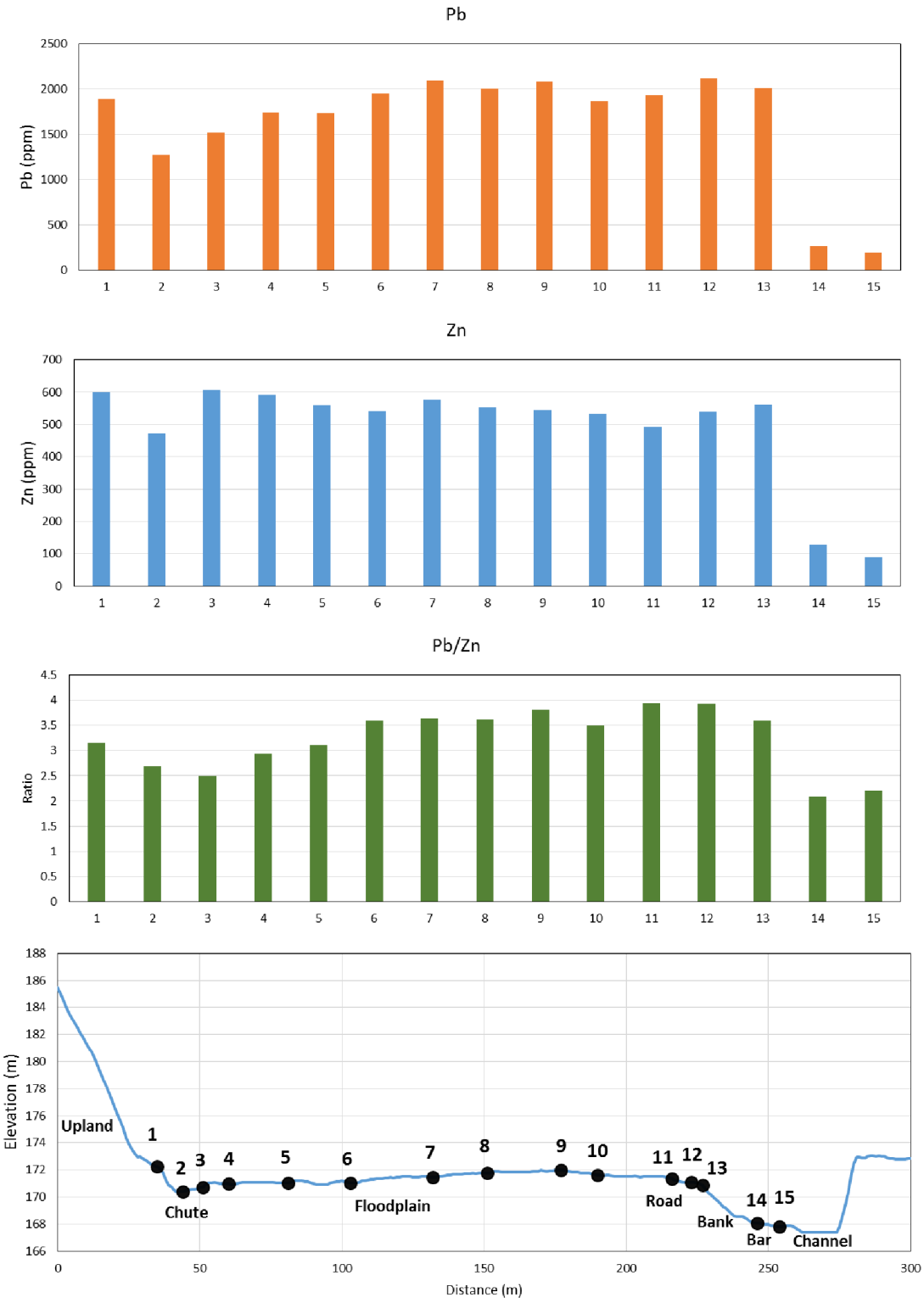

Figure 30 – Geochemical cross section at WSP. Cross section location can be found on Figure 29. Numbers are reference points for use in text.

Interpolation. Interpolation maps show high and relatively uniform Pb concentrations across the floodplain (Figure 31). Unlike St. Francois, there does not appear to be an inverse relationship between distance from the channel and concentrations. The little variability seen across the floodplain that does exist can be attributed to the channelized chutes and drainage features where lower concentrations occur. Areas in and around the bank tend to have lower Pb concentrations, likely related to the coarser grained deposition typically in these areas.

Zinc however does not show the same pattern as Pb (Figure 32). Chutes do not appear to correlate visually with lower concentrations. High concentrations of Zn seem to concentrate more in the west end of the study site where the drainage feature leads. However, it is important to note that the pattern variations may be a factor of magnitude. Concentration values for Zn are significantly less than that of Pb, so variations on the order of a 100 ppm visually look more significant for Zn than would for Pb.

Calcium is again limited to areas close to the channel where sand deposition likely dominates (Figure 33). Calcium will be significantly limited because Washington is much farther downstream than the other two sites, so coarser-grained mining sediment likely will not be readily transported this far downstream.

Iron is concentrated near the bluff and decreases closer to the channel (Figure 34). It is likely that Fe concentrations could be related to areas where natural sediment such as weathered residuum is eroding off of the uplands is being deposited on the floodplain. This may have an effect on the relationship between Pb and Fe.

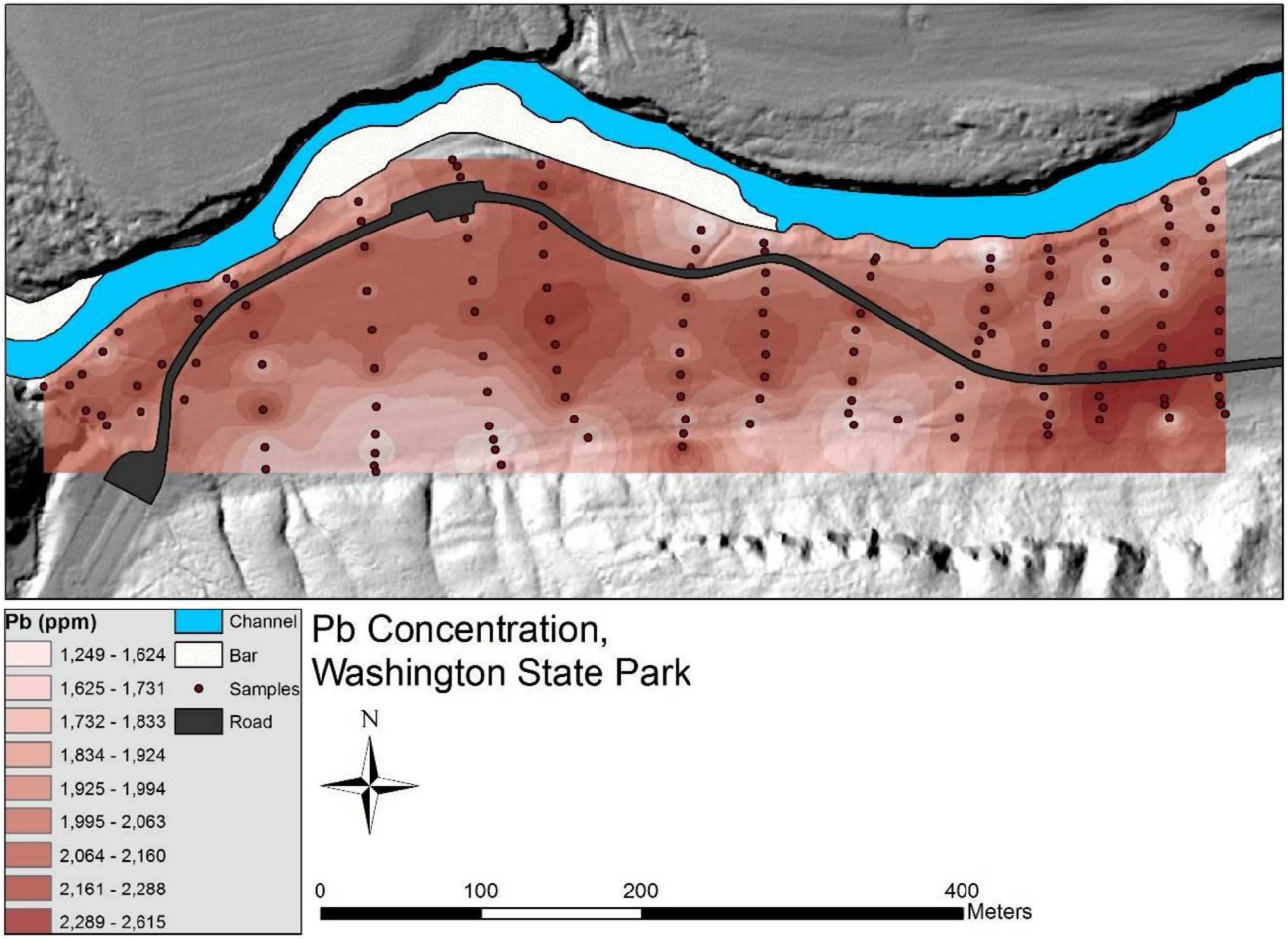

Figure 31 – Pb interpolation at the WSP site.

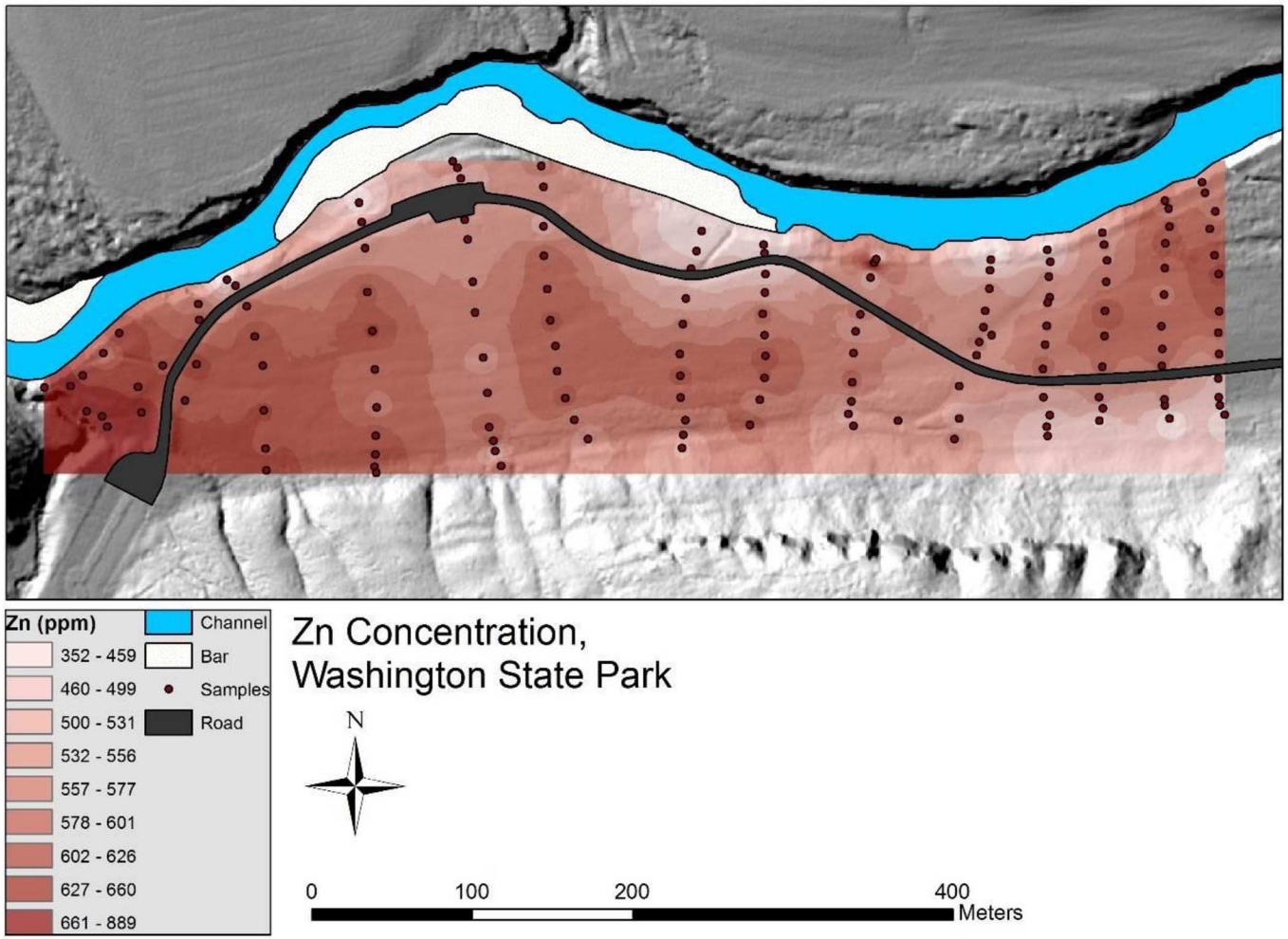

Figure 32 – Zn interpolation at the WSP site.

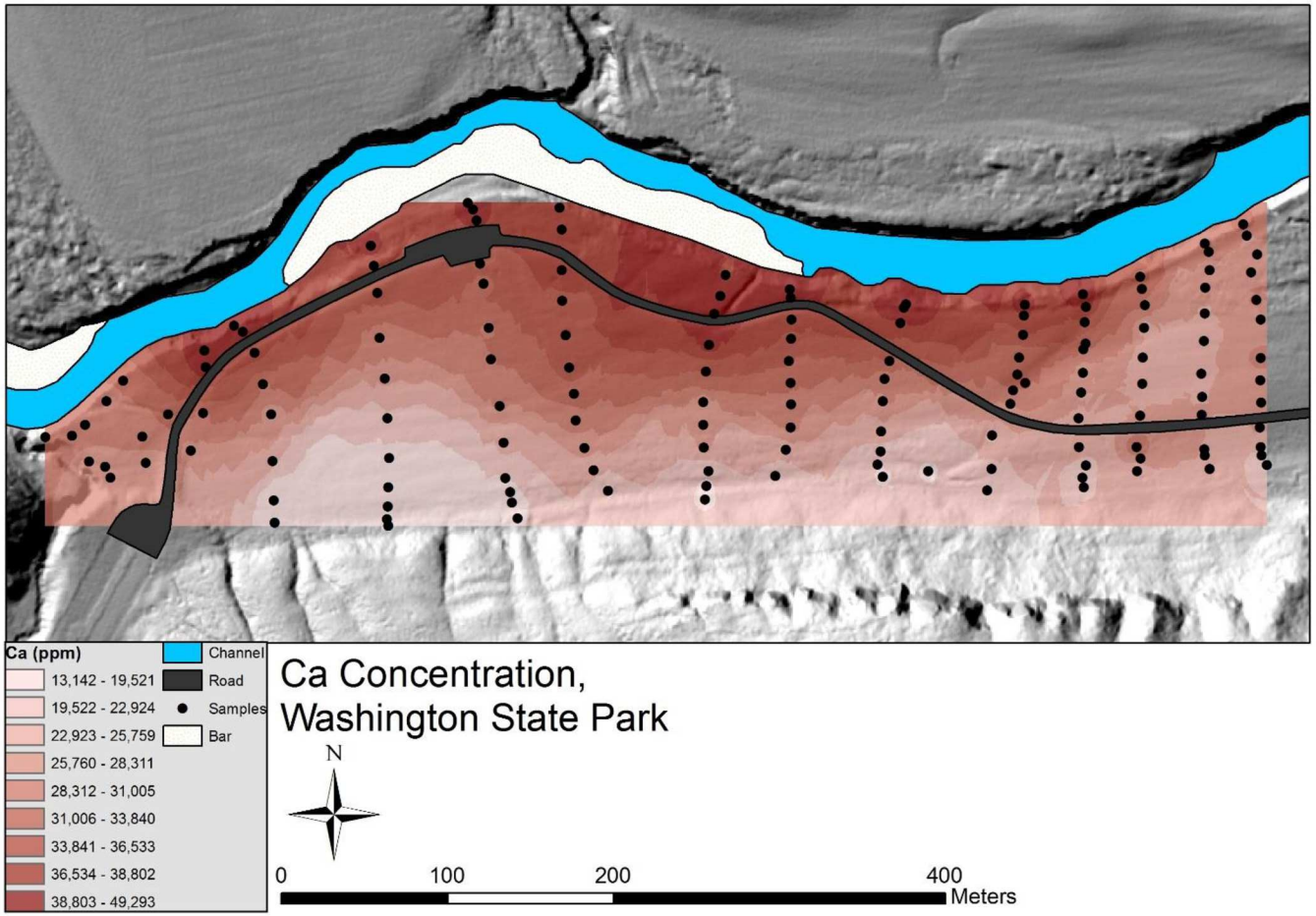

Figure 33 – Ca interpolation at the WSP site.

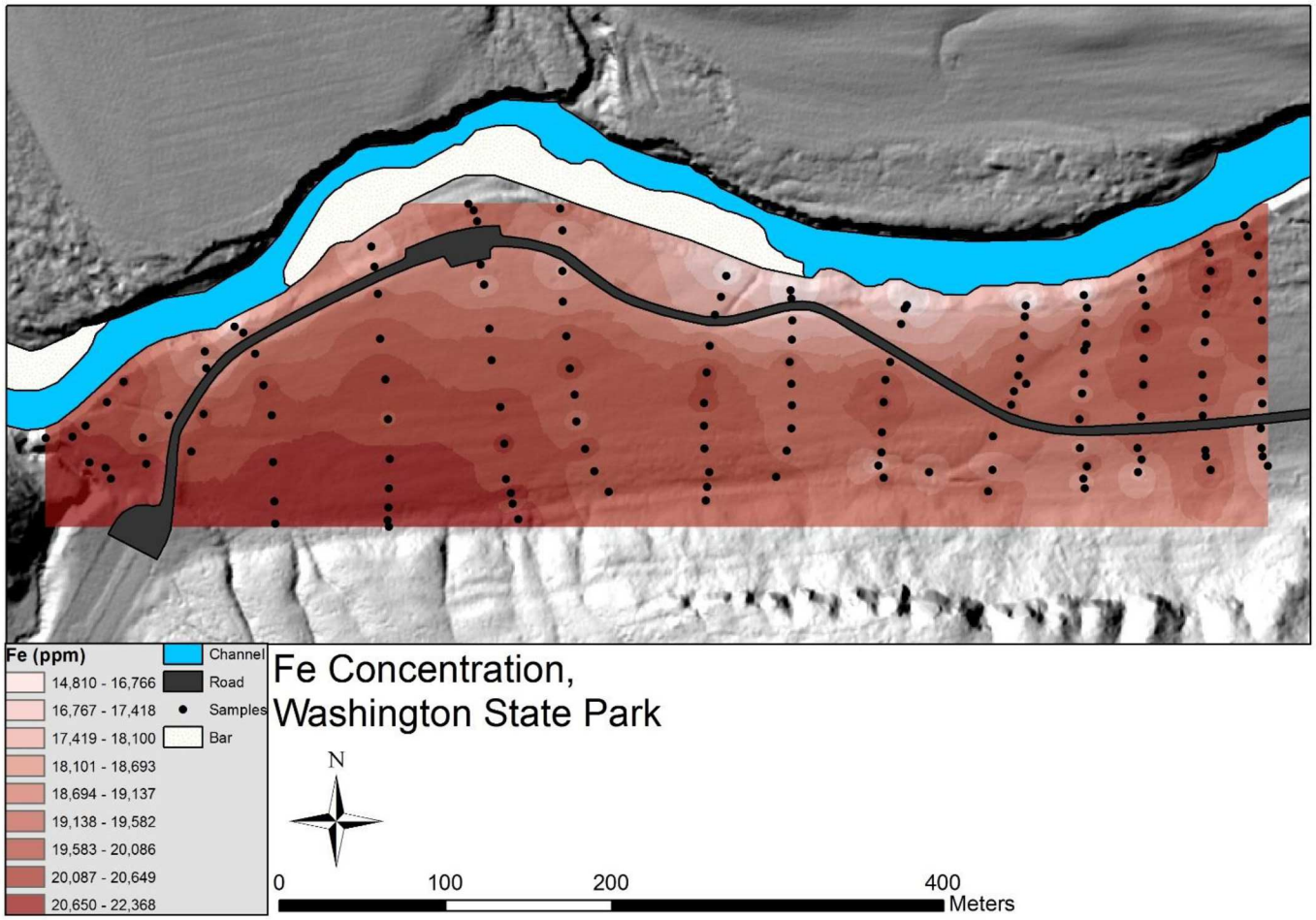

Figure 34 – Fe interpolation at the WSP site.

Geographic Trends

Effects of Source and Proximity to Source. As discussed in chapter one, the general trend in contamination in fluvial systems is a downstream decay in concentrations with increased distance from the source. This is attributed to dilution, tributary input, and storage of sediment in channels and floodplains (Lecce and Pavlowsky, 2001; Axtmann and Luoma, 1991). However, upon looking at contamination trends in floodplains in the Big River, it becomes apparent that there are more factors affecting longitudinal trends than strictly distance from the source.

Among the three sites examined for this study, there is not a consistent pattern of decay of Pb as expected (Figure 35). Beginning at the Big River/Flat River confluence site and moving approximately 14.5 river kilometers downstream to St. Francois State Park, there is a 34% decrease in mean Pb concentration in floodplain surface soils. This shows expected downstream decrease; however, in another 38.5 river kilometers downstream at Washington State Park, there is a 134% increase in mean Pb concentration. Recalling Washington State Park had the highest average lead concentrations of any of the three sites, and is the farthest away from the source.

Since mining tailings in the Old Lead Belt contain both zinc and lead (Smith and Schumacher 1993), it would be expected to see the same longitudinal trends between the two elements. Zinc concentrations do decay between the confluence and St. Francois State Park, and then increase at Washington State Park (Figure 35). Concentrations decrease 71% from the Big River/Flat River confluence to St. Francois State Park, then increase to a smaller degree from St. Francois State Park to Washington State. Unlike with lead, Washington State Park does not have the highest Zn concentrations; there is a

51% decrease from the Big River/Flat River confluence. The difference in relative concentrations of Zn and Pb longitudinally is due to both the difference in tailing geochemical signatures between piles along the Flat River and the Big River, and background dilution of Zn from natural sediment.

Calcium concentrations see a significant decay downstream of the Big River/Flat River confluence (Figure 35). Mean Ca concentrations are roughly 20,000 ppm higher at the Big River/Flat River confluence than the other two sites. Iron concentrations remain relatively unchanged across the three study sites, likely because Fe is present in natural sediment (Figure 35).

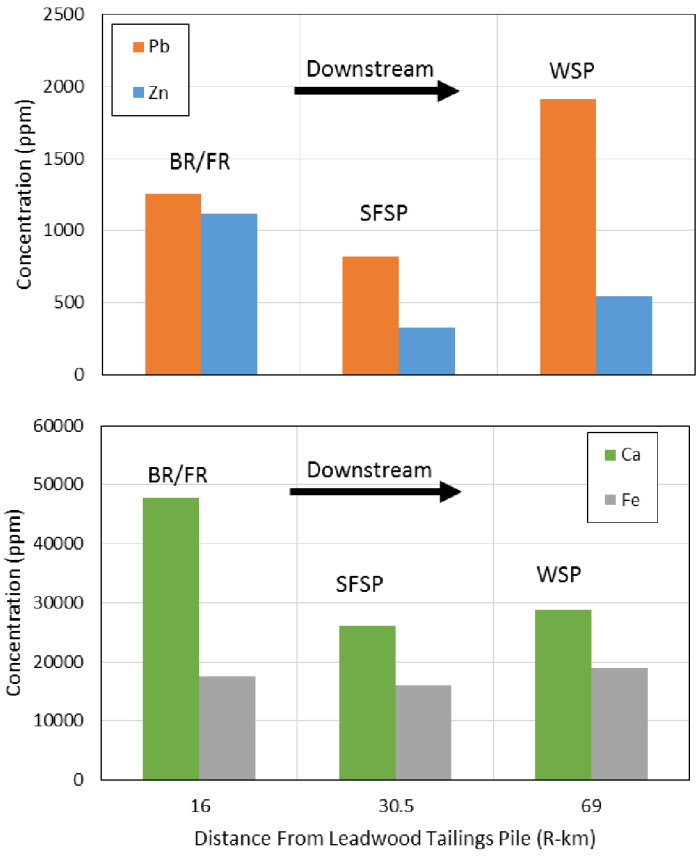

Figure 35 – Geochemistry in relation to river kilometer below Leadwood tailings pile.

Effects of Downstream Sorting. Grain size is an important factor in the distribution trends of these elements. Fine-grained sediment has: more downstream mobility than coarse sediment, the highest concentrations of Pb in mining contaminants, and more lateral mobility across floodplains making it important in surface soil contamination (Axtmann and Luoma, 1991; Lecce and Pavlowsky, 2001). Since fine-grained materials can remain entrained within the river for greater distances, significant mining sediment with high Pb concentrations, can be transported the as far downstream as Washington State Park and spread across the floodplain during floods. The ability for fine-grained sediment to remain entrained within the stream, allows for a large longitudinal extent of heavy metal contamination. This mobility of fine-grained materials, paired with the large floodplain area for sedimentation, allows for high concentrations to accumulate at Washington State Park.

Conversely, coarser fractions of mining sediment will be limited in mobility, and consequently remain in the upstream segments of the stream. This paired with the proximity to the source is the reason mean Ca concentrations are so much higher at the Big River/Flat River confluence than downstream. Sand deposition from the coarser mining sediment is high in Ca, and represents the main source of Ca for the stream. High Ca concentrations will be more limited longitudinally due to the limits on the streams ability to transport this coarser fraction, hence the significant decay.

Effects of Valley Width. St. Francois State Park has significantly lower concentrations in Pb than both Washington State Park and the Big River/Flat River confluence, and it is located in between the two sites. This can best be explained by valley width. St. Francois State Park has a valley width more than four times smaller than

the Big River/Flat River confluence site, and more than five times smaller than the Washington State Park site. The resulting narrower floodplain will tend to transport more sediment downstream with limited floodplain area for storage, whereas the wider valleys at the other two sites will deposit more sediment and have the ability to store higher concentrations of contaminants (Figure 36). This trend indicates that valley width plays a significant factor in longitudinal distribution of floodplain contamination, and is the reason for high concentrations in the wide valley at Washington State Park (Leece and Pavlowsky, 2015; Howard, 1996; Magilligan, 1985).

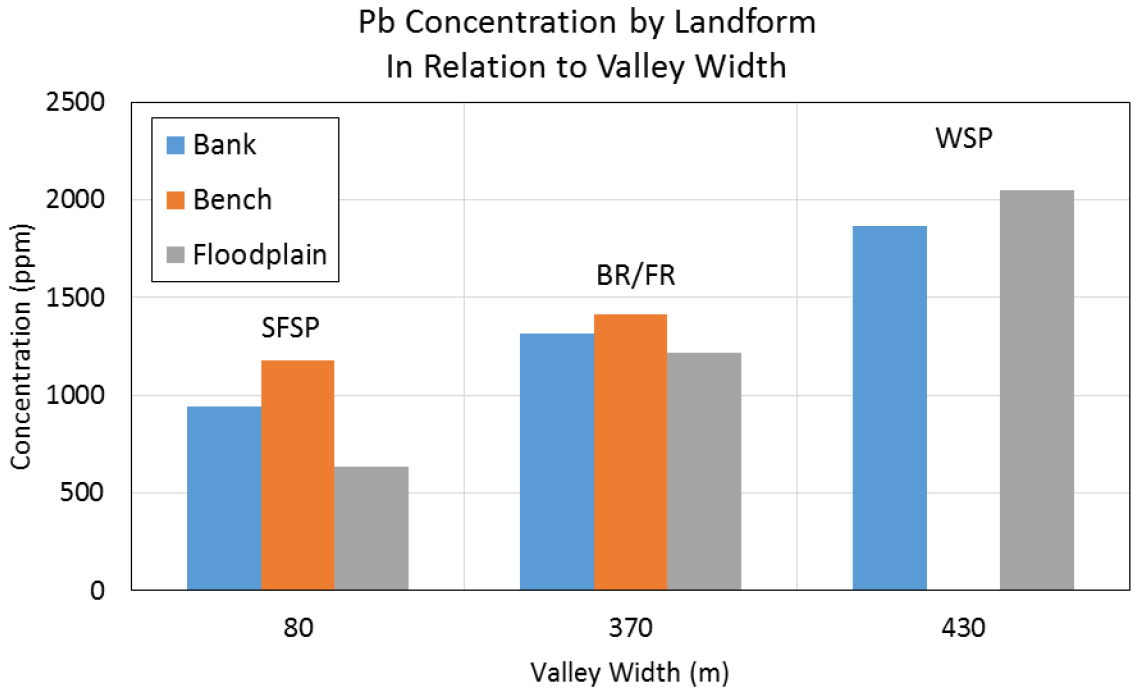

Figure 36 – Pb concentration by landform in relation to valley width.

Spatial and Geochemical Variables and Pb Concentrations

On a smaller scale, there are variations in geochemistry seen across floodplain landforms. Contamination is summarized by landform in Chapter 4, but in order to quantify the spatial patterns of Pb concentrations across a study site, it is important to examine the physical and geochemical characteristics of the landscape in order to look for correlation between them and Pb concentration. Correlation matrices between Pb and elevation, distance from the channel, Ca and Fe were created for two sample groupings. One grouping included all samples at a study site, and the other was a subsample of only samples in the floodplain class to see if correlation coefficients varied with the largest landform kept constant. At the Big River/Flat River confluence, the floodplain and disturbed classes were combined for the subsample. Pearson coefficients relating Pb concentrations to these variables are displayed in Figures 37, 38, and 39. Floodplain subsamples showed the same trends as the grouping with all the samples at all sites for all variables except distance from the channel at Washington State Park. In general, correlation coefficients were stronger at St. Francois State park where variability is higher (CV = 55%), than at the Big River/Flat River Confluence (CV = 29%) and Washington State Park (CV = 21%).

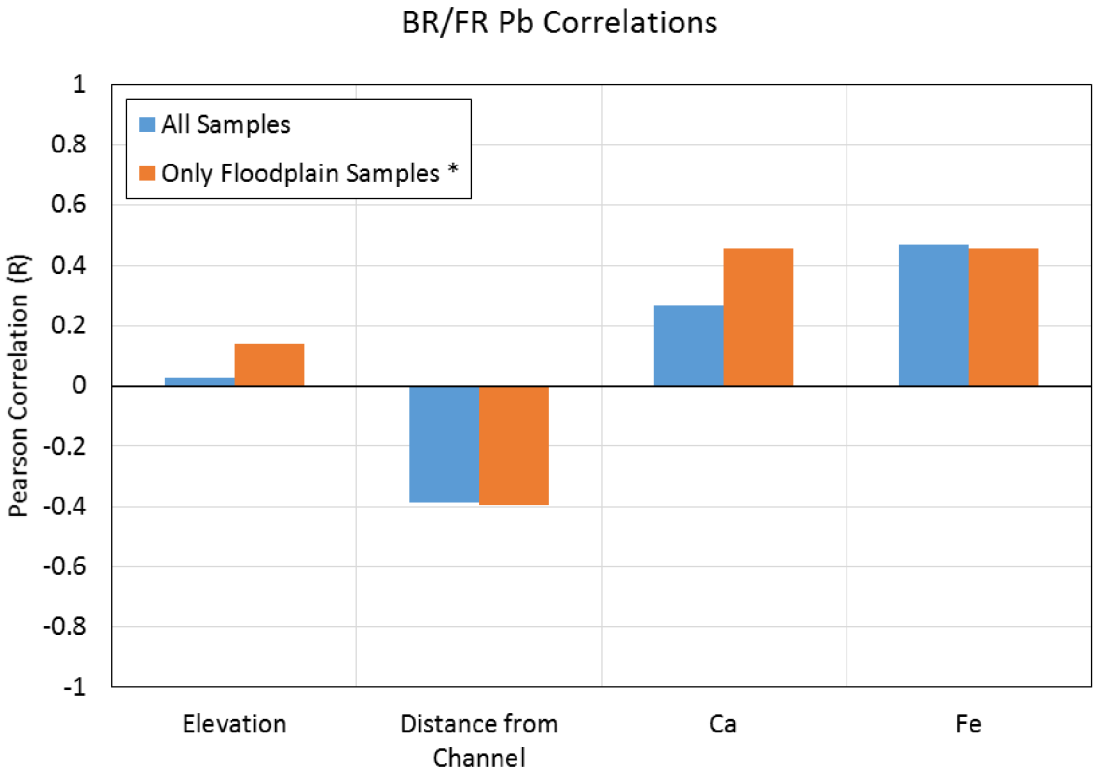

Figure 37 – Pearson correlation coefficients for Pb with elevation, distance from the channel, Ca, and Fe at the BR/FR site.

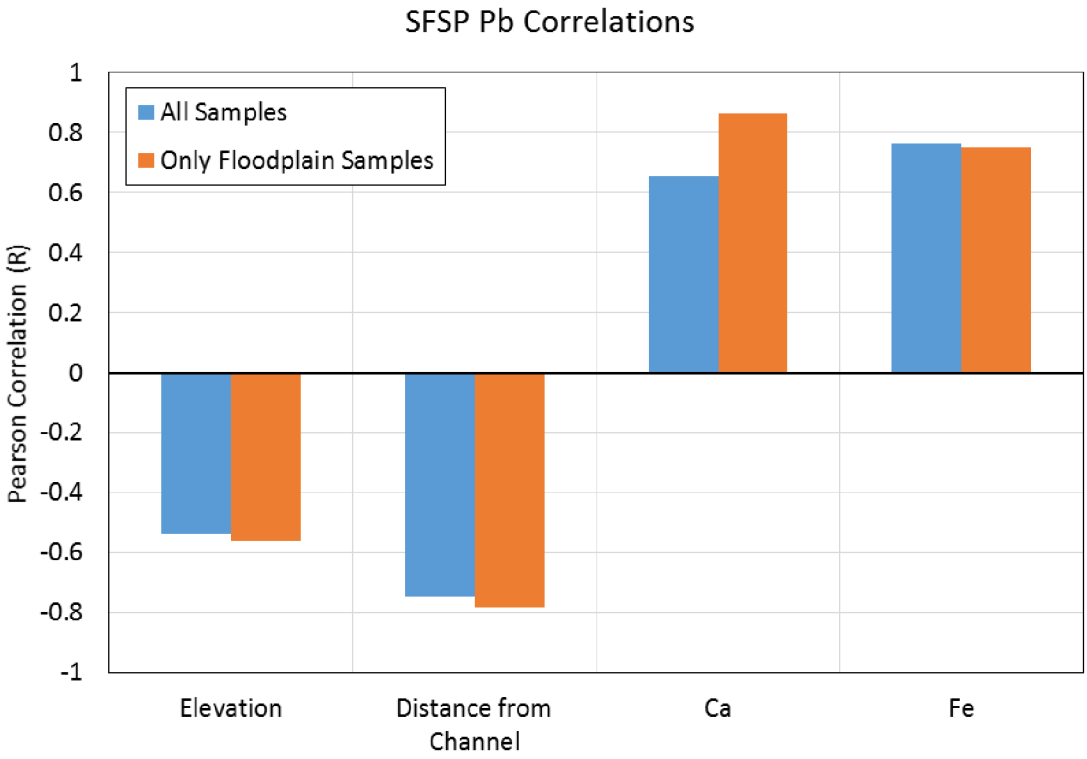

Figure 38 – Pearson correlation coefficients for Pb with elevation, distance from the channel, Ca, and Fe at the SFSP site.

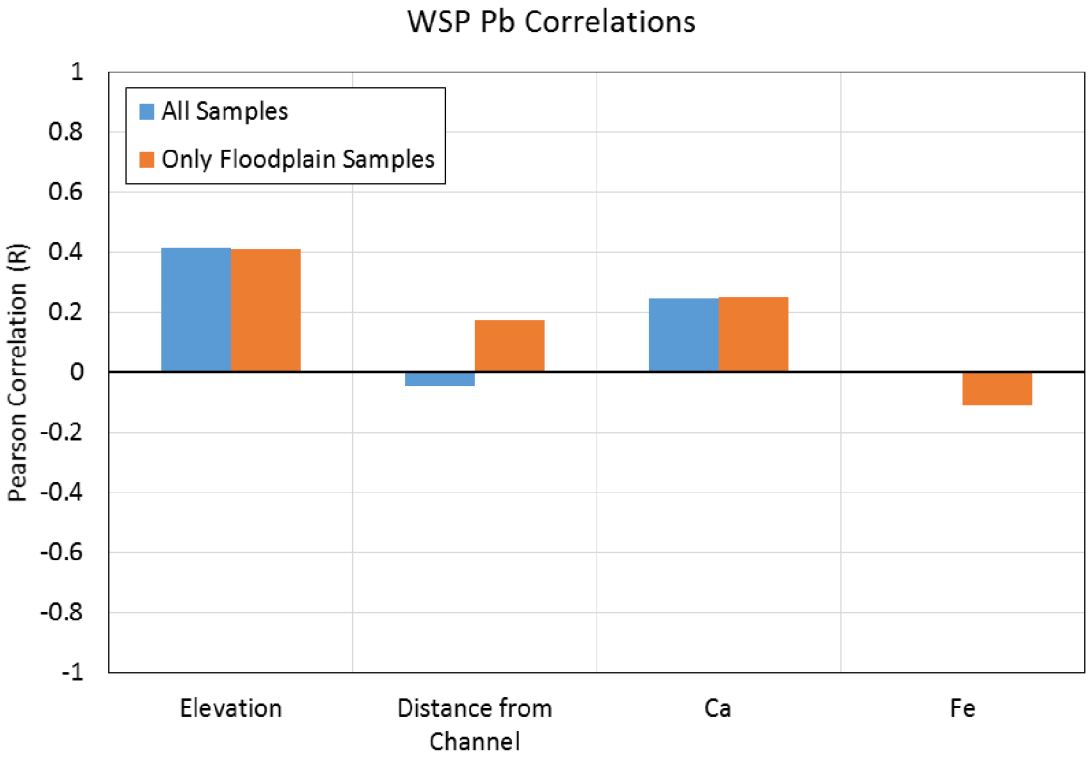

Figure 39 – Pearson correlation coefficients for Pb with elevation, distance from the channel, Ca, and Fe at the WSP site.

Elevation Correlation. At the Big River/Flat River confluence, Pearson correlation coefficients for elevation are weakly positive showing no significant correlation. At St. Francois State Park, coefficients are significantly negative indicating a decrease in Pb concentrations with increasing elevation. At Washington State Park, coefficients are significantly positive, meaning increasing elevation corresponds with increased Pb concentrations.

As described in Chapter 1, there is an expectation that landforms at higher elevation would have a lessened flooding frequency, thus depositing less contaminated

sediment (Chen et al., 2012; Howard, 1996; Ciszewski and Malik, 2004). Lower elevation landforms would conversely be inundated more frequently, and an increased deposition of contaminated sediment would be expected. Therefore, elevation theoretically should be inversely related to Pb concentrations on Big River floodplains.

At the Big River/Flat River site, the correlation is negative as expected, but is not significant, likely due to the variation of hydrologic conditions at similar elevation landforms. The small channelized area that connects the Big River excavated/disturbed basin to the channel is at a similar low elevation to the basin in the disturbed area. The channelized flows will likely scour and prevent significant deposition, whereas the ability for sediment to settle in the disturbed basin will allow for increased deposition (Howard, 1996). The variable flows will likely cause a difference among Pb contaminant concentrations at similar elevations, thus weakening the elevation-Pb relationship by adding spatial variability. At St. Francois State Park, the negative correlation is highly significant. This is likely related to the rapid elevation rise in the narrow valley limiting sediment deposition in the upper floodplain. At Washington State Park, the correlation between these variables is positive and opposite of what was expected from the literature. Higher landform elevations were correlated with an increase in Pb concentrations. This is likely due to the chute/drainage influence at this site. These areas occur at the lowest elevations within the study site and have lower concentrations of Pb than floodplain surfaces. This could be due to channelized scouring in the chute during inundation (Howard, 1996), and the dilution of contaminants from upland erosion by the drainage off nearby hillslopes (Lecce and Pavlowsky et al, 2001). Higher, non-channelized

floodplains at this site will allow for sediment to settle out under lower velocity conditions, and thus there is higher concentrations in the higher elevation floodplain unit.

Distance to the Channel Correlation. Distance from the channel shows a significant negative relationship with Pb concentrations at St. Francois State Park and the Big River/Flat River confluence. At Washington State Park, coefficients for the grouping with all of the samples is insignificant and negative, and the coefficient for the floodplain grouping shows an insignificant positive trend.

It is expected that the soil metal concentration would be highest at locations closer to the river and decrease away due to deposition losses and dilution from valley slope sediment. Overbank flows will lose sediment transport capacity as they flow over a floodplain, so increased deposition and the resulting higher concentrations are expected to be closer to the channel (Chen et al., 2012; Middelkoop, 2000). Therefore, Pb concentration should be inversely related to distance from the channel.

At the Big River/Flat River site, distance from the channel is significantly negatively correlated with soil Pb concentrations (Figure 37). The bench has a recurrence interval of less than a year, meaning it has the potential to receive contaminated sediment more frequently than higher areas. The road, which is inundated with larger floods of 1.5-2 year recurrence intervals, would limit access of sediment transport in overbank flows to the disturbed area/floodplain. As discussed in earlier, the majority of sediment deposited in the disturbed area/floodplain would occur when the southern end of the study area is inundated every 1.05-1.25 years. These factors would likely cause the declining contamination seen with distance from the channel. At St. Francois State Park, the strong inverse relationship is likely related to the narrow valley (Figure 38). Contaminated

sediment would be limited to areas closer to the channel because of the valley confinement (Howard, 1996; Leece and Pavlowsky, 2014). Finally, at Washington State Park, the weak correlations are likely due to the general lack of variability in Pb concentrations across the study site (Figure 29) (CV = 21%). High concentrations across the site, likely related to the increased deposition rates associated with a wide valley, tend to mask the small variability making correlations largely insignificant.

Geochemical Correlations. Coefficients for Ca and Pb concentrations at all sites for both groupings are positive and significant. Coefficients for Fe and Pb concentrations, the Big River/Flat River confluence show a significant positive relationship when all samples are used, but a significant negative relationship when only floodplain samples are used (Figure 37). St. Francois State Park has high coefficients in both subgroups for Fe (Figure 38), and Washington State Park does not show any significant correlation for either subgroup (Figure 39).

Calcium content in the Big River is related to dolomite tailings containing significant amounts of Pb (Smith and Schumacher, 1993). Therefore, Ca content can likely be a proxy for tailings deposition on floodplains. Iron can be related to both natural Fe/Mn-oxides and clays which can absorb heavy metals (Laing et al., 2009; Schröder et al., 2008; Smith and Schumacher, 1993). Therefore, positive relationships are expected between Pb and both Ca and Fe in mining affected environments.

At the Big River/Flat River confluence, Ca shows a significant positive relationship with Pb as expected, likely related to the high availability both coarse and fine-grained tailings due to the proximity to the tailings piles. With Fe, the expected positive relationship is observed and was and significant. This is likely related to fine

grained deposition in the disturbed area. A more detailed chemical analysis of Fe is needed for a better understanding of this relationship. At St. Francois St. Park, the relationships are as expected and strong. This is likely to Fe/Mn-oxides and clays in the bench. At Washington State Park, the relationship for Ca was significant, again likely due to mine tailing deposition close to the channel as previously noted. With Fe, the insignificant relationship may be due to both input of Fe from upland erosion, and the general lack of variability discussed in the last section.

Overall, these correlations indicate that with increased complexity in floodplain morphology, comes an increased complexity in floodplain hydrology and consequently contaminated sediment deposition patterns. Narrow valley floodplains such as St. Francois State Park produce the expected relationships, while wider floodplains like the Big River/Flat River confluence and Washington State Park tend to have a more complex planform with chutes and drainage features causing weaker relationships.

Stepwise Regression Analysis

Since no single variable accurately explains the variation in Pb contamination, multiple linear regression analysis was conducted in order to determine if multiple variables together could explain the Pb variability. The most significant models were developed by evaluating results using multiple variables in both logarithmic and arithmetic forms. The best model had the highest Pearson R^2 value with a small standard estimate of error, an α value less than 0.05 for each variable, and no significant multicollinearity problems. Table 10 displays preliminary models with all samples and Table 11 displays results with the removal of possible outliers (Rogerson, 2010).

Table 10 – Regression equations for Pb variability.

Site	Dept. Variable	n	R^2	S.E of Est.	b_0	b_1	b_2	b_3	b_4
BR/FR	Log(Pb)	162	0.412	0.116	-4.252	0.352 *Log(Ca)* *α = 0.000*	1.351 *Log(Fe)* *α = 0.000*		
SFSP	Log(Pb)	131	0.839	0.131	-81.299	33.783 *Log(Elev)* *α = 0.001*	-0.011 *Dist* *α = 0.000*	1.691 *Log (Fe)* *α = 0.000*	
WSP	Log(Pb)	148	0.462	0.042	-7.270	0.034 *Elev* *α = 0.000*	0.029 *Log(Dist)* *α = 0.000*	0.796 *Log(Fe)* *α = 0.000*	0.294 *Log(Ca)* *α = 0.000*

[a]Regression equation form: $Y = b_0 + b_1X_1 + b_2X_2 + b_3X_3 + b_4X_4$

[b]Independent variables: Ca = Calcium; Fe = Iron; Elev = Elevation; Dist = Distance to the levee

Table 11 – Regression equations for Pb variability without possible outliers.

Site	Dept. Variable	n	R^2	S.E. of Est.	b_0	b_1	b_2	b_3	b_4
BR/FR	Log(Pb)	159	0.386	0.091	-4.387	0.225 *Log(Ca)* *α = 0.000*	1.521 *Log(Fe)* *α = 0.000*		
SFSP	Log(Pb)	131	0.839	0.131	-81.299	33.783 *Log(Elev)* *α = 0.001*	-0.011 *Dist* *α = 0.000*	1.691 *Log (Fe)* *α = 0.000*	
WSP	Log(Pb)	146	0.449	0.039	-5.871	0.031 *Elev* *α = 0.000*	0.027 *Log(Dist)* *α = 0.000*	0.608 *Log(Fe)* *α = 0.000*	0.272 *Log(Ca)* *α = 0.000*

[a]Regression equation form: $Y = b_0 + b_1X_1 + b_2X_2 + b_3X_3 + b_4X_4$

[b]Independent variables: Ca = Calcium; Fe = Iron; Elev = Elevation; Dist = Distance to the levee

At the Big River/Flat River confluence, spatial variables were not significant in the distribution Pb concentrations. This is likely due to the anthropogenic alteration of landscape in the disturbed areas, as well as the complexity of floodplain planform including the development of chutes, and the two different sources of contaminated sediment (Hupp et al., 2015; Pavlowsky, et al., 2010a; Howard, 1996). The best model still only accounted for 41% of the variability using Ca and Fe indicating geochemistry as a proxy for tailings and fine-grained sediment may provide some explanation for Pb distribution.

At St. Francois State Park, a much more significant model was created for Pb contamination. As expected, due to the narrow confining valley, elevation and distance from the channel were important variables (Magilligan, 1985; Leece and Pavlowsky, 2001). The rapid rise in elevation away from the channel significantly controlled the deposition of contaminated sediment in the areas farther from the channel. By adding in Fe, this model was further improved. When looking at both Pb (Figure 25) and Fe (Figure 28) interpolation maps, it is clear that the highest concentrations of both elements were found in the bench in a very similar looking spatial distribution, indicating the possible correlation between Fe/Mn-oxides or Fe tailings signatures correlating with Pb. It is possible that significant clay content may be present in the bench, and could be investigated further in future studies (Smith and Schumacher, 1993; Schröder et al., 2008; Laing et al., 2009).

At Washington State Park, the best model included all variables, both geochemical and spatial. As seen in the correlation analysis, distance and elevation were positively related to Pb, as well as Ca and Fe. Each variable was significant and no

multicollinearity problems were found, but overall the model only explained 46% of the variability. This is likely due in part to the presence of the chutes and drainage features adding complexity to the deposition patterns (Hupp et al., 2015; Howard, 1996), as well as the overall high contamination across the floodplain that result in weak relationships between Pb and these variables. High concentrations were fairly uniform across the whole floodplain, making it difficult to model the subtle changes.

Stepwise Analysis with Possible Outliers Removed. Linear regression equations for Pb versus elevation, distance from the channel, Ca, and Fe were developed for each site. Residuals were then plotted in order to further examine relationships between Pb and these variables, and identify possible outliers that may affect the fit of the model. (Rogerson, 2010). Any sample that had a residual that looked much larger than other samples on the plot was considered a possible outlier, and equations were run with and without this sample to see if model fit improved (Table 11).

Three outliers at the Big River/Flat River confluence site were removed based on anomalously high or low values yielding large residuals. One sample was located in the excavation fill, one in the disturbed area, and one in the upland. At St. Francois State Park, no outliers were identified. At Washington State Park, two outliers stood out in residual plots for elevation, distance from the channel, and Ca were removed. One sample was in the bank, and the other was in the drainage feature/chute.

Without the outliers, the models for the Big River/Flat River confluence and Washington State Park were not improved. The R^2 value for the Big River/Flat River confluence decreased by 0.026, and the R^2 value at Washington State Park decreased by 0.013. However, the standard error of the estimate at each site was improved, indicating

the values removed did have an effect on the accuracy of predictions made with the initial regression line.

Summary of Regression Results. Regression modelling showed that it was difficult to use selected spatial and geochemical variables to effectively model the variability across the Big River floodplains. This is likely due to the general lack of variation in these highly contaminated floodplains as indicated by the low coefficients of variation (Figure 40). In using the selected variables for modeling, planform and hydrologic complexity (i.e. chutes and drainage features, and human influence on topography) caused some variation from expected relationships between Pb and selected spatial variables for modeling (elevation, distance from the channel). Natural inputs of Fe which dilute mining input of Fe, and complex relationships between Pb and Ca that are not fully understood, also make geochemical variables used in this study less effective than anticipated.

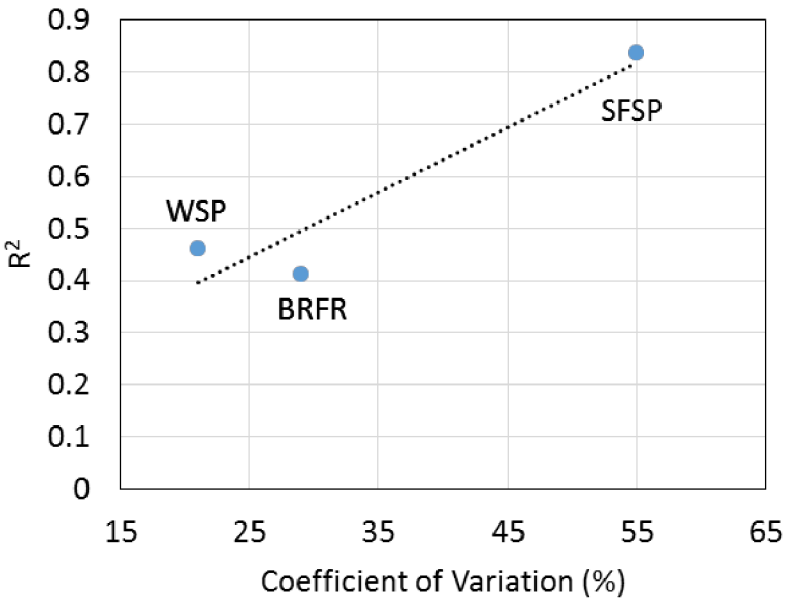

Figure 40 – Relationship between Pb variation and fit of best Pb distribution model.

Implications of Findings

The extent and concentration of Pb concentrations found in this study can pose a significant ecological and health risk to the area. According to the Toxic Substance Control Act, the Pb threshold for soils is 400 ppm where children may be present (EPA, 2015). According to a 2014 report by Stratus Consulting on Missouri mining districts, Pb concentrations above 345 ppm in soils have a reasonable likelihood to cause physiological damage to local songbirds. All three sites studied show Pb contamination concentrations well above these standards with averages of 1,257 ppm at the Big River/Flat River confluence, 820 ppm at St. Francois State Park, and 1,915 ppm at Washington State Park. The excessive Pb in the soil and the potential harm it can cause to wildlife demonstrates the need for effective remediation planning.

Landform concentration summarized by site in Figure 16 also showed how classified landforms differ in contamination concentrations at different study sites. Landform mapping and flood frequency calculations in this study showed that benches and floodplains inundate at < 2 year recurrence intervals and are typically contaminated with Pb to higher levels than other landform classes. Similar findings were found at all three sites in this study, which indicates bench and floodplain landforms throughout the Big River may contain relatively high concentrations of contaminants. Therefore project managers could utilize landform maps with summarized geochemistry to focus remediation efforts on bench and floodplain classifications. These results support findings of Pavlowsky et al., 2010a which reported floodplain Pb contamination for 171 river kilometers from Leadwood to Eureka where the Big River flows into the Meramec River.

Stepwise linear regression results indicated that it was difficult to use selected spatial and geochemical variables to effectively model the variability across the Big River floodplains. This is likely due to the general lack of variation in the highly contaminated floodplains, as indicated by the low coefficients of variation. In using the selected variables for modeling, planform and hydrologic complexity (i.e. chutes and drainage features) caused significant variation from expected relationships between Pb and selected spatial variables for modeling (elevation, distance from the channel). Natural inputs of Fe which dilute mining input of Fe, and complex relationships between Pb and Ca that are not fully understood, also make geochemical variables used in this study less effective than anticipated.

This study suggests that localized "hot spots" of Pb do not occur in surface soils on the Big River floodplains. Contaminated soil areas appear to be extensive and widespread. Therefore, focused remediation planning through floodplain mapping, landform classification, and risk assessment is needed. The use of USDA soil series maps can allow for the general display of contamination extent on the Big River. As described in Pavlowsky, et al, 2010a, Kaintuck, Haymond, Wilbur, and Sturkie soil series are contaminated with heavy metals. Contaminated soil samples in this study were predominately located within mapped Kaintuck and Haymond series, and unmapped Wilbur series areas. In the 171 river kilometers of Big River floodplain, mapped Haymond and Kaintuck series cover an area of approximately 25 and 8 km^2 respectively. If these series are assumed to be contaminated to a similar extent as what was found in this study, these soils represent 36 km^2 of contaminated soil area. While this study did not collect samples mapped as the Wilbur or Sturkie series, Pavlowsky et al., 2010a

described these soil series as high floodplains and low terraces, respectively. If these soils represent the same landforms as the landforms sampled in this study, then it can be assumed these series are highly contaminated as well. This means that between the Kaintuck, Haymond, Wilbur, and Sturkie soil series, there is a total of approximately 39 km^2 of contaminated soils may be located on Big River floodplains below the tailings piles in St. Francois, Washington, and Jefferson Counties, Missouri. The use of landform maps and soil series in conjunction can provide a preliminary indicator of mining-related contamination.

CHAPTER 5 – SUMMARY AND CONCLUSIONS

Lead contamination in the Big River from historical mining activity has been extensively studied in order to quantify the extent of contamination (Pavlowsky et al., 2010a; Meneau, 1997; Smith and Schumacher 1993; Mosby et al., 2009; Young, 2011). Large volumes of contaminated sediment were discharged into the Big River by historical mining activities since 1892, where it has been transported downstream, reworked by fluvial processes, and deposited in floodplain and channel areas. Floodplains are a significant sink for fine-grained contaminated sediment and can pose a serious long-term pollution problem to streams. Floodplains along the Big River have been found to contain significant concentrations of heavy metals for 171 kilometers downstream of Leadwood, MO (Pavlowsky et al., 2010a). Ongoing remediation efforts have been underway to mitigate the ecological damage. However, more information on site-scale trends in heavy metals across floodplain surfaces is needed to be studied in order to develop the most effective remediation plans.

Elevation data and field observations were used to develop geomorphic maps of floodplain landforms at three approximately 1 kilometer long sites along the Big River. One site was at the Big River/Flat River confluence, 16 km downstream of the Leadwood tailings pile, and represents a moderately wide floodplain with a human-altered floodplain through excavation. The second study site was at St. Francois State Park, 30.5 kilometers downstream of the Leadwood tailings pile, and represents a narrow floodplain with a confining valley. The last study site was at Washington State Park, 69 kilometers downstream of the Leadwood tailings pile, and represents a wide valley and floodplain.

Lead concentrations were quantified for each study site by collecting and analyzing 468 top soil samples. Geochemical data was then used to develop interpolation maps for the examination of spatial trends of contaminants.

Using correlation and regression analysis, spatial and geochemical variables were used to model Pb concentrations across each site. Elevation, distance from the channel, calcium concentrations, and iron concentrations were used to model variations in Pb at all three sites. Based on previous studies, an increase in elevation, and an increase in the distance from the channel should be related to a decrease in Pb (Chen et al., 2012; Howard, 1996; Ciszewski and Malik, 2004; Owen et al, 2011; Middelkoop, 2000). Increases in Ca and Fe should be related to an increase in Pb in sediment related to the tailing input in the Big River (Smith and Schumacher, 1993; Pavlowsky et al., 2010a).

Average lead concentrations at the Big River/Flat River confluence, St Francois State Park, and Washington State Park were 1,257, 820, and 1,915 ppm respectively. Variation at the Big River/Flat River confluence and Washington State Park was small with coefficients of variation of 29% and 21% respectively. At St. Francois State Park, significantly more variation in Pb was found, with a coefficient of variation of 55%. At all three sites, benches and floodplains were found to have high concentrations of Pb, while chutes and drainage features were found to have low concentrations.

Geographic and physiographic controls such as distance from the source and valley width played a more important role in explaining the degree of contamination at a site compared to site-specific controls. While variation was minimal at a single site, notable differences in mean Pb concentrations at the three different sites were found (CV = 21 to 55%). Much of the variation between sites was interpreted to be a result of valley

width (Howard, 1996). Narrow valleys such as St. Francois State Park tend to transport contaminated sediment downstream and deposit less on floodplain surfaces. Wider valleys, such as Washington State Park and the Big River/Flat River confluence, act as significant sinks for contaminants and consequently have much higher concentrations of Pb (Howard, 1996; Leece and Pavlowsky, 2001).

Using elevation, distance from the channel, Ca, and Fe as independent variables, it proved difficult to develop effective models that explained the variability in Pb across a floodplain using stepwise regression. Much of this difficulty can be explained by the lack of variation in Pb concentrations at a site. With the low CV values at the Big River/Flat River confluence and Washington State Park, models only accounted for 41% and 46% of the variation in Pb concentrations respectively. The limited variation in dependent variables, paired with hydrologic and geomorphic complexities associated with the development of chutes and drainage features made it difficult to create effective predictive models. Ultimately, the spatial distribution of floodplain contamination was relatively uniform making within-site modelling largely ineffective using methods of this study.

United State Department of Agriculture soil series which correlate with areas sampled in this study, and areas related to landforms mapped in this study suggest that an estimated 39 km^2 of floodplain soils along 171 river kilometers of the Big River may be highly contaminated with Pb to a level of serious risk to both riparian ecosystems and human health (EPA, 2015; Stratus, 2014).

Key Findings

The key findings of this study include:

1) Top soil deposits along the Big River are highly contaminated with heavy metals from historical mining activity. The Environmental Protection Agency threshold for lead in soils where children are present is 400 ppm, and mean Pb concentrations found at three different floodplain sites ranged from 820-1915 ppm, indicating a significant threat to human and riparian ecosytem health;

2) Low floodplain surfaces such as benches contain some of the highest concentrations of Pb measured in this study. Increased flood frequency of these surfaces allow for more contaminated sediment to be deposited in these areas, and consequently tend to be the most contaminated;

3) The development of chute and drainages features, as well as human influence on topography, create complex hydrology and geomorphology patterns which affect the spatial distribution of contaminated sediment across a floodplain. Specifically, chute and drainage features where flow velocity is high can cause scour and dilution of contaminated sediment, causing a decrease in contamination in these areas;

4) Valley width controls that affect sedimentation rates on floodplains also similarly affect contamination levels and variation among sites. Wider valleys in general have a tendency to accrete more sediment, consequently sites with wider valleys accumulate higher concentrations of contamination, whereas sites with narrow valleys tend to transport more contamination downstream;

5) Low variability of Pb concentrations across floodplains studied made significant linear regression modeling difficult, especially in wide-valley floodplains;

6) The best regression models for sites with a wider floodplain, Washington State Park and the Big River/Flat River confluence, yielded models with R^2 values of 0.46 and 0.41 respectively. However, at the narrow floodplain site at St. Francois State Park, models were more effective in describing the variability ($R^2 = 0.84$);

7) Soil series associated with contamination concentrations found in this study are mapped on Big River floodplains for 39 km^2 and could likely represent areas of significant contamination. Using soils series maps and floodplain maps, a better understanding of contamination distribution may be estimated.

Future Work

This study provided a more detailed analysis of the spatial trends and the factors controlling contaminant distribution along Big River floodplains. However, it is important to assess the methodology used in this study and discuss future work that needs to be conducted in order to better understand the ecological risks surrounding Big River floodplain contamination. Interpolation maps used in this study allowed for the visualization of contamination trends across the study site. This was a beneficial technique to qualitatively view geochemical variations at a site for the purpose of interpreting geomorphic controls. However, if spatial continuity with higher accuracy is desired, comparison of interpolated concentration values to collected control values needs to done. This can be accomplished through cross validation techniques. Samples collected would be divided into two subgroups. One subgroup would be used to run the interpolation calculation, and the other subgroup would be used to compare to interpolated values. This allows for the calculation of the error between the predicted sample from the interpolation and a known control point (O'Sullivan and Unwin, 2010; Kravchenko, 2003; Gotway et al., 1995). Future studies should consider the use of cross validation to ensure accuracy to the degree desired. Previous studies have shown a relationship between grain size and contamination (Pavlowsky et al., 2010b; Axtmann and Luoma, 1991). Models in the Big River may be improved by adding the grain size as an independent variable in regression analysis, and should be considered in future studies. Other geospatial modelling methods could also be explored such as geographically weighted regression (GWR). Geographically weighted regression allows for the development of models with a consideration of spatial heterogeneity (Zhang et al., 2009;

Brunson et al., 1996). Exploring these ideas may improve the results of this study to better understand and model distribution of heavy metals in Big River floodplain surfaces.

REFERENCES

Adamski, J.C., Petersen, J.C., Freiwald, D.A., Davis, J.V., 1995. Environmental and hydrologic setting of the Ozark Plateau study unit, Arkansas, Kansas, Missouri, and Oklahoma. U.S. Geological Survey. Water-Resources Investigations Report 94-4022.

Appleton, J. D., Williams, T. M., Orbea H., Carrasco, M., 2001. Fluvial contamination associated with artisanal gold mining in the Ponce Enriquez, Portovelo-Zaruma and Nambija Areas, Ecuador. Water, Air, and Soil Pollution 131 (1-4), 19-39.

Andronikov, S.V., Davidson, D.A., Spiers, R.B., 2000. Variability in contamination by heavy metals: sampling implications. Water, Air, and Soil Pollution 120 (1-2), 29-45.

Axtmann, E.V., Luoma, S.N., 1991. Large-scale distribution of metal contamination in the fine-grained sediments of the Clark Fork River, Montana, U.S.A. Applied Geochemistry 6, 75-88.

Box, J.B., Mossa, J., 1999. Sediment, land use, and freshwater mussels: prospects and problems. Journal of the North American Benthological Society 18 (1), 99-117.

Bradley, D.C., Leach, D.L., 2003. Tectonic controls of Mississippi Valley-type lead-zinc mineralization in orogenic forelands. Mineralium Deposita 38, 652-667.

Bretz, J.H., 1962. Dynamic equilibrium and the Ozark land Forms. American Journal of Science 260, 427-438.

Brewer, P.A., Taylor, M.P., 1997. The spatial distribution of heavy metal contaminated sediment across terraced floodplains. Catena 30, 229-249.

Brunsdon, C., Fotheringham, A.S., Carlton, M.E., 1996. Geographically weighted regression: A method for exploring spatial nonstationary. Geographical Analysis 28 (4), 281-298.

Bussiere, B., 2007. Colloquium 2004: Hydrogeotechnical properties of hard rock tailings from metal mines and emerging geoenvironmental disposal approaches. Canadian Geotechnical Journal 44, 1019-1052.

Chen Y., Liu, Y., Liu, Y., Liu, A., Kong, X., Liu, D., Li, X., Zhang, Y., Gao, Y., Wang D., 2012. Mapping of CU and Pb contaminants in soil using combined geochemistry, topography, and remote sensing: A case study in the Le'an River floodplain, China. International Journal of Environmental Research and Public Health 9 (5), 1874-1886.

Ciszewski, D., Malik, I., 2004. The use of heavy metal concentrations and dendrochronology in the reconstruction of sediment accumulation, Mala Panew River Valley, southern Poland. Geomorphology 58, 161-174.

Ciszewski, D., Turner, J., 2009. Storage of sediment-associated heavy metals along the channelized Odra River, Poland. Earth Surface Processes and Landforms 34 (4), 558-572.

Clements, W.H., Carlisle, D.M., Lazorchak, J.M., Johnson, P.C., 2000. Heavy metals structure benthic communities in Colorado mountain streams. Ecological Applications 10 (2), 626-638.

Dennis, I. A., Coulthard, T. J., Brewer, P., Macklin, M.G., 2009. The role of floodplains in attenuating contaminated sediment fluxes in formerly mined drainage basins. Earth Surface Processes and Landforms 34 (3), 453-466.

Environmental Protection Agency (EPA), 2015. Regional Screening Levels (RSL) for Chemical Contaminants at Superfund Sites. Retrieved December 3, 2015 from EPA website at http://www.epa.gov/region09/superfund/prg/index.html.

Environmental Protection Agency (EPA), 2007. Field portable x-ray fluorescence spectrometry for the determination of elemental concentrations in soil and sediment. Report for Method 6200, 1-32.

Faulkner, D.J., 1998. Spatially variable historical alluviation and channel incision in West-Central Wisconsin. Annals of the Association of American Geographer 88 (4), 666-685.

Fleming K.L., Westfall, D.G., Bausch, W.C., 2000. Evaluating management zone technology and grid soil sampling for variable rate nitrogen application. Proceedings of the 5th International Conference on Precision, 179-184.

Franke, R., 1981. Scattered Data Interpolation: Tests of Some Methods. Mathematics of Computation, 38 (157), 181-200.

Gäbler H.E., Schneider, J., 1999. Assessment of heavy-metal contamination of floodplain soils due to mining and mineral processing in the Harz Mountains, Germany. Environmental Geology 39 (7), 774-482.

Gazdag, E.R., Sipter, E., 2008. Geochemical Background in Heavy Metals and Human Health Risk Assessment at an Ore Mine Site, Gyöngyösoroszi (North Hungary). Carpathian Journal of Earth and Environmental Sciences 3 (2), 83-92.

Gilvear, D.J., Waters, T.M., Milner, A.M., 1995. Image analysis of aerial photography to quantify changes in channel morphology and instream habitat following placer mining in interior Alaska. Freshwater Biology 34, 389-398.

Gotway, C.A., Ferguson, R.B., Hergert, G.W., Peterson, T.A., 1995. Comparison of Kriging and inverse-distance methods for mapping soil parameters. Soil Science Society of America Journal 60 (4), 1237-1247.

Graf, W. L., 1996. Transport and deposition of plutonium-contaminated sediments by fluvial processes, Los Alamos Canyon, New Mexico. Geological Society of America Bulletin 108 (10), 1342-1355.

Gregg, J.M., Shelton, K.L., 1989. Minor- and trace-element distributions in the Bonneterre Dolomite (Cambrian), southeast Missouri: Evidence for possible multiple-basin fluid sources and pathways during lead-zinc mineralization. Geological Society of America Bullitin 101, 221-230.

Heeren D.M., Mittelstet, A.R., Fox, G.A., Storm, D.E., Al-Madhhachi, A.T., 2012. Using rapid geomorphic assessment to assess streambank stability in Oklahoma Ozark streams. Biological Systems Engineering: Papers and Publications 55 (3), 957-968.

Hohenthal, J., Alho, P., Hyyppa, J., Hyyppa, H., 2011. Laser scanning applications in fluvial studies. Progress in Physical Geography 35 (6), 782-809.

Howard, A.D., 1996. Modelling Channel Evolution and Floodplain Morphology. Floodplain Processes. John Wiley and Sons Ltd., 15-62.

Huggett, R.J., 2007. Fundamentals of Geomorphology: Second Edition, Routledge.

Hupp C.R., Schenk, E.R., Kroes, D.E., Willard, D.A., Townsend, P.A., Peet, R.K., 2015. Patterns of floodplain sediment deposition along the regulated lower Roanoke River, North Carolina: Annual, decadal, centennial scales. Geomorphology 288, 666-680.

Hürkamp, K., Raab, T., Völkel, J., 2009. Lead Pollution of Floodplain Soils in a Historic Mining Area - Age, Distribution and Binding Forms. Water, Air, and Soil Pollution 201 (1-4), 331-345.

International Organization for Standardization (ISO), 2011. Accuracy (trueness and precision) of measurement methods and results – Part 1: Introduction and basic principles. Working document 15725-1, 1-8.

Jacobson, R.B., Primm, A.T., 1994. Historical land-use changes and potential effects on stream disturbance in the Ozark Plateaus, Missouri. U.S. Geological Survey Water-Supply Paper 2484, 1-85.

Jain, V., Fryirs, K., 2008. Where do floodplains begin? The role of total stream power and longitudinal profile form on floodplain initiation process. GSA Bulletin 120 (1), 127-141.

Jones, A.F., Brewer, P. A., Johnstone, E. Macklin, M. G., 2007. High-resolution interpretative geomorphological mapping of river valley environments using airborne LiDAR data. Earth Surface Processes and Landforms 32 (10), 1574-1592.

Kooistra L., Lueven, R.S.E.W., Nienhuis, P.H., Wehrens, R., Buydens, L.M.C., 2001. A procedure for incorporation spatial variability in ecological risk assessment of Dutch River floodplains. Environmental Management 28 (3), 359-373.

Kravchenko, A.N., 2003. Influence of spatial structure on accuracy of interpolation methods. Soil Science Society of America Journal 67, 1564-1571.

Laing, G.D., Rinklebe, J., Vandecasteele, B., Meers, E., Tack, F.M.G., 2009. Trace metal behavior in estuarine and riverine floodplain soils and sediments: A review. Science of the Total Environment 407, 3972-3958.

Leenears, H., Burrough, P.A., Okx, J., 1989. Efficient mapping of heavy metal pollution on floodplains by co-kriging from elevation data. Three Dimensional Applications in GIS, 37-51.

Lecce, S. A., Pavlowsky, R. T., 1997. Storage of mining-related zinc in floodplain sediments, Blue River, Wisconsin. Physical Geography 18 (5), 424-439.

Lecce, S. A., Pavlowsky, R. T., 2001. Use of mining-contaminated sediment tracers to investigate the timing and rates of historical flood plain sedimentation. Geomorphology 38 (1-2), 85-108.

Lecce, S. A., Pavlowsky, R. T., 2014. Floodplain storage of sediment contaminated by mercury and copper from historic gold mining at Gold Hill, North Carolina, USA. Geomorphology 206, 122-132.

Leopold, L.B., Maddock Jr., T., 1953. The Hydraulic Geometry of Stream Channels and Some Physiographic Implications. United States Geologic Survey Professional Paper 252.

Leopold, L.B., 1980. Techniques and interpretation: The sediment studies of G. K. Gilbert. Geological Society of America Special Paper 183, 125-128.

Leopold, L.B., 1994. Flood Hydrology and the Floodplain, in Coping with the Flood: The Next Phase. Water Resources Update Spring issue, 11-15.

Liu, G., Yang, X., 2007. Spatial variability analysis of soil properties within a field. Computer and Computing Technologies in Agriculture 2, 1341-1344.

Macklin, M.G., Brewer, P.A., Hudson-Edwards, K.A., Bird, G., Coulthard, T.J., Dennis, I.A., Lechler, P.J., Miller, J.R., Turner, J.N., 2006. A geomorphological approach

to the management of rivers contaminated by metal mining. Geomorphology 79, 423-447.

Magilligan, F.J., 1985. Historical floodplain sedimentation in the Galena River Basin, Wisconsin and Illinois. Annals of the Association of American Geographers 75 (4), 583-594.

Martin, C.W., 2009. Recent changes in heavy metal storage in flood-plain soils of the Lahn River, central Germany. Environmental Geology 58, 803-814.

McCann, C.M., Gray, N.D., Tourney, J., Davenport, R.J., Wade, M., Finlay, N., Hudson-Edwards, K.A., Johnson, K.L., 2015. Remediation of historically Pb contaminated soil using a model natural Mn oxide waste. Chemosphere 138, 211-215.

Meneau, K.J., 1997. Big River Watershed Inventory and Assessment. Retrieved 15 April, 2015 from Missouri Department of Conservation at http://mdc.mo.gov/fish/wastershed/big/contents.

Middelkoop H., 2000. Heavy-metal pollution of the Rhine and Meuse floodplains in Neatherlands. Neatherlands Journal of Geosciences 79 (4), 411-428.

Miller, J.R., 1996. The role of fluvial geomorphic processes in the dispersal of heavy metals from mine sites. Journal of Geochemical Exploration 58, 101-118.

Missouri Department of Natural Resources (MDNR), 2007. Total Maximum Daily Load Information Sheet: Big River and Flat River Creek. Retrieved November 20, 2014 at http://www.dnr.mo.gov/env/wpp/tmdl/info/2074-2080-2168-big-r-info.pdf.

Mosby, D.E., Weber, J.S., Klahr, F., 2009. Final phase 1 damage assessment plan for the southeast Missouri lead mine district: Big River Mine Tailings Superfund Site, St. Francois County, and Viburnum Trend sites, Reynolds and Iron counties. Retrieved on November 20, 2014 from Missouri Department of Natural Resources at http://dnr.mo.gov/env/hwp/docs/semofinaldraft.pdf.

Nanson, G.C., Croke, J.C., 1992. A genetic classification of floodplains. Geomorphology 4 (6), 459-486.

Notebaert, B., Verstraeten, G., Govers, G., Poesen, J., 2009. Qualitative and quantitative applications of LiDAR imagery in fluvial geomorphology. Earth Surface Processes and Landforms 34 (2), 217-231.

O'Sullivan, D., Unwin, D.J., 2010. Geographic Information Analysis: Second Edition. John Wiley & Sons, Inc.

Owen, M.R., Pavlowsky, R.T., Womble, P.J., 2011. Historical disturbance and contemporary floodplain development along an Ozark river, southwest Missouri. Physical Geography 32 (5), 423-444.

Pavlowsky, R.T., Owen, M.R., Martin, D.J., 2010a. Distribution, geochemistry, and storage of mining sediment in channel and floodplain deposits of the Big River system in St. Francois, Washington, and Jefferson Counties, Missouri. Report prepared for U.S. Fish and Wildlife Service, Columbia Missouri Field Office, Columbia, Missouri.

Pavlowsky, R.T., Lecce, S.A., Bassett, G., Martin, D.J., 2010b. Legacy Hg-Cu contamination of active stream sediments in the Gold Hill Mining District, North Carolina. Southeastern Geographer 50 (4), 503-522.

Pavlowsky, R.T., 2013. Coal-tar pavement sealant use and polycyclic aromatic hydrocarbon contamination in urban stream sediments. Physical Geography 34 (4-5), 392-415.

Phillips J.D., Marden, M., Gomez, B., 2007. Residence time of alluvium in aggrading fluvial systems. Earth Surface Processes and Landforms 32, 307-316.

Piegay, H., Hupp, C.R., Citterio, A., Dufour, S., Moulin, B., Walling, D.E., 2008. Spatial and temporal variability in sedimentation rates associated with cutoff channel infill deposits: Ain River, France. Water Resources Research 44**,** W05420, 1-18.

Rogerson, P.A., 2010. Statistical Methods for Geography: A Student's Guide, Third Edition. Sage Publications Ltd.

Schipper, A.M., Wijnhoven, S., Leuven, R.S.E.W., Ragas, A.M.J., Hendriks, A.J., 2008. Spatial distribution and internal metal concentrations of terrestrial arthropods in a moderately contaminated lowland floodplain along the Rhine River. Environmental Pollution 151, 17-26.

Schröder T.J., van Riemsdijk, W.H., van der Zee, S.E.A.T.M., Vink, J.P.M., 2008. Monitoring and modelling of the solid-solution partitioning of metals as in a river floodplain redox sequence. Applied Geochemistry 23, 2350-2363.

Smith, B.J., Schumacher, F.G., 1993. Surface-Water and Sediment Quality in the Old Lead Belt, southeastern Missouri 1988-89. Report prepared by The U.S. Geological Survey, Rolla Missouri Office, Rolla, Missouri.

Smith E., Naidu, R., Alston, A.M., 1998. Arsenic in the Soil Environment: A Review. Advances in Agronomy 64, 149-195.

Stratus Consulting, 2014. Associating soil lead with adverse effects on songbirds in the Southeast Missouri Mining District. Report prepared for the U.S. Fish and Wildlife Service.

Thonon, I., Middelkoop, H., van der Perk, M., 2007. The influence of floodplain morphology and river works on spatial patterns of overbank deposition. Netherlands Journal of Geosciences 86 (1), 63-75.

United States Department of Agriculture (USDA), 1981. Soil Survey of St. Francois County, Missouri. National Cooperative Soil Survey.

United States Department of Agriculture (USDA), 2000. Soil Survey of Jefferson County, Missouri. National Cooperative Soil Survey.

United States Department of Agriculture (USDA), 2001. Soil Survey of Washington County, Missouri. National Cooperative Soil Survey.

United States Department of Agriculture (USDA), 2002. Horsecreek Series. Retrieved on December 2, 2015 from the National Cooperative Soil Survey at https://soilseries.sc.egov.usda.gov/OSD_Docs/H/HORSECREEK.html.

United States Department of Agriculture (USDA), 2006. Kaintuck Series. Retrieved on December 2, 2015 from the National Cooperative Soil Survey at https://soilseries.sc.egov.usda.gov/OSD_Docs/K/KAINTUCK.html

United States Department of Agriculture (USDA), 2011. Haymond Series. Retrieved on December 2, 2015 from the National Cooperative Soil Survey at https://soilseries.sc.egov.usda.gov/OSD_Docs/H/HAYMOND.html.

United States Department of Agriculture (USDA), 2012. Ogborn Series. Retrieved on December 2, 2015 from the National Cooperative Soil Survey at https://soilseries.sc.egov.usda.gov/OSD_Docs/O/OGBORN.html.

United States Fish and Wildlife Service (USFWS), 2008. Big River mine tailings site, St. Francois County, Missouri. Preassessment Screen and Determination. 1-20.

Ward, A.D., Elliot, W.J., 1995. Environmental Hydrology. CRC Press LLC.

Wolman, M.G., Leopold, L.B., 1957. River flood plains: Some observations on their formation. Geological Survey Professional Paper 282-C.

Xiao, R., Bai, J., Wang, Q., Gao, H., Huang, L., Liu, X., 2011. Assessment of heavy metal contamination of wetland soils from a typical aquatic-terrestrial Ecotone in Haihe River Basin, North China. Clean – Soil, Air, Water 39 (7), 612-618.

Young, B., 2011. Historical channel change and mining-contaminated sediment remobilization in the lower Big River, eastern, Missouri. Master's Thesis for Missouri Start University.

Zhang, L., Zhilhai, M., Luo, G., 2009. An evaluation of spatial autocorrelation and heterogeneity in the residuals of six regression models. Forest Science 55 (6), 533-548.

Zornoza, R., Carmona, D.M., Acosta, J.A., Martinez-Martinez, S., Weiss, N., Faz, A., 2011. The effect of former mining activities on contamination dynamics in sediments, surface water and vegetation in El Avenque Stream, SE Spain. Water Air Soil & Pollution 223, 519-532.

APPENDICES

Appendix A – Sampling Permit, Missouri Department of Natural Resources

MISSOURI
STATE PARKS

April 3, 2015

David Huggins
1029 W Battlefield #D302
Springfield, MO 65807

Dear Mr. Huggins:

Thank you for your application requesting permission to conduct the research *Geospatial Mapping of Soil Properties and Pb Concentration on Floodplains* at St. Francois and Washington State Parks.

Because of natural and culturally significant resources within these state parks, only the designated areas that have been discussed and agreed upon are open to this research. Vehicle access to the project area is restricted to dry weather or dry ground surface conditions in order to avoid rutting and compaction. In the event that cultural (archaeological) resources are identified during the project activities, Missouri State Park's Cultural Resource Management Section (CRMS) will be notified and provided with the location (GPS data and physical description) and depth of the material/features. All archaeological materials located during the project are the property of Missouri State Parks and shall be returned to CRMS for curation.

As stated on the application, it is imperative that you notify the park superintendent or naturalist in advance of each visit and provide two copies of your research results (thesis, papers, reports, lists, etc.) to Ken McCarty, Missouri State Parks, Resource Management and Interpretation Program, PO Box 176, Jefferson City, MO 65102-0176 (ken.mccarty@dnr.mo.gov). Electronic submission is preferable. Your approval begins 4/3/15 and expires 12/31/15.

Please contact us if you have questions or need assistance. We wish you the very best with regard to your research.

Sincerely,

MISSOURI STATE PARKS

Ken McCarty
Chief, Natural Resource Management Section

KM/cc

c: St. Francois State Park Washington State Park

PO Box 176 Jefferson City MO 65102 800-334-6946 mostateparks.com

Missouri State Parks is a division of the Missouri Department of Natural Resources

Appendix B - Sample Geochemistry

Appendix B-1 - Big River/Flat River Confluence Samples

Sample Name	Pb (ppm)	Zn (ppm)	Ca (ppm)	Fe (ppm)
BRDH-1	1,618	1,378	49,169	17,031
BRDH-2	1,560	1,129	42,823	18,040
BRDH-3	1,524	1,181	35,713	19,351
BRDH-4	1,958	1,066	43,492	20,497
BRDH-5	1,639	1,253	48,976	19,226
BRDH-6	1,414	825	27,329	18,646
BRDH-7	698	727	122,316	15,402
BRDH-8	698	569	189,746	20,735
BRDH-9	1,392	1,310	86,757	19,394
BRDH-10	1,397	958	52,772	17,169
BRDH-11	1,240	902	26,103	16,502
BRDH-12	1,384	951	22,730	18,281
BRDH-13	1,453	1,048	28,378	18,375
BRDH-14	1,672	1,111	29,703	19,396
BRDH-15	1,786	1,382	67,943	18,057
BRDH-16	1,078	1,008	95,710	16,295
BRDH-17	1,484	1,165	58,129	18,759
BRDH-18	1,454	1,193	41,523	17,430
BRDH-19	1,536	1,037	39,005	18,594
BRDH-20	1,323	954	37,047	17,551
BRDH-21	1,541	899	35,538	17,468
BRDH-22	1,829	1,261	25,192	16,106
BRDH-23	1,798	1,121	39,287	21,010
BRDH-24	1,502	1,302	28,014	18,379
BRDH-25	1,086	898	26,164	17,686
BRDH-26	1,088	952	19,563	16,952
BRDH-27	952	875	23,060	18,611
BRDH-28	1,237	1,164	30,286	16,279
BRDH-29	1,908	1,767	164,359	23,978
BRDH-30	1,645	1,413	39,326	18,334
BRDH-31	1,826	1,151	54,944	20,491
BRDH-32	1,689	1,050	48,854	18,514
BRDH-33	1,574	1,085	42,215	19,236
BRDH-34	1,070	896	17,854	19,614

Appendix B-1 Continued

Sample Name	Pb (ppm)	Zn (ppm)	Ca (ppm)	Fe (ppm)
BRDH-36	1,557	1,394	36,356	16,704
BRDH-37	936	865	19,150	17,983
BRDH-38	1,243	1,164	28,149	18,544
BRDH-39	736	557	18,530	17,348
BRDH-40	1,382	1,250	123,841	21,216
BRDH-41	1,323	1,576	77,619	15,877
BRDH-42	1,269	1,482	65,672	17,071
BRDH-43	2,203	2,446	29,446	20,235
BRDH-44	1,684	1,754	44,186	17,650
BRDH-45	1,700	1,017	66,076	19,355
BRDH-46	1,298	986	39,414	15,103
BRDH-48	1,159	948	58,754	16,761
BRDH-49	1,367	1,044	35,842	18,324
BRDH-50	1,561	1,012	28,281	18,300
BRDH-51	1,829	1,397	45,955	18,836
BRDH-53	1,109	693	26,248	17,588
BRDH-54	928	722	19,053	16,156
BRDH-55	1,272	1,096	18,691	20,119
BRDH-56	1,130	1,060	23,661	16,989
BRDH-57	1,902	1,978	28,854	17,966
BRDH-59	1,387	1,237	26,063	17,291
BRDH-60	146	172	5,491	17,355
BRDH-61	1,003	790	15,608	18,525
BRDH-62	858	700	14,684	18,572
BRDH-63	1,174	937	72,875	16,010
BRDH-64	1,580	1,631	60,757	18,666
BRDH-65	1,337	1,300	57,213	16,353
BRDH-66	1,281	1,262	53,182	15,433
BRDH-67	1,388	1,175	50,598	16,957
BRDH-68	982	994	25,153	14,508
BRDH-69	1,400	1,025	30,436	18,480
BRDH-70	1,353	1,444	51,231	15,640
BRDH-71	813	961	76,861	14,443
BRDH-72	795	624	19,248	16,749
BRDH-73	681	524	25,030	14,953
BRDH-74	1,230	1,276	41,142	16,272
BRDH-75	826	1,214	64,412	14,185
BRDH-76	1,383	1,219	36,076	17,163

Appendix B-1 Continued

Sample Name	Pb (ppm)	Zn (ppm)	Ca (ppm)	Fe (ppm)
BRDH-78	1,308	1,192	34,274	16,384
BRDH-79	1,320	1,110	27,366	17,929
BRDH-80	869	702	14,194	15,836
BRDH-81	371	263	7,225	13,790
BRDH-82	1,164	950	102,370	18,810
BRDH-83	1,454	1,464	135,038	19,787
BRDH-84	1,017	924	105,812	16,095
BRDH-85	1,777	1,283	57,182	18,949
BRDH-86	1,291	1,503	56,381	16,209
BRDH-87	1,476	1,174	48,427	17,825
BRDH-88	1,352	964	29,268	17,849
BRDH-89	913	858	39,709	20,391
BRDH-90	1,142	936	41,981	17,507
BRDH-91	850	552	35,952	14,789
BRDH-92	1,178	1,039	36,597	16,703
BRDH-94	1,225	1,171	29,530	17,206
BRDH-95	1,259	1,137	27,282	18,448
BRDH-97	1,494	947	30,753	16,783
BRDH-98	237	233	4,298	23,159
BRDH-99	882	649	108,181	24,334
BRDH-100	1,110	490	141,518	19,748
BRDH-101	1,811	1,363	113,602	21,632
BRDH-102	1,394	1,086	57,509	17,832
BRDH-103	1,193	1,298	33,542	16,403
BRDH-104	1,276	1,334	44,074	16,142
BRDH-106	1,123	883	26,031	17,471
BRDH-107	1,122	920	40,002	17,449
BRDH-108	3,264	1,459	126,898	26,514
BRDH-109	926	1,094	31,826	14,853
BRDH-110	1,382	1,243	36,875	15,951
BRDH-111	1,476	1,292	29,843	18,023
BRDH-112	1,269	1,064	30,968	16,401
BRDH-113	1,274	1,141	25,892	17,502
BRDH-114	1,149	1,020	26,235	18,261
BRDH-115	1,141	979	21,513	18,245
BRDH-117	1,268	1,118	41,432	16,375
BRDH-118	1,470	1,158	31,351	17,178
BRDH-119	1,333	1,001	59,559	18,887

Appendix B-1 Continued

Sample Name	Pb (ppm)	Zn (ppm)	Ca (ppm)	Fe (ppm)
BRDH-121	1,107	990	73,839	15,857
BRDH-122	1,190	1,485	72,019	17,022
BRDH-123	1,314	1,742	57,271	17,504
BRDH-124	1,262	1,190	55,343	16,428
BRDH-125	1,290	1,394	56,277	16,514
BRDH-126	827	1,023	71,391	15,072
BRDH-127	1,374	1,380	48,664	15,657
BRDH-128	1,314	1,340	46,326	15,457
BRDH-129	1,243	1,060	40,429	15,669
BRDH-130	1,066	1,061	25,667	17,297
BRDH-131	1,316	1,180	25,842	17,816
BRDH-132	1,129	896	22,474	18,267
BRDH-133	1,091	902	15,134	18,955
BRDH-134	598	510	8,969	19,724
BRDH-135	2,323	1,076	81,870	16,067
BRDH-136	1,184	1,520	117,393	21,695
BRDH-137	1,556	1,236	119,925	18,576
BRDH-138	1,141	992	29,273	17,725
BRDH-139	1,369	1,175	47,033	17,518
BRDH-140	1,532	1,465	43,500	19,416
BRDH-141	999	1,038	47,222	15,519
BRDH-142	1,150	1,040	39,247	16,567
BRDH-143	1,354	1,251	35,966	17,909
BRDH-146	535	488	9,526	18,223
BRDH-147	485	452	9,039	17,643
BRDH-148	1,109	752	118,107	21,344
BRDH-149	1,196	1,389	49,119	16,342
BRDH-150	1,431	1,054	51,816	17,668
BRDH-152	1,654	1,316	54,045	18,128
BRDH-153	1,088	1,158	70,272	16,594
BRDH-154	1,360	1,507	58,910	15,649
BRDH-155	1,215	1,460	52,104	17,236
BRDH-156	1,091	1,569	60,269	15,122
BRDH-157	1,270	1,118	42,766	15,459
BRDH-158	1,105	1,173	37,421	16,679
BRDH-160	1,073	1,206	41,331	15,257
BRDH-161	1,204	1,023	29,910	17,895
BRDH-162	1,173	1,070	25,291	17,221

Appendix B-1 Continued

Sample Name	Pb (ppm)	Zn (ppm)	Ca (ppm)	Fe (ppm)
BRDH-164	1,038	833	19,491	16,906
BRDH-165	1,309	1,128	94,611	19,047
BRDH-166	752	1,470	82,039	14,234
BRDH-167	743	1,392	76,464	12,543
BRDH-168	948	1,122	74,011	15,161
BRDH-169	1,096	1,329	51,934	13,793
BRDH-170	1,239	1,130	59,210	16,041
BRDH-171	860	3,375	83,794	15,937
BRDH-172	1,284	2,287	60,266	15,475
BRDH-173	711	914	103,510	15,035
BRDH-174	1,182	1,343	32,600	15,237
BRDH-47	1,518	1,233	41,778	18,903
BRDH-52	1,000	711	31,205	17,222
BRDH-58	1,177	1,080	22,660	16,769
BRDH-93	1,161	1,142	50,108	16,633
BRDH-96	666	465	14,558	16,597
BRDH-105	1,348	1,029	36,620	15,864
BRDH-116	1,074	884	18,220	18,995
BRDH-145	1,233	1,006	20,230	18,365
BRDH-144	1,267	1,105	21,884	18,367
BRDH-151	1,136	1,202	45,548	17,277
BRDH-159	1,121	1,221	38,852	15,491

Appendix B-2 - St. Francois State Park (DH-1 to DH-132; DH-288 to DH-295), and Washington State Park (DH-133 to DH-287) Samples

Sample Name	Pb (ppm)	Zn (ppm)	Ca (ppm)	Fe (ppm)
DH-1	1,018	495	33,505	18,128
DH-2	926	417	26,306	18,939
DH-3	954	462	23,702	19,752
DH-4	857	363	32,347	16,263
DH-5	921	399	20,076	18,458
DH-6	1,092	414	37,484	16,821
DH-7	1,366	492	39,746	17,526
DH-8	1,428	476	35,160	18,091
DH-9	435	379	30,051	14,535
DH-10	449	206	9,304	15,258
DH-11	672	285	9,974	16,543
DH-12	494	149	5,036	16,781
DH-13	506	194	5,906	14,441
DH-14	461	154	2,953	13,239
DH-15	1,014	471	30,445	18,625
DH-16	1,190	461	40,249	17,445
DH-17	1,128	436	32,158	17,365
DH-18	1,000	356	27,320	15,490
DH-19	1,845	700	53,265	19,362
DH-20	1,252	456	19,747	17,148
DH-21	855	362	14,100	17,692
DH-22	770	305	8,643	16,212
DH-23	450	170	4,023	14,859
DH-24	423	172	4,972	13,462
DH-25	946	480	60,449	17,682
DH-26	1,063	492	40,621	17,678
DH-27	909	398	29,326	17,876
DH-28	1,201	448	25,618	17,960
DH-29	1,469	539	34,642	18,808
DH-30	1,070	427	23,775	17,531
DH-31	721	277	13,609	16,566
DH-32	351	164	4,289	13,992
DH-33	451	189	5,441	14,379
DH-34	736	298	64,570	14,668
DH-35	1,032	400	49,346	16,731
DH-36	1,182	485	27,255	18,233
DH-37	1,075	394	33,553	18,492

Appendix B-2 Continued

Sample Name	Pb (ppm)	Zn (ppm)	Ca (ppm)	Fe (ppm)
DH-39	1,004	423	26,523	16,768
DH-40	467	198	18,391	14,491
DH-41	346	159	7,950	12,585
DH-42	488	196	6,970	12,589
DH-43	535	271	67,340	12,299
DH-44	1,247	603	50,691	17,116
DH-45	1,339	555	56,611	17,263
DH-46	1,349	473	33,233	17,436
DH-47	1,156	354	18,576	17,023
DH-48	402	161	13,106	17,285
DH-49	342	136	6,524	12,525
DH-50	278	111	4,427	11,680
DH-51	656	314	64,337	14,903
DH-52	641	293	47,310	13,615
DH-53	1,251	450	24,662	17,280
DH-54	1,094	392	18,321	17,153
DH-55	986	327	17,021	15,949
DH-56	462	172	11,787	15,559
DH-57	815	279	9,348	14,900
DH-58	346	136	4,340	11,070
DH-59	695	350	22,187	18,943
DH-60	985	407	46,677	17,474
DH-61	557	237	21,956	13,637
DH-62	640	285	13,621	16,473
DH-63	982	546	51,681	16,741
DH-64	1,302	501	34,445	17,718
DH-65	1,306	347	31,170	15,668
DH-66	2,098	580	42,334	18,357
DH-67	1,109	366	17,765	15,530
DH-68	787	291	16,514	15,723
DH-69	783	271	21,386	15,112
DH-70	654	213	23,848	16,560
DH-71	1,232	450	55,176	16,921
DH-72	959	369	34,862	19,980
DH-73	449	167	4,302	12,338
DH-74	382	179	9,677	12,788
DH-75	290	111	4,564	11,207
DH-76	239	99	4,054	11,879

Appendix B-2 Continued

Sample Name	Pb (ppm)	Zn (ppm)	Ca (ppm)	Fe (ppm)
DH-78	58	44	2,160	11,957
DH-79	701	280	47,555	12,117
DH-80	1,070	466	26,964	18,500
DH-81	1,590	582	28,436	18,890
DH-82	1,542	468	26,280	17,725
DH-83	705	244	11,810	13,197
DH-84	788	286	15,379	16,314
DH-85	451	199	6,462	13,403
DH-86	381	143	3,796	11,974
DH-87	328	121	3,187	11,625
DH-88	258	132	8,814	11,026
DH-89	196	83	2,576	12,089
DH-90	148	68	1,988	14,163
DH-91	80	52	1,778	12,415
DH-92	654	249	15,474	17,280
DH-93	637	238	16,248	16,231
DH-94	825	356	44,562	16,357
DH-95	294	114	5,088	12,480
DH-96	230	93	2,921	11,779
DH-97	158	74	2,203	14,709
DH-98	84	43	1,615	13,403
DH-99	1,217	526	30,320	17,861
DH-100	1,227	504	30,041	17,592
DH-101	1,328	515	28,152	15,957
DH-102	2,176	732	30,606	17,318
DH-103	970	360	17,444	14,944
DH-104	826	312	20,799	14,806
DH-105	1,121	360	26,758	16,169
DH-106	529	204	7,245	14,103
DH-107	385	150	6,121	13,498
DH-108	206	88	2,669	12,951
DH-109	208	87	2,497	13,236
DH-110	120	66	2,144	13,891
DH-111	80	48	1,869	14,660
DH-112	1,333	658	43,777	17,908
DH-113	1,237	483	18,884	17,822
DH-114	1,859	591	33,864	16,892
DH-115	1,569	580	34,467	16,165

Appendix B-2 Continued

Sample Name	Pb (ppm)	Zn (ppm)	Ca (ppm)	Fe (ppm)
DH-117	969	326	23,901	15,544
DH-118	1,104	322	29,293	14,598
DH-119	934	332	10,291	16,464
DH-120	499	194	3,494	13,809
DH-121	371	170	5,554	15,002
DH-122	220	99	2,408	13,068
DH-123	153	74	2,100	14,029
DH-124	756	461	110,911	30,859
DH-125	464	227	76,358	15,216
DH-126	687	593	52,184	19,344
DH-127	672	245	128,054	20,844
DH-128	1,603	836	105,749	35,153
DH-129	481	217	93,135	18,873
DH-130	1,201	508	76,944	19,814
DH-131	545	266	98,005	15,824
DH-132	554	293	72,178	15,919
DH-133	1,539	388	22,890	20,216
DH-134	2,380	502	26,223	19,422
DH-135	2,430	555	25,617	19,619
DH-136	2,615	584	28,950	19,183
DH-137	2,330	599	24,459	20,006
DH-138	2,234	592	23,483	19,901
DH-139	1,866	562	22,122	19,171
DH-140	1,880	592	24,064	19,599
DH-141	2,119	624	26,818	20,383
DH-142	1,917	610	21,400	21,072
DH-143	1,746	540	31,622	19,437
DH-144	1,968	597	32,865	20,500
DH-145	2,180	443	50,358	15,524
DH-146	1,910	459	41,080	18,331
DH-147	2,142	558	37,356	19,504
DH-148	2,030	541	33,664	19,725
DH-149	1,935	560	28,878	19,258
DH-150	1,981	581	22,021	19,674
DH-151	1,982	569	24,298	18,778
DH-152	2,163	602	24,482	19,911
DH-153	1,871	520	27,161	18,402
DH-154	1,979	495	16,496	20,028

Appendix B-2 Continued

Sample Name	Pb (ppm)	Zn (ppm)	Ca (ppm)	Fe (ppm)
DH-156	2,414	464	20,363	18,796
DH-157	1,248	352	43,636	14,960
DH-158	1,952	497	39,443	19,107
DH-159	2,132	558	36,683	19,250
DH-160	2,094	552	30,223	19,620
DH-161	1,994	546	34,499	19,215
DH-162	2,010	567	31,715	19,038
DH-163	1,952	540	33,592	19,339
DH-164	1,937	554	27,024	19,965
DH-165	1,801	551	19,573	19,402
DH-166	1,912	502	21,676	18,611
DH-167	1,919	568	22,242	19,791
DH-168	1,619	542	14,811	18,922
DH-169	1,624	419	42,548	16,431
DH-170	1,823	422	39,257	15,404
DH-171	1,981	482	39,173	17,720
DH-172	1,975	509	33,786	17,931
DH-173	1,898	367	11,513	17,923
DH-174	2,480	508	21,903	18,796
DH-175	2,094	501	23,117	18,283
DH-176	2,076	484	29,083	18,160
DH-177	2,526	568	28,629	18,525
DH-178	2,455	581	27,365	19,492
DH-179	2,449	620	32,523	19,808
DH-180	2,198	641	27,559	20,092
DH-181	2,013	620	31,147	19,738
DH-182	1,856	583	25,102	19,509
DH-183	1,703	568	25,988	20,182
DH-184	1,707	579	25,247	20,542
DH-185	1,988	551	40,040	19,330
DH-186	2,143	524	39,997	18,042
DH-187	1,970	561	31,127	18,642
DH-188	1,858	554	31,489	19,724
DH-189	1,613	575	18,187	20,831
DH-190	1,956	631	21,825	19,987
DH-191	2,078	599	22,568	20,145
DH-192	2,317	589	25,501	19,597
DH-193	2,476	557	40,791	19,303

Appendix B-2 Continued

Sample Name	Pb (ppm)	Zn (ppm)	Ca (ppm)	Fe (ppm)
DH-195	2,418	438	18,635	17,631
DH-196	1,578	558	16,806	20,248
DH-197	1,614	488	16,790	17,225
DH-198	1,649	557	20,819	19,458
DH-199	2,083	594	26,670	19,808
DH-200	1,970	576	29,431	20,259
DH-201	1,784	532	26,143	20,099
DH-202	2,294	563	35,570	19,094
DH-203	1,988	476	37,205	17,798
DH-204	2,150	897	42,316	17,502
DH-205	1,539	340	51,276	14,745
DH-206	1,446	380	37,704	16,181
DH-207	1,819	455	43,559	17,549
DH-208	1,946	466	45,394	17,952
DH-209	2,135	513	44,303	19,203
DH-210	2,006	561	34,018	20,360
DH-211	1,853	589	23,132	20,410
DH-212	2,171	614	29,960	19,657
DH-213	2,054	594	28,730	19,615
DH-214	1,671	573	19,427	19,947
DH-215	2,096	597	32,722	19,840
DH-216	2,142	570	31,416	19,516
DH-217	2,151	623	30,675	19,388
DH-218	2,221	604	31,298	19,391
DH-219	1,818	556	23,566	19,335
DH-220	1,657	587	16,617	20,085
DH-221	1,618	539	17,135	19,621
DH-222	1,793	561	24,347	19,562
DH-223	2,187	618	28,305	20,412
DH-224	2,080	593	32,920	19,269
DH-225	2,217	600	34,403	19,944
DH-226	2,310	607	37,553	20,295
DH-227	2,162	583	38,280	19,832
DH-228	2,114	603	36,262	18,841
DH-229	2,074	515	40,406	17,976
DH-230	2,218	539	39,348	18,127
DH-231	2,016	573	36,738	19,590
DH-232	266	128	40,000	8,513

Appendix B-2 Continued

Sample Name	Pb (ppm)	Zn (ppm)	Ca (ppm)	Fe (ppm)
DH-234	308	134	24,784	9,670
DH-235	472	147	24,327	8,849
DH-236	281	124	5,940	8,369
DH-237	308	134	24,784	9,670
DH-238	2,192	560	43,427	18,944
DH-239	2,157	592	45,555	18,332
DH-240	2,011	647	35,261	20,735
DH-241	1,781	568	28,659	20,048
DH-242	2,200	650	31,714	19,583
DH-243	1,888	682	24,376	21,030
DH-244	1,871	700	23,192	21,429
DH-245	2,185	649	28,046	21,381
DH-246	2,125	740	27,807	21,384
DH-247	2,061	740	28,110	20,959
DH-248	1,888	648	30,216	20,303
DH-249	1,998	619	28,660	20,394
DH-250	1,733	547	15,320	19,732
DH-251	2,476	518	15,984	20,141
DH-252	1,892	599	17,951	21,169
DH-253	1,273	473	15,157	20,240
DH-254	1,520	607	16,905	21,217
DH-255	1,747	592	18,622	20,147
DH-256	1,737	559	21,574	20,766
DH-257	1,952	542	29,653	20,205
DH-258	2,097	576	30,468	19,868
DH-259	2,005	553	28,602	19,572
DH-260	2,080	544	29,710	18,392
DH-261	1,865	532	34,867	19,004
DH-262	1,933	491	39,890	19,075
DH-263	2,124	540	43,695	20,166
DH-264	2,011	561	37,821	19,133
DH-265	1,779	422	45,190	18,541
DH-266	1,963	525	36,187	18,139
DH-267	2,096	545	35,867	19,248
DH-268	1,987	607	27,394	20,076
DH-269	2,070	631	26,564	20,555
DH-270	2,040	578	23,549	20,000
DH-271	1,655	562	17,539	20,751

Appendix B-2 Continued

Sample Name	Pb (ppm)	Zn (ppm)	Ca (ppm)	Fe (ppm)
DH-273	1,542	609	12,935	21,624
DH-274	1,615	629	14,623	22,027
DH-275	1,730	599	15,594	20,973
DH-276	1,638	657	15,923	22,369
DH-277	1,665	620	14,867	21,001
DH-278	2,154	627	23,199	20,878
DH-279	1,770	602	20,780	20,425
DH-280	2,110	628	28,238	20,360
DH-281	2,212	603	38,722	19,476
DH-282	2,036	517	42,198	19,238
DH-283	1,773	397	50,012	16,121
DH-284	2,084	622	34,101	19,051
DH-285	1,943	603	25,563	20,608
DH-286	2,024	638	29,106	20,171
DH-288	1,336	582	27,849	18,460
DH-289	1,366	530	30,159	16,998
DH-290	1,638	617	32,145	18,487
DH-291	1,505	510	31,187	17,835
DH-292	932	348	15,758	16,011
DH-293	800	287	17,216	14,799
DH-294	911	329	20,831	16,008
DH-295	604	231	6,593	14,156

Appendix C – Aqua-Regia Correction Data

Appendix C-1 – Aqua-Regia Results

Pb (ppm)

Chemex Name	Sample Name	Location	XRF	AQ	AQ/XRF
H-1	BRDH-60	BR/FR	178	160	0.899
H-2	BRDH-98	BR/FR	289	253	0.875
H-3	BRDH-81	BR/FR	452	356	0.788
H-4	DH-50	SFSP	339	279	0.823
H-5	DH-41	SFSP	422	271	0.642
H-6	BRDH-73	BR/FR	831	641	0.771
H-7	BRDH-68	BR/FR	1,198	1,060	0.885
H-8	BRDH-26	BR/FR	1,327	1,140	0.859
H-9	DH-55	SFSP	1,203	1,030	0.856
H-10	DH-34	SFSP	898	701	0.781
H-11	BRDH-57	BR/FR	2,319	1,430	0.617
H-12	BRDH-118	BR/FR	1,793	1,550	0.864
H-13	BRDH-32	BR/FR	2,060	1,630	0.791
H-14	DH-53	SFSP	1,525	1,250	0.820
H-15	DH-29	SFSP	1,791	1,530	0.854

Zn (ppm)

Chemex Name	Sample Name	Location	XRF	AQ	AQ/XRF
H-1	BRDH-60	BR/FR	196	151	0.770
H-2	BRDH-98	BR/FR	265	227	0.857
H-3	BRDH-81	BR/FR	299	250	0.836
H-4	DH-50	SFSP	126	113	0.897
H-5	DH-41	SFSP	181	121	0.669
H-6	BRDH-73	BR/FR	596	553	0.928
H-7	BRDH-68	BR/FR	1,130	1,070	0.947
H-8	BRDH-26	BR/FR	1,082	1,020	0.943
H-9	DH-55	SFSP	372	344	0.925
H-10	DH-34	SFSP	339	313	0.923
H-11	BRDH-57	BR/FR	2,248	1,450	0.645
H-12	BRDH-118	BR/FR	1,316	1,160	0.881
H-13	BRDH-32	BR/FR	1,193	1,020	0.855
H-14	DH-53	SFSP	511	451	0.883
H-15	DH-29	SFSP	613	556	0.907

Appendix C-1 Continued

Ca (ppm)

Chemex Name	Sample Name	Location	XRF	AQ	AQ/XRF
H-1	BRDH-60	BR/FR	5,491	5,400	0.983
H-2	BRDH-98	BR/FR	4,298	6,400	1.489
H-3	BRDH-81	BR/FR	7,225	6,100	0.844
H-4	DH-50	SFSP	4,427	3,300	0.745
H-5	DH-41	SFSP	7,950	5,400	0.679
H-6	BRDH-73	BR/FR	25,030	22,100	0.883
H-7	BRDH-68	BR/FR	25,153	29,400	1.169
H-8	BRDH-26	BR/FR	19,563	19,600	1.002
H-9	DH-55	SFSP	17,021	22,900	1.345
H-10	DH-34	SFSP	64,570	53,000	0.821
H-11	BRDH-57	BR/FR	28,854	44,000	1.525
H-12	BRDH-118	BR/FR	31,351	42,200	1.346
H-13	BRDH-32	BR/FR	48,854	46,500	0.952
H-14	DH-53	SFSP	24,662	34,200	1.387
H-15	DH-29	SFSP	34,642	40,300	1.163

Fe (ppm)

Chemex Name	Sample Name	Location	XRF	AQ	AQ/XRF
H-1	BRDH-60	BR/FR	22,539	17,400	0.772
H-2	BRDH-98	BR/FR	30,076	21,700	0.722
H-3	BRDH-81	BR/FR	17,909	13,700	0.765
H-4	DH-50	SFSP	15,169	12,000	0.791
H-5	DH-41	SFSP	16,344	10,600	0.649
H-6	BRDH-73	BR/FR	19,420	14,100	0.726
H-7	BRDH-68	BR/FR	18,842	15,600	0.828
H-8	BRDH-26	BR/FR	22,015	16,500	0.749
H-9	DH-55	SFSP	20,713	16,400	0.792
H-10	DH-34	SFSP	19,049	15,600	0.819
H-11	BRDH-57	BR/FR	23,332	16,600	0.711
H-12	BRDH-118	BR/FR	22,309	19,300	0.865
H-13	BRDH-32	BR/FR	24,044	18,500	0.769
H-14	DH-53	SFSP	22,442	18,200	0.811
H-15	DH-29	SFSP	24,426	19,600	0.802

Appendix C-2 – Regression Equations for XRF to Aqua-Regia Correction

Metal	Relationship*	n	r2
Pb	Y = -16.45 + 0.8445 x	14	0.992
Zn	Y = -12.339 + 0.9153 x	14	0.994
Ca	$Y = 0.00001 x^2 + 1.7844 x - 4{,}776.40$	15	0.938
Fe	Y = 634.98 + 0.7415 x	15	0.861

* x = XRF concentration (ppm), Y = Aqua-regia concentration (ppm)

Appendix C-3 – Aqua-Regia:XRF Ratio

	Ratio Distribution	Pb	Zn	Ca	Fe	Mn	Co
	75%	0.86	0.92	1.35	0.81	1.01	0.22
(n=15)	Median	0.82	0.88	1.00	0.77	0.94	0.18
	25%	0.78	0.85	0.86	0.74	0.87	0.17
	RPD%	5	4	24	4	7	14

Appendix D – Landform Geochemical Frequency Distribution

Appendix D-1 – Big River/Flat River Confluence

Lead Concentration (ppm) by Landform

Landform	n	Min	25%	Median	75%	Max
Bank	14	1,017	1,179	1,288	1,391	1,786
Bench	22	752	1,277	1,359	1,568	2,203
Floodplain	66	237	1,081	1,294	1,512	1,958
Drainage/Chute	0	NA	NA	NA	NA	NA
Backswamp/Disturbed	52	146	1,069	1,182	1,277	1,902
Fill	8	850	923	1,123	1,195	3,264

Zinc Concentration (ppm) by Landform

Landform	n	Min	25%	Median	75%	Max
Bank	14	752	1,015	1,143	1,361	1,576
Bench	22	990	1,174	1,282	1,469	2,446
Floodplain	66	237	959	1,055	1,218	1,742
Drainage/Chute	0	NA	NA	NA	NA	NA
Backswamp/Disturbed	52	172	898	1,096	1,201	3,375
Fill	8	552	876	928	997	1,459

Calcium Concentration (ppm) by Landform

Landform	n	Min	25%	Median	75%	Max
Bank	14	29,273	39,853	62,726	90,363	123,841
Bench	22	29,446	45,780	52,499	58,973	82,039
Floodplain	66	4,298	28,305	39,351	54,401	95,710
Drainage/Chute	0	NA	NA	NA	NA	NA
Backswamp/Disturbed	52	5,491	20,063	26,200	36,064	103,510
Fill	8	26,031	31,187	37,831	40,497	126,898

Iron Concentration (ppm) by Landform

Landform	n	Min	25%	Median	75%	Max
Bank	14	15,877	16,350	17,452	18,265	21,344
Bench	22	14,234	16,245	17,398	18,374	20,235
Floodplain	66	12,543	16,119	17,195	18,505	23,159
Drainage/Chute	0	NA	NA	NA	NA	NA
Backswamp/Disturbed	52	13,790	16,278	17,326	18,263	20,119
Fill	8	14,789	16,800	17,489	18,484	26,514

Appendix D-2 – St. Francois State Park

Lead Concentration (ppm) by Landform

Landform	n	Min	25%	Median	75%	Max
Bank	11	656	781	946	1,016	1,333
Bench	39	402	1,018	1,190	1,337	2,098
Floodplain	66	58	281	493	897	2,176
Drainage/Chute	15	342	451	557	875	1,251
Backswamp/Disturbed	0	NA	NA	NA	NA	NA
Fill	0	NA	NA	NA	NA	NA

Zinc Concentration (ppm) by Landform

Landform	n	Min	25%	Median	75%	Max
Bank	11	280	335	471	510	658
Bench	39	161	396	462	507	617
Floodplain	66	43	112	201	329	732
Drainage/Chute	15	136	167	231	308	450
Backswamp/Disturbed	0	NA	NA	NA	NA	NA
Fill	0	NA	NA	NA	NA	NA

Calcium Concentration (ppm) by Landform

Landform	n	Min	25%	Median	75%	Max
Bank	11	26,306	31,975	44,562	56,065	64,570
Bench	39	13,106	26,402	30,159	35,965	67,340
Floodplain	66	1,615	3,570	9,491	20,536	55,176
Drainage/Chute	15	4,023	6,493	7,950	17,789	46,677
Backswamp/Disturbed	0	NA	NA	NA	NA	NA
Fill	0	NA	NA	NA	NA	NA

Iron Concentration (ppm) by Landform

Landform	n	Min	25%	Median	75%	Max
Bank	11	12,117	15,630	17,682	18,018	18,939
Bench	39	12,299	16,795	17,444	17,918	19,752
Floodplain	66	11,026	13,100	14,684	16,226	19,361
Drainage/Chute	15	12,525	13,814	14,859	16,627	19,980
Backswamp/Disturbed	0	NA	NA	NA	NA	NA
Fill	0	NA	NA	NA	NA	NA

Appendix D-3 – Washington State Park

Lead Concentration (ppm) by Landform

Landform	n	Min	25%	Median	75%	Max
Bank	15	1,249	1,698	1,968	2,070	2,180
Bench	0	NA	NA	NA	NA	NA
Floodplain	83	1,618	1,924	2,070	2,162	2,615
Drainage/Chute	50	1,273	1,661	1,911	2,035	2,480
Backswamp/Disturbed	0	NA	NA	NA	NA	NA
Fill	0	NA	NA	NA	NA	NA

Zinc Concentration (ppm) by Landform

Landform	n	Min	25%	Median	75%	Max
Bank	15	340	408	524	556	897
Bench	0	NA	NA	NA	NA	NA
Floodplain	83	422	549	583	613	740
Drainage/Chute	50	367	504	557	584	657
Backswamp/Disturbed	0	NA	NA	NA	NA	NA
Fill	0	NA	NA	NA	NA	NA

Calcium Concentration (ppm) by Landform

Landform	n	Min	25%	Median	75%	Max
Bank	15	32,865	37,763	42,316	44,443	51,276
Bench	0	NA	NA	NA	NA	NA
Floodplain	83	14,473	24,792	29,083	34,451	45,555
Drainage/Chute	50	11,513	16,963	22,984	28,712	45,394
Backswamp/Disturbed	0	NA	NA	NA	NA	NA
Fill	0	NA	NA	NA	NA	NA

Iron Concentration (ppm) by Landform

Landform	n	Min	25%	Median	75%	Max
Bank	15	14,745	16,151	18,042	19,232	20,500
Bench	0	NA	NA	NA	NA	NA
Floodplain	83	15,404	19,193	19,808	20,331	21,429
Drainage/Chute	50	17,225	19,041	19,607	20,076	22,369
Backswamp/Disturbed	0	NA	NA	NA	NA	NA
Fill	0	NA	NA	NA	NA	NA